ENGINEERING RESEARCH INSTITUTE
UNIVERSITY OF MICHIGAN
ANN ARBOR

THEORETICAL STUDY, DESIGN, AND CONSTRUCTION OF C-W MAGNETRONS FOR FREQUENCY MODULATION

FINAL REPORT

Technical Report No. 13
Electron Tube Laboratory
Department of Electrical Engineering

BY

J. R. BLACK
J. A. BOYD
G. R. BREWER
G. HOK
J. S. NEEDLE
W. PETERSON
S. RUTHBERG
R. F. STEINER
H. W. WELCH, JR.

Approved by: W. G. DOW

Project M921

CONTRACT NO. DA-36-039 sc-5423
SIGNAL CORPS, DEPARTMENT OF THE ARMY
DEPARTMENT OF THE ARMY PROJECT NO. 3-99-13-022
SIGNAL CORPS PROJECT 27-112B-0

January 1952

TABLE OF CONTENTS

		Page
	PERSONNEL OF UNIVERSITY OF MICHIGAN ELECTRON TUBE LABORATORY	ii
	MAJOR REPORTS ISSUED TO DATE	iii
	ABSTRACT	v
	LIST OF ILLUSTRATIONS	vi
I.	INTRODUCTION	1
	1. Purpose	1
	2. Outline of Procedure	2
	A. Status at Beginning of Period	2
	B. Theoretical Program	3
	C. Voltage-Tunable Tubes - Experimental	4
	D. Variable Reactance F-M Tubes - Experimental	4
	E. Experimental Study of Space Charge	4
II.	BASIC THEORY	6
	3. Dynamic Frequency Characteristics of the Magnetron Space Charge; Frequency Pushing and Voltage Tuning (H.W. Welch, Jr.)	6
	4. The Propagation of Electromagnetic Waves in a Magnetron-Type Space Charge (G.R. Brewer)	23
	5. Space Charge Equilibrium in a Magnetron - A Statistical Approach (G. Hok)	36
III.	EXPERIMENTAL RESULTS	
	6. Model 9 Low-Power Insertion Magnetron (J.S. Needle)	48
	7. Model 8 Double-Anode Set Interdigital Magnetron (J.R. Black)	80
	8. Model 6 and Model 7 F-M Magnetron (S. Ruthberg)	88
	9. Model 13 Low-Power External Cavity Interdigital Magnetron (J. Boyd)	109
	10. The Trajectron, a Tube for Study of Magnetron Space Charge (W. Peterson)	115
IV.	CONCLUSIONS	122
	11. Summary of Results	122
	12. Work in Prospect	123
V.	APPENDIX	126
	13. Tubes Construction Within the Period Covered by this Report (R.F. Steiner)	126
	14. New Laboratory Facilities (J.R. Black)	126
	15. Construction Techniques (R.F. Steiner)	134
	16. Assembly Drawings of Tubes and Special Cavities	140

PERSONNEL

Scientific and Engineering Personnel		Time Worked in Man Months*
W. G. Dow	Professor of Electrical Engineering	Supervisor
H. W. Welch, Jr.	Research Physicist	3.23
J. R. Black	Research Engineer	6.54
G. Hok	Instructors in Electrical Engineering	3.25
J. Needle		5.28
J. A. Boyd		2.36
R. Hegler		.41
G. R. Brewer	Research Associates	3.45
S. Ruthberg		7.41
M. Miller		.49
W. W. Peterson	Research Assistant	4.88
Service Personnel		
V. R. Burris	Machine Shop Foreman	2.23
R. F. Steiner	Assembly Technicians	6.93
J. W. Van Natter		10.25
R. Hansen	Technicians	1.23
C. Jaycox		2.37
E. A. Kayser	Instrument Makers	2.62
R. F. Denning		5.23
T. G. Keith		6.18
D. L. McCormick		1.69
N. Navarre	Draftsman	6.98
P. Moore	Laboratory Assistant	.11
S. Spiegelman	Stenographers	1.95
J. Long		1.54
A. Kline		.16
E. Brewer		.16
M. Gotanda		3.08

* Time worked is based on 172 hours per month.

MAJOR REPORTS ISSUED TO DATE

Contract No. W-36-039 sc-32245. Subject: Theoretical Study, Design and Construction of C-W Magnetrons for Frequency Modulation.

Technical Report No. 1

H. W. Welch, Jr., "Space-Charge Effects and Frequency Characteristics of C-W Magnetrons Relative to the Problem of Frequency Modulation," November 15, 1948.

Technical Report No. 2

H. W. Welch, Jr., G. R. Brewer, "Operation of Interdigital Magnetrons in the Zero-Order Mode," May 23, 1949.

Technical Report No. 3

H. W. Welch, Jr., J. R. Black, G. R. Brewer, G. Hok, "Final Report," May 27, 1949.

Contract No. W-36-039 sc-35561. Subject: Theoretical Study, Design and Construction of C-W Magnetrons for Frequency Modulation.

Technical Report No. 4

H. W. Welch, Jr., "Effects of Space Charge on Frequency Characteristics of Magnetrons," Proc. I.R.E., 38, 1434-1449, December 1950.

Technical Report No. 5

H. W. Welch, Jr., S. Ruthberg, H. W. Batten, W. Peterson, "Analysis of Dynamic Characteristics of the Magnetron Space Charge, Preliminary Results," January 1951.

Technical Report No. 6

J. S. Needle, G. Hok, "A New Single-Cavity Resonator for a Multianode Magnetron," January 8, 1951.

Technical Report No. 7

J. R. Black, H. W. Welch, Jr., G. R. Brewer, J. S. Needle, W. Peterson, "Theoretical Study, Design, and Construction of C-W Magnetrons for Frequency Modulation," Final Report, February 1951.

Contract No. DA-36-039 sc-5423. Subject: Theoretical Study, Design and Construction of C-W Magnetrons for Frequency Modulation.

Technical Report No. 8

G. R. Brewer, "The Propagation of Electromagnetic Waves in a Magnetron-Type Space Charge," July 1951.

Technical Report No. 10

G. Hok, "Space-Charge Equilibrium in a Magnetron: A Statistical Approach," July 13, 1951.

Technical Report No. 11

J. S. Needle, "The Insertion Magnetron: A New External-Cavity Magnetron for Low-Power Electronically-Tunable Operation in the 10 to 20-cm Wavelength Range," August 1951.

Technical Report No. 12

H. W. Welch, Jr., "Dynamic Frequency Characteristics of the Magnetron Space Charge; Frequency Pushing and Voltage Tuning," November 1951.

ABSTRACT

Two methods for frequency modulating magnetrons have been investigated. One method employs voltage tuning or "frequency pushing" while the other utilizes a magnetron-type space charge to produce a variable reactance.

Voltage tuning has been experimentally accomplished using two distinct types of tubes. A new type of mechanically-tunable magnetron has been constructed and operated giving a tuning range of 2.1.

Basic theory concerning the propagation of electromagnetic waves in a magnetron-type space charge, the space charge equilibrium in a magnetron and the dynamic frequency characteristics of the magnetron space charge including frequency pushing and voltage tuning have been developed in order to give a more complete understanding of the problem.

The design factors and operating characteristics of eight different types of tubes are presented as well as the special construction techniques employed for one of these types. Progress made towards the development of a new type of tube to be used for the study of the magnetron-type space charge is given.

A general outline of the new laboratory facilities of this laboratory is discussed. Suggestions are offered for the direction to be taken in future research in this field. Assembly drawings are given for all tubes designed and constructed in this laboratory in the period covered by this report.

LIST OF ILLUSTRATIONS

Fig.	Title	Page
3.1	Basic Physical Picture of the Magnetron Space Charge with Large Signal R-F Potential on the Anode	8
3.2	Illustration of Graphical Method for Determining Spoke Width and Phase Angle	13
3.3	Phase Focussing Diagram	16-17
3.4	Current Induced by Spoke into Circuit on Time Scale	16-17
3.5	Phase Focussing Diagrams for a Typical Magnetron Volt-Ampere Characteristic	18
3.6	Typical Volt-Ampere Characteristic Used in Making Phase-Focussing Diagrams of Fig. 3.5	19
4.1	ε_{eff} for Plane Magnetron Propagation Normal to Magnetic Field	26
4.2	ε_{eff} for Cylindrical Magnetron Propagation in $\pm$ Z-Direction.	27
4.3	ε_{eff} for Cylindrical Magnetron Propagation in r Direction. .	30
4.4	X-Directed Electric Field Distribution in Space Charge . .	32
4.5	Y-Directed Electric Field Distribution in Space Charge . .	34
4.6	Susceptance of Electron Stream as Seen from Anode	35
5.1	Space-Charge Distribution at Thermal Equilibrium	38
5.2	Regions in Phase Space Accessible to Electrons whose Orbits Intersect the Anode or Cathode Plane	40
5.3	Brillouin Distribution in Phase Space	43
5.4	Double-Stream Distribution in Phase Space	43
5.5	Space-Charge-Limited Conditions	45
5.6	Temperature Limited Conditions	45

LIST OF ILLUSTRATIONS (Cont'd)

Fig.	Title	Page
6.1	Variation of Wavelength with Distance ℓ_3	52
6.2	Upper Mode Boundary Current vs. Wavelength Showing the Effect of the Cathode Line Circuit	54
6.3	Operating Wavelength vs. Shorting Plunger Position Showing the Effect of the Cathode Line Circuit	55
6.4	Arrangement Used to Study the Effect of the Load on Upper-Mode-Boundary Current and Frequency Pushing	58
6.5	Effect of Load on Upper-Mode-Boundary Current and Frequency Pushing	59
6.6	Normalized G_{shunt} and B_{shunt} vs. Wavelength with "d" as a Parameter for Cavity No. 2 with Reactance Tuner	61
6.7a	Comparison of the Observed Wavelength at the Upper Mode Boundary with the Computed Resonance Wavelength	62
6.7b	Correlation of Upper-Mode-Boundary Current with Normalized Shunt Conductance at the Computed Resonance Wavelength . .	62
6.8	Sketch of Experimental Set Up for Low Q Operation in Cavity No. 1	65
6.9	Sketch of Experimental Set Up for Low Q Operation in Cavity No. 2	67
6.10	E_b and P_o vs. I_b for Two Values of Cathode Heater Current .	68
6.11	Volt-Ampere Characteristic	69
6.12	Comparison of Voltage Tuning Data with the Hartree Relation.	72
6.13	Experimental Set Up Using Insertion Tube as Local Oscillator for Spectrum Analyzer	73
6.14	Oscillograph Traces Obtained with the Experimental Arrangement Shown in Fig. 6.13	75

LIST OF ILLUSTRATIONS (Cont'd)

Fig.	Title	Page
7.1	Possible Types of Magnetrons Employing the Model 8 Resonant System	81
7.2	Photograph of Model 8B	84
7.3	Pulsed Performance Oscillograms Model 8B	85
7.4	Tuning Curves for Model 8C	87
8.1	View Showing Vane Protruding Through Slot. Model 7E	90
8.2	Volt Ampere Characteristics Model 7E	91
8.3	Performance Chart for Coaxial Single-Cavity Magnetron	95
8.4	Resonance Curve Model 7D No. 42 Magnetron	96
8.5	Voltage Standing Wave Ratio vs. Wavelength Model 7D-42	99
8.6	Voltage Standing Wave Ratio vs. Wavelength Model 7F No. 55	100
8.7	Tuner Position vs. Wavelength for Model 7F Tunable Magnetron Showing Pushing	101
8.8	Performance Chart Model 7F Tunable Magnetron	103
8.9	Performance Chart Model 7F Tunable Magnetron	104
8.10	Performance Chart Model 7F Tunable Magnetron	105
8.11	Performance Chart Model 7F Tunable Magnetron	106
8.12	Wavemeter Behavior for Single Frequencies and for Doublets Showing Dispersion Increase with Plunger Position	107
8.13	Wavemeter Response for Close Spaced and Separated Doublets.	108
8.14	Performance Characteristics vs. Heater Power for Model 7F No. 55 Magnetron	110

LIST OF ILLUSTRATIONS (Cont'd)

Fig.	Title	Page
8.15	Mode Jump Current vs. Heater Power Model 7F Tunable Magnetron	111
9.1	Schematic Diagram of Circuit Used in Experiment No. 3	114
10.1	View of Trajectron No. 3	117
10.2	Typical Magnetron Diode Volt-Ampere Curve Showing Negative Resistance	119
10.3	Points where Negative Resistance has been Observed in the Magnetron Diode	120
14.1	General View of Room 3515	129
14.2	Model 9 Coaxial Test Bench	129
14.3	Model 9 Parallel Plate Test Bench	131
14.4	Waveguide Arrangement for Interdigital Magnetron	131
14.5	View of test Bench in Room 3506-A	133
14.6	Test Bench in Room 3506-A	133
15.1	Model 9B Magnetron Assembly Glassing Operation	136

ASSEMBLY DRAWINGS OF TUBES AND SPECIAL CAVITIES

	F-M Magnetron Model 6A	141
	Co-axial Magnetron Model 7A	142
	Coaxial Magnetron Model 7B	143
	Co-axial Magnetron Model 7D	144
	Tunable Coaxial Magnetron Model 7F	145

ASSEMBLY DRAWINGS OF TUBES AND SPECIAL CAVITIES (Cont'd)

Title	Page
Push-Pull Magnetron Model 8B	146
Tunable Magnetron Model 8C	147
Low-Power Magnetron Model 9B	148
Low-Power Magnetron Model 9C	149
Magnetron Cavity No. 1 Assembly Model 9	150
Cavity No. 2, Mod. 9 Mag.	151
Cavity No. 3 Mod. 9 Mag.	152

THEORETICAL STUDY, DESIGN, AND CONSTRUCTION OF C-W MAGNETRONS FOR FREQUENCY MODULATION

FINAL REPORT

I. INTRODUCTION

1. Purpose

This report summarizes the progress in the University of Michigan Electron Tube Laboratory during the period from December 1, 1950, through November 30, 1951, on Contract No. DA-36-039 sc-5423 for the Signal Corps. The general objectives of the program under this contract are to increase the knowledge of space-charge effects and frequency characteristics in c-w magnetrons and to apply this knowledge to the development of magnetrons which can be frequency modulated. Prior to March 1, 1950, the emphasis had been in the 2000 to 2400 megacycle range. The general technique adapted for f-m was to employ a magnetron-type space charge as a variable reactance element within the same vacuum envelope as the oscillator magnetron. Three models of f-m tubes were under development using this principle.

On March 1, 1950, a study of a new type of frequency modulation was initiated. Wilbur of General Electric Laboratories had discovered that under certain conditions very wide frequency pushing at uniform levels could be obtained at frequencies below 1000 mc. Frequency shifts were observed between 1.5 to 1 and 15 to 1 depending on loading,

efficiency, and cathode temperature. The loading conditions were quite restrictive and consisted of a load placed directly across the terminals of the tube producing a Q in the order of 10 or less.

Since March 1, 1950, the objective on this phase of the program was to obtain a sufficient understanding of voltage-tunable operation in order to be able to extend this type of operation to microwave frequencies.

2. Outline of Procedure

A. Status at Beginning of Period. Results obtained at the Michigan Vacuum Tube Laboratory prior to the period covered by this report were presented in Technical Report Nos. 1 through 6. (See Major Reports Issued to Date at the front of this report.)

The status as of December 1, 1950, was as follows:

a. The understanding of the magnetron-type space charge concerning its effects on frequency was fairly complete based on theoretical and experimental observations presented in Technical Report Nos. 1 and 4. The concept was also based on a partially completed extension of this work covering effects not presented in the above reports.

b. Factors influencing the design of interdigital magnetrons for operation in the zero order mode were evaluated, several tubes contructed and results presented in Technical Report No. 2.

c. A preliminary analysis of dynamic characteristics of the magnetron space charge was made and presented in Technical Report No. 5. This work was concerned with initial concepts including such phenomena as induced current, maximum current boundary, frequency pushing, and voltage tuning. Low-Q operation and temperature-limited conditions were also considered.

d. A new geometry for a single-resonant-cavity magnetron was developed and presented, along with experimental results of such structures, in Technical Report No. 6. A tube using this new geometry was built to operate with an external resonant circuit, lending a large degree of freedom to the study and analysis of magnetron behavior. The first model

of this external-cavity magnetron was completed at the beginning of the period covered by this report and was expected to be a valuable tool for the study of voltage tuning.

e. Three designs for frequency-modulated magnetrons employing a magnetron-type space charge for a variable reactance was developed. One of these models (Model 5) was discontinued because of constructional difficulties. Several tubes of the Model 6 design were constructed and sketchy modulation data were obtained on one. A preliminary model of the third structure (Model 8), having both anode sets designed as oscillators rather than one oscillator set and one modulator set, was constructed and operated.

f. Work was started on the development of a smooth-bore diode magnetron for experimentally verifying theories on the magnetron space charge. Tests indicated that changes were necessary in the first model to eliminate distorted magnetic fields which prohibit accurate alignment of an exploring electron beam. This tube is called the "Trajectron" and is Model 11.

B. Theoretical Program.

a. In order to arrive at a quantitative understanding of frequency characteristics of the oscillating magnetron, namely frequency pushing and voltage tuning and magnetron operation in general, a program was initiated to theoretically analyze these phenomena. Phase focussing and the resulting effect of the magnitude of r-f voltage on the anodes were to receive attention. This work would be an extension of the preliminary analysis of dynamic characteristics of the magnetron space charge presented in Technical Report No. 5. It was to be a large-signal approach to the magnetron problem.

b. Theoretical study of the propagation of electromagnetic waves in a magnetron space charge was to be completed and presented as a technical report. This study is applicable to all magnetrons since it enables one to predict the effect of the inner swarm of electrons on the operating frequency. The above study also is important in the design of f-m magnetrons using the magnetron-type space charge as a reactive element.

c. A statistical approach to the problem of the space-charge distribution in a d-c or oscillating magnetron in the non-conducting (or approximately non-conducting) condition was to be investigated. It was felt that this approach which had not been attempted before would lend considerable insight to a number of magnetron problems.

C. Voltage-Tunable Tubes - Experimental. An experimental program for obtaining voltage-tunable operation at microwave frequencies was to be undertaken using the coaxial Model 9 external-cavity magnetron. With a circuit external to the interaction space a study could be conveniently made to determine the effect of the circuit on the magnetron operation.

In addition to the above program an investigation was to be started at a somewhat later date to determine how an interdigital anode structure operating directly into a waveguide could be used as a voltage-tunable tube. It was planned to experimentally determine the effect of the circuit on such a structure by using the Sylvania 3J22 magnetron and later to design an interdigital tube which would eliminate undesirable characteristics inherent in the 3J22 anode structure.

D. Variable Reactance F-M Tubes - Experimental. Effort was made to continue the development of the Model 6 coaxial resonator f-m magnetron for operation in the 2000 to 2400 megacycle range employing reactance-tube modulation. It was felt that the basic oscillator structure (Model 7) should be improved before incorporating the reactance tube structure into the circuit.

The Model 8 rectangular-cavity magnetron was to be developed for operation in the 2000 to 2400 megacycle range. This geometry has possibilities for reactance-tube tuning, voltage tuning, mechanical tuning or high-power operation.

E. Experimental Study of Space Charge. Tubes were to be constructed to experimentally confirm the theory developed in the study of propagation of electromagnetic waves in a magnetron space charge. (See section 2Bb.)

The trajectron, a tube for experimentally determining the space-charge distribution in a magnetron, was to continue to receive attention at a reduced rate (1/3 man month per month). The results of this work should lead to a more complete understanding of magnetron behavior.

II. BASIC THEORY

3. Dynamic Frequency Characteristics of the Magnetron Space Charge; Frequency Pushing and Voltage Tuning (H. W. Welch, Jr.)

This section summarizes the results of theoretical and experimental study of space-charge behavior in the oscillating magnetron. This investigation has been directed toward the attainment of a quantitative understanding of frequency characteristics of the oscillating magnetron, namely, frequency pushing and voltage tuning. A report presenting the results in detail has been issued.[1] What follows is, essentially, a summary of the content of this report.

Posthumus,[2] in 1935, described qualitatively the mechanism by which electrons are focussed into a phase position, relative to the r-f potential between the magnetron anode sets, which permits delivery of energy from the electrons to the circuit. Since the first presentation by Hartree and Stoner[3] of the method for self-consistent field calculations of the space-charge distribution in the oscillating magnetron, it has been theoretically possible to describe quantitatively the mechanism of phase focussing of electrons in the magnetron.

---

1 H. W. Welch, Jr., "Dynamic Frequency Characteristics of the Magnetron Space Charge; Frequency Pushing and Voltage Tuning," Technical Report No. 12, Electron Tube Laboratory, University of Michigan, Ann Arbor, November 1951.

2 K Posthumus, "Oscillations in a Split-Anode Magnetron, Mechanism of Generation," Wireless Engineer, Vol. 12, pp. 126-132, 1935.

3 This work is reviewed in detail by Walker in Chapter 6 of Microwave Magnetrons, Massachusetts Institute of Technology, Radiation Laboratory Series, Vol. 6, New York, 1948.

The number of calculations required by the self-consistent field method makes prohibitive the application of the method to the quantitative analysis of practically important magnetron characteristics such as frequency pushing. Methods for small-signal analysis, such as that proposed by Buneman[1] cannot be extended to the large-signal problem. The works of several other investigators have been studied and evaluated.[2] The conceptual picture of the space charge in the multianode magnetron under large-signal conditions, which seems to be generally agreed upon, is that shown in Fig. 3.1. The anode segments which are shown in this picture are assumed attached to an external circuit which is not shown. The distribution of space charge shown in Fig. 3.1 corresponds to the π-mode which is so named because there exists a phase differences between the potentials on adjacent segments of π-radians. It is found to be possible to represent this distribution of potential, which is stationary in space, by the Fourier sum of a number of travelling waves which proceed in opposite directions around the interaction space. For the π-mode of operation electrons interact primarily with the fundamental wave which is moving in the direction of the electron drift around the cathode. The velocity is such that the maximum of the wave proceeds from one anode segment to the next in one-half cycle. Electrons with this same velocity are said to be in "synchronism" with the wave. The synchronism angular velocity is defined by

$$\omega_n = \frac{2\pi f}{N} \tag{3.1}$$

---

1 Also described by Walker, op. cit.

2 See Section 1.3 and Bibliography of Technical Report No. 12.

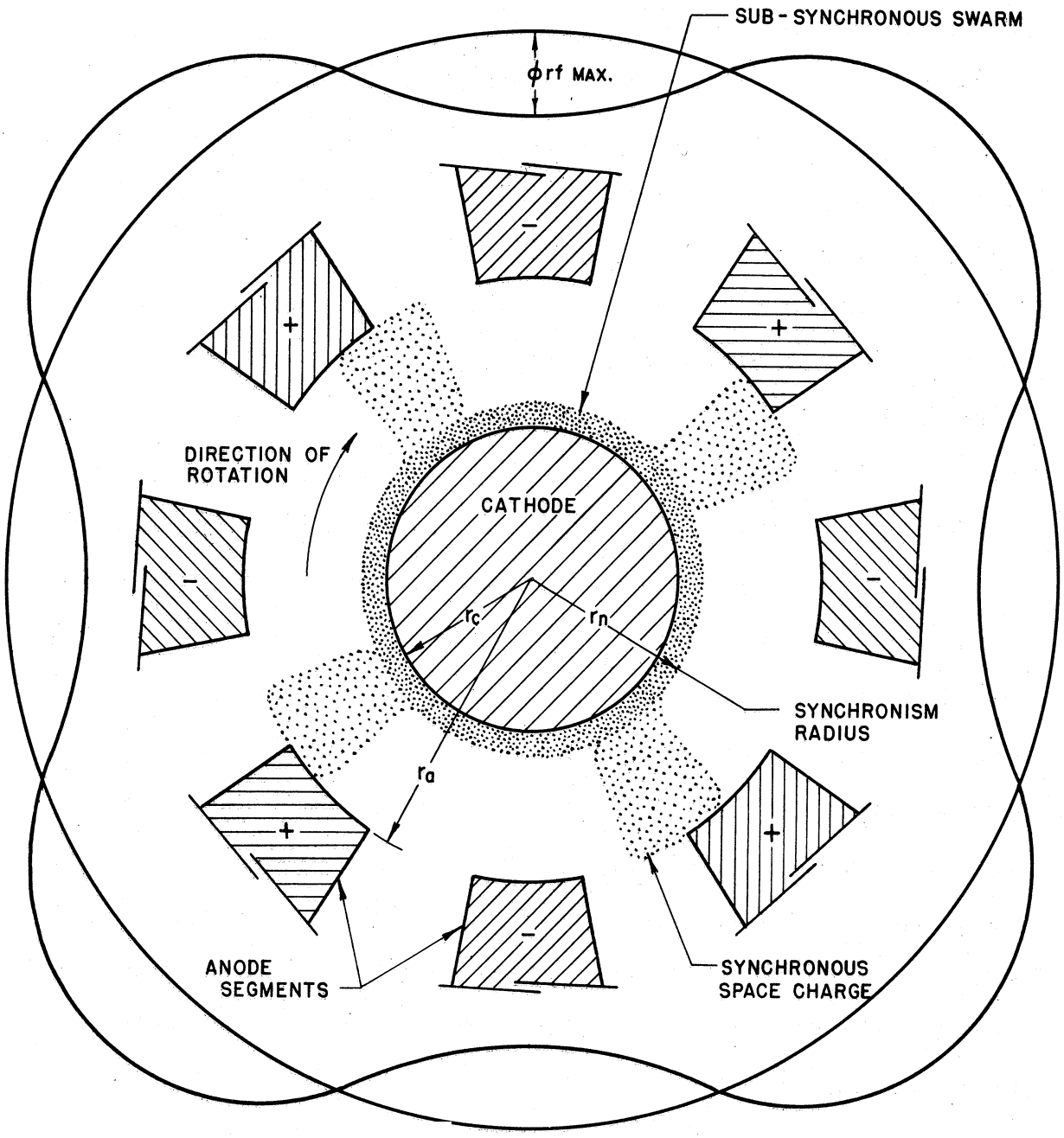

FIG. 3.1
BASIC PHYSICAL PICTURE OF THE MAGNETRON SPACE CHARGE WITH LARGE SIGNAL R-F POTENTIAL ON THE ANODE

$$n = \frac{N}{2}$$

N = number of anode segments.

The space bounded by the anode segments and the cathode surface is the region of interaction between the electrons and the fields. The presence of the d-c electric and magnetic fields causes the electrons to have a drift motion parallel to the cathode and anode surfaces in this region. The electrons are assumed to leave the cathode surface with zero initial velocities. The synchronism drift velocity must be reached or exceeded at some point in the interaction region if energy is to be delivered to the fundamental travelling-wave component. The conditions for this to be the case have been established for the planar and cylindrical magnetron geometry. In the planar magnetron the synchronism velocity is given by

$$v_n = x_n f \tag{3.2}$$

where $x_n/2$ is the distance between centers of adjacent anodes.

Since the mathematics of electron behavior is considerably less complicated for the planar magnetron than for the cylindrical magnetron, both have been carried through with the discussion centered around the planar magnetron geometry. The motion of the electron is determined through the force equation which in vector form is

$$\frac{\vec{dv}}{dt} = -\frac{e}{m}\left(\vec{E} + \vec{v} \times \vec{B}\right) \tag{3.3}$$

$\vec{v}$ = Vector velocity of the electron.

$\vec{E}$ = Vector value of electric field.

$\vec{B}$ = Vector value of magnetic field.

e = Absolute value of electronic charge.

m = Mass of electron.

After a change of variables to the reference frame moving with the synchronism velocity, resolution of the vector values into components, and algebraic manipulation, the force equations in component form become

$$\frac{d}{dt}\left(\frac{1}{2}mv_y^2\right) = e\frac{\partial\phi}{\partial y}\frac{dy}{dt} - Be\,(v_x' + v_n)\,\frac{dy}{dt}\quad , \tag{3.4}$$

$$\frac{dv_x'}{dt} = \frac{e}{m}\frac{\partial\phi}{\partial x} + \frac{Be}{m}\frac{dy}{dt}\quad , \tag{3.5}$$

in the planar system, and

$$\frac{d}{dt}\left(\frac{1}{2}mv_r^2\right) = e\frac{\partial\phi}{\partial r}\frac{dr}{dt} - \left[Be(\omega' + \omega_n)\,r - m(\omega' + \omega_n)^2 r\right]\frac{dr}{dt}\quad , \tag{3.6}$$

$$\frac{d(\omega' + \omega_n)r}{dt} = \frac{e}{m}\frac{\partial\phi}{\partial\theta} + \left[\frac{Be}{m} - (\omega' + \omega_n)\,\frac{dr}{dt}\right]\quad , \tag{3.7}$$

in the cylindrical system. ϕ is electric potential. The primed values refer to the moving reference frame, i.e.,

$$v_x = v_x' + v_n \tag{3.8}$$

$$\omega = \omega' + \omega_n \tag{3.9}$$

These equations can be integrated if v_x' and ω' are expressed as functions of distance y, or r. For the static magnetron the result is the cutoff potential. The synchronism anode potential required to bring electrons to the synchronism velocity may also be defined (given by Eq 2.25 and 2.36 in Technical Report No. 12). It is shown that, if a large-signal r-f

potential is present, the electron tends to remain in synchronism after it has reached the synchronism velocity. In this case

$$v_x' = \omega' = 0.$$

By making use of this condition and assuming that the r-f field has negligible effect on the subsynchronous electron it is possible to derive the threshold Hartree potential equation. This potential defines the energy which the electron must receive from the electric field to reach the anode. It is given by

$$\frac{\phi}{\phi_o} = 2\frac{B}{B_o} - 1 \tag{3.10}$$

$$\phi_o = \frac{1}{2}\frac{m}{e} v_n^2 \quad \text{for the planar magnetron} \tag{3.11}$$

$$\phi_o = \frac{1}{2}\frac{m}{e} \omega_n^2 r_a^2 \quad \text{for the cylindrical magnetron} \tag{3.12}$$

$$B_o = \frac{m}{e}\frac{v_n}{y_a} \quad \text{for the planar magnetron} \tag{3.13}$$

$$B_o = \frac{2\frac{m}{e}\omega_n}{1 - \frac{r_c^2}{r_a^2}} \quad \text{for the cylindrical magnetron} \tag{3.14}$$

y_a = cathode-anode distance

r_c/r_a = ratio of cathode radius to anode radius

The region of the interaction space which is accessible to the electrons is determined by an approximate method. This method makes use of the threshold potential condition and of the fact that electrons may have a component of drift velocity toward the anode when there is an appreciable

component of electric field parallel to the cathode surface. This is the case when there is an r-f potential difference between the anode segments. Electrons are found to drift toward the anode in the region where the r-f electric field is opposing the drift motion parallel to the cathode surface. In the rest of the interaction region, where the r-f electric field is aiding the tangential drift, electrons drift away from the anode. Since all electrons are presumed to originate from the cathode it is assumed that electrons will not exist in the immediate vicinity of the anode in the region where drift motion is away from the anode. Thus two conditions determining the approximate location of the spokes of electrons are established: a certain threshold potential must be exceeded at the anode, and a drift velocity toward the anode must exist at the anode. Application of these principles in a useful graphical construction is illustrated by Fig. 3.2.

The threshold energy level is represented by the line labeled ϕ_{at}, the actual anode voltage by the line ϕ_a. An r-f potential is represented with peak amplitude ϕ_f. This is the peak value of the fundamental travelling-wave component which appears stationary in the moving reference frame. Fig. 3.2a illustrates the possibility that, even though the threshold potential is not exceeded by ϕ_a, <u>if</u> an r-f potential exists, the threshold <u>may</u> be exceeded during part of the cycle designated by the interval A-B. In Fig. 3.2b the effect of the drift velocity condition is illustrated. The drift motion of the electrons is toward the anode in the region C-E and away from the anode in the region D-C. Therefore, although the threshold energy is exceeded in the entire region A-B, electrons can only drift toward the anode in half of this region bounded by C-B. In the

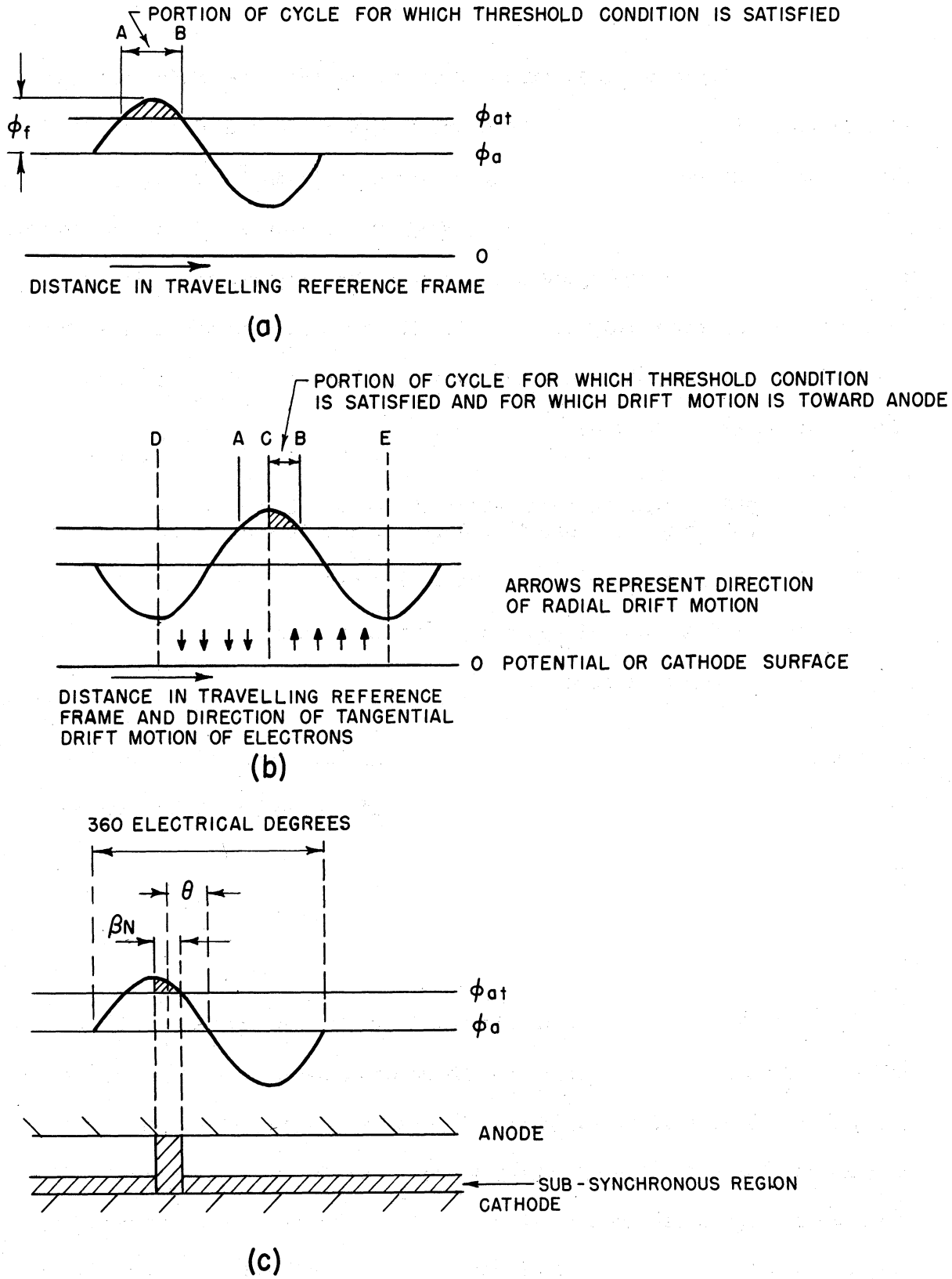

FIG. 3.2

ILLUSTRATION OF GRAPHICAL METHOD FOR DETERMINING SPOKE WIDTH AND PHASE ANGLE

region A-C electrons can only exist if they come fron the anode, and the assumption is that all electrons are emitted from the cathode. The final picture to be derived from this line of argument is shown in Fig. 3.2c. Here the potential distribution is plotted over a diagram of the interaction region. The width of the spoke and its phase angle relative to the r-f potential are approximately determined. These quantities are defined by the following symbols which are used when the current induced into the circuit is to be calculated.

θ = phase angle between center of spoke and zero of r-f potential in electrical degrees, negative as shown.

βN = width of spoke in electrical degrees.

β = half the actual space angle width of the spoke.

N = number of anodes.

There are N/2 full wavelengths (each 360 electrical degrees) around the cylindrical magnetron structure. The width of a spoke in electrical degrees, therefore is

$$\frac{N}{2}.2\beta = \beta N$$

The real value in this diagram is in its determination of the angle θ. θ is shown to be equal to the phase angle between the current induced in the circuit by the motion of the spoke parallel to the anode surface and the r-f potential which is developed between anode sets. In other words, for a particular set of conditions in the "phase focussing" diagram, there is a particular circuit which can produce these conditions since the phase angle and magnitude of the current induced by the spoke

will be determined once the anode potential, r-f potential, magnetic field and frequency are determined.

The use of the phase-focussing diagram is illustrated by Figs. 3.3, 3.4, 3.5, and 3.6. The phase-focussing diagram is in the moving reference frame so that the anode structure which is at rest in the stationary system may be thought of as moving to the left in Fig. 3.3. The resulting current is shown in Fig. 3.4. In Fig. 3.5, the phase-focussing diagrams for a typical volt-ampere characteristic given in 3.6 are shown. This illustrates space-charge behavior over a typical frequency-pushing characteristic. The significant properties are the large change in frequency and a relatively large change in anode potential. This is exactly the behavior to be expected from operation with a high Q resonant system.

The quantities defined in Fig. 3.2 may be expressed analytically. Using Fig. 3.2c we see that

$$- \cos \beta N = \cos 2\theta = \frac{\phi_a - \phi_{at}}{\phi_f} \tag{3.15}$$

ϕ_f, the peak value of the fundamental travelling-wave, is related to the actual peak r-f potential between anode segments by a constant which depends only on electrode geometry

$$\phi_f = K \phi_{rf\ max} \tag{3.16}$$

A condition of particular interest arises when $\theta = 0$, i.e., when resonance is reached. In this case

$$\phi_a - \phi_{at} = \phi_f \ ,$$

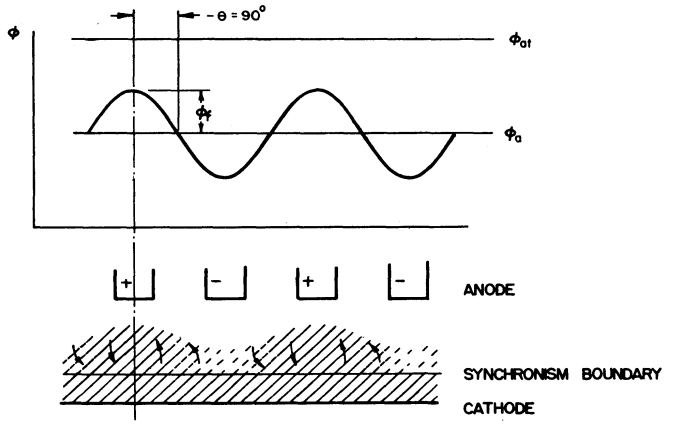

FIG. 3.3a

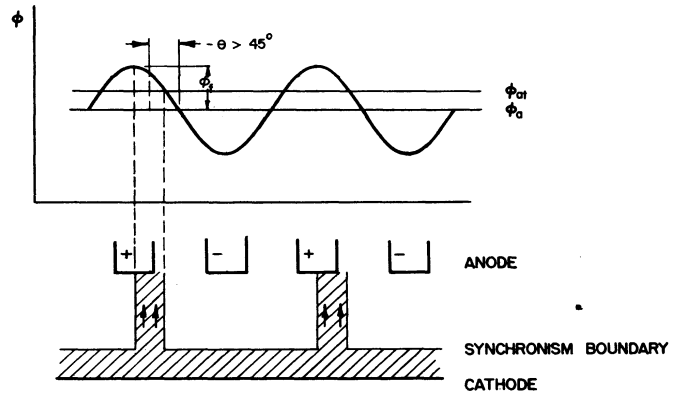

FIG. 3.3b

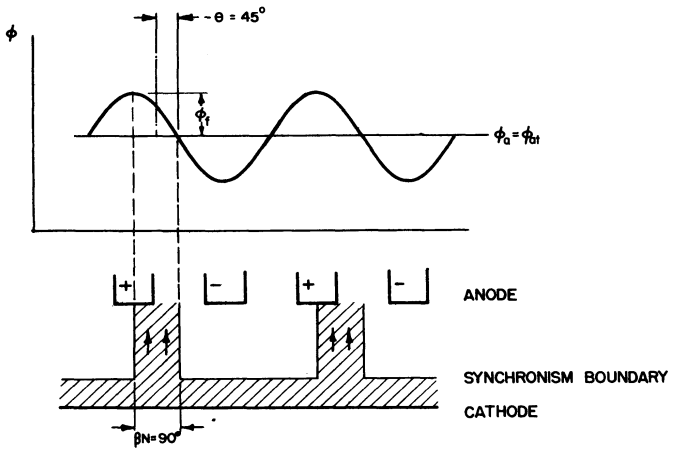

FIG. 3.3c

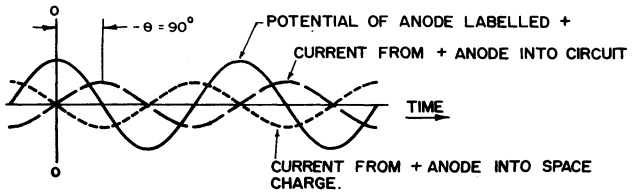

ELECTRONS CAPACITIVE

FIG. 3.4a

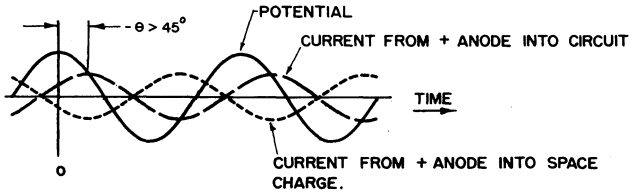

CIRCUIT INDUCTIVE

FIG. 3.4b

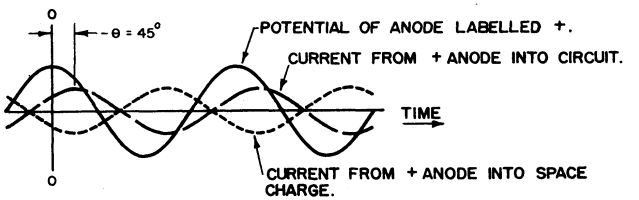

CIRCUIT INDUCTIVE AT HALF POWER POINT.

FIG. 3.4c

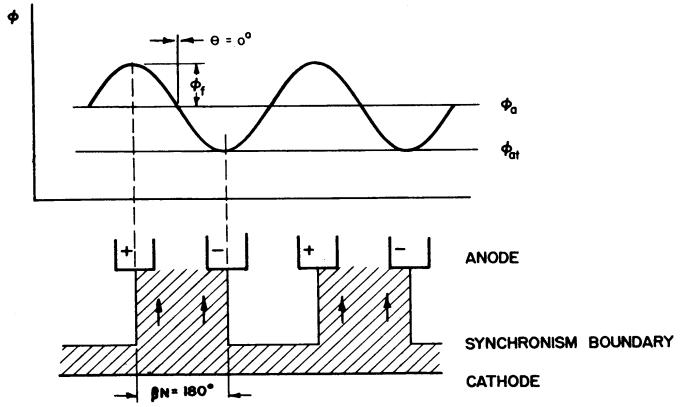

FIG. 3.3 d

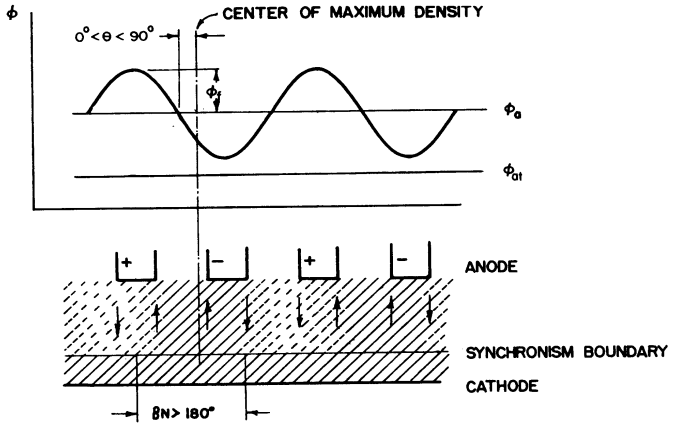

FIG. 3.3e

FIG. 3.3

PHASE FOCUSSING DIAGRAM. GRAPHICAL DEVELOPMENT OF RELATIONSHIP BETWEEN PHASE ANGLE θ AND ANODE POTENTIAL. CONSTANT R-F POTENTIAL AND FREQUENCY ARE ASSUMED. ARROWS INDICATE DIRECTION OF ELECTRON DRIFT BETWEEN ANODE AND CATHODE.

THIS FIGURE SHOULD BE STUDIED WITH FIG. 3.4

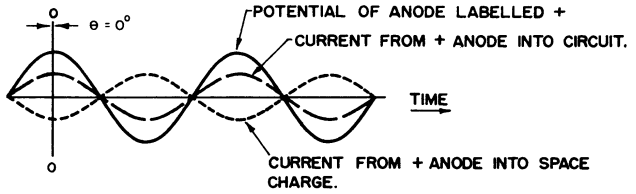

CIRCUIT RESISTIVE ON RESONANCE.

FIG. 3.4d

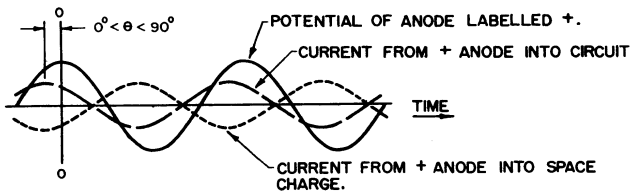

CIRCUIT CAPACITIVE

FIG. 3.4e

FIG. 3.4

CURRENT INDUCED BY SPOKE INTO CIRCUIT ON TIME SCALE. TIME O-O MARKS THE INSTANT OBSERVED IN ILLUSTRATION LABELLED BY THE SAME LETTER IN FIG. 3.3.

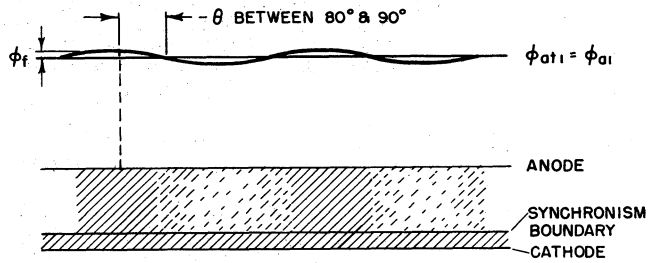

FIG. 3.5 a

MAGNETRON JUST STARTING. ϕ_f IS VERY SMALL. FREQUENCY IS 5 OR 10 % OFF RESONANCE. BUNCHING NOT COMPLETE, POSSIBLY NOISY OPERATION

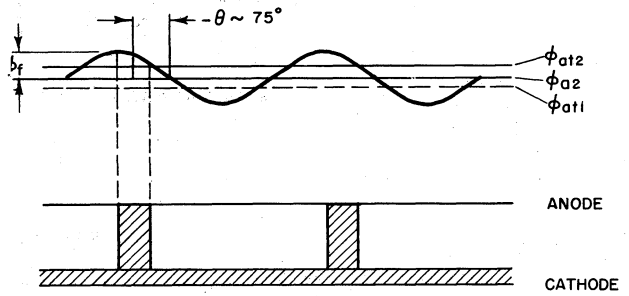

FIG. 3.5 b

MAGNETRON IS OSCILLATING STRONGLY. ϕ_f IS GREATER THAN 10% OF ϕ_a. FREQUENCY IS 1 TO 3 % OFF RESONANCE. BUNCHING IS COMPLETE BUT BUNCHES AND INDUCED CURRENT ARE MUCH LESS THAN MAXIMUM.

FIG. 3.5
PHASE FOCUSSING DIAGRAMS FOR A TYPICAL MAGNETRON VOLT-AMPERE CHARACTERISTIC

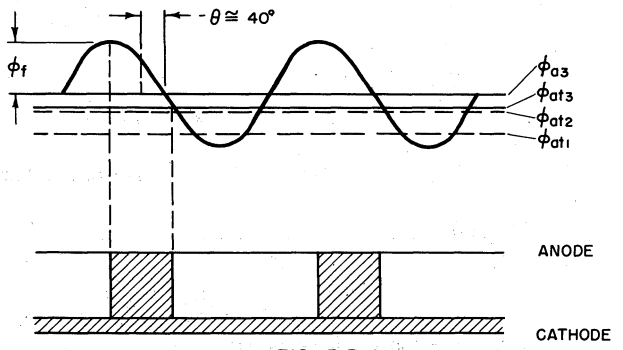

FIG. 3.5 c

MAGNETRON IS OSCILLATING AT A MEDIUM POWER LEVEL ϕ_f IS 30 OR 40% OF ϕ_a FREQUENCY IS LESS THAN 1% OFF RESONANCE. BUNCH HAS INCREASED IN SIZE AND INDUCED CURRENT IS GREATER THAN IN LAST PICTURE

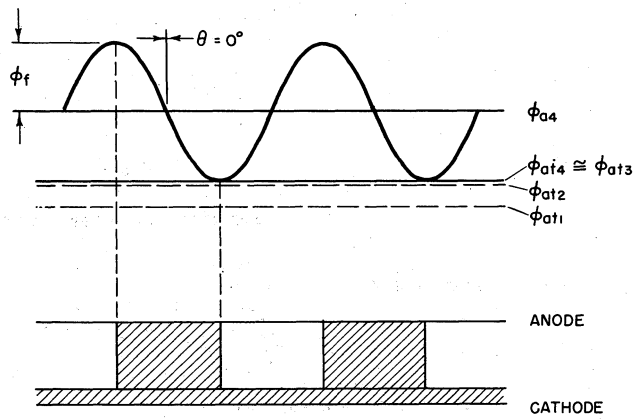

FIG. 3.5 d

MAGNETRON IS OSCILLATING AT HIGHEST POSSIBLE LEVEL ϕ_f IS OF THE ORDER OF HALF ϕ_a. FREQUENCY IS ON RESONANCE BUNCHES OCCUPY HALF OF THE SPACE. INDUCED CURRENT IS MAXIMUM.

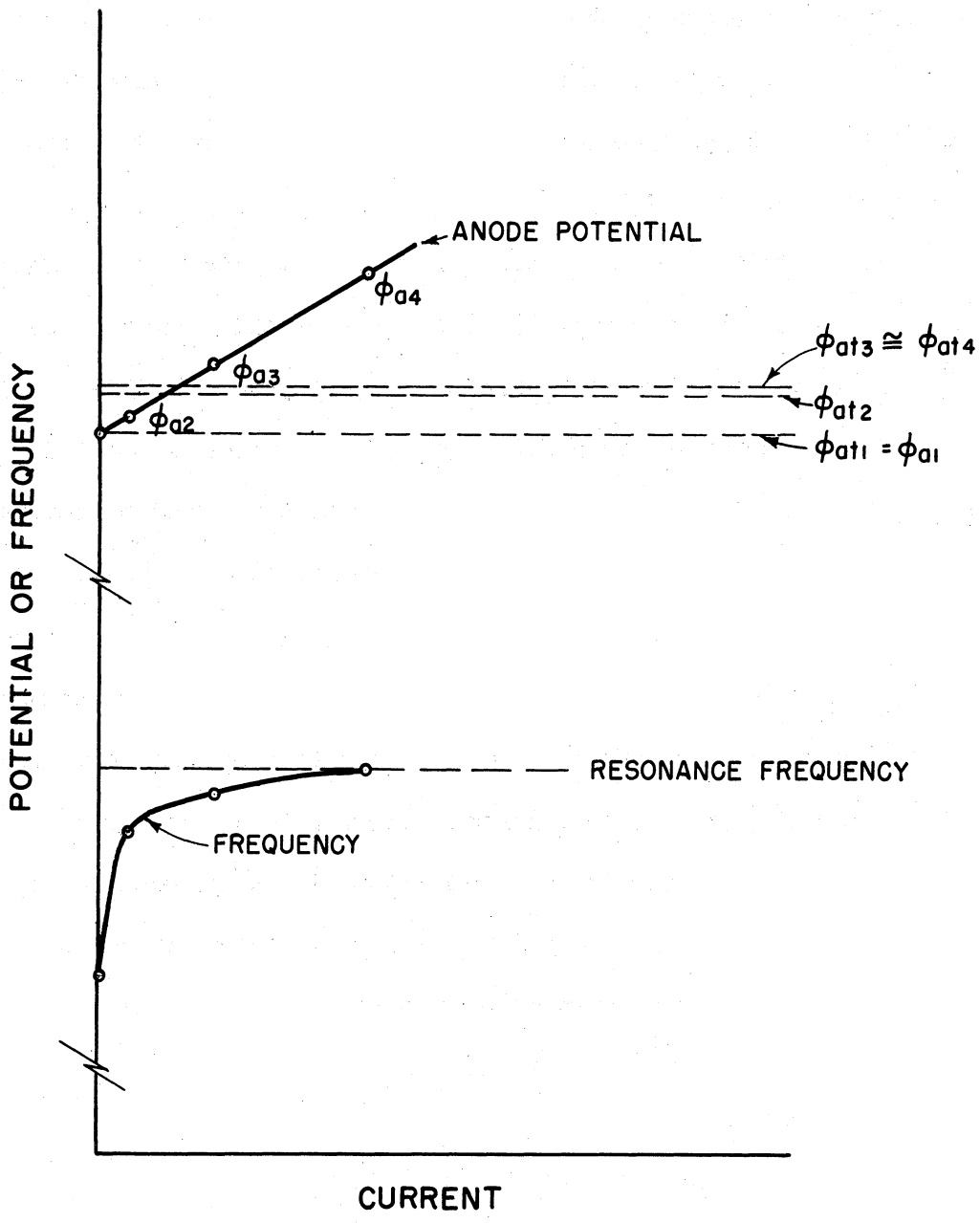

FIG. 3.6
TYPICAL VOLT-AMPERE CHARACTERISTIC
USED IN MAKING PHASE-FOCUSSING DIAGRAMS
OF FIG. 3.5

and the spoke appears as in Fig. 3.3d or Fig. 3.5d. For higher d-c potential the potential in the moving reference frame is greater than the threshold value everywhere in the interaction region. It is no longer possible to have good phase focussing, and debunching will be expected as illustrated in Fig. 3.3e. The magnetron will not be expected to oscillate, therefore, when $\phi_a - \phi_{at} >> \phi_f$.

Voltage-tuning characteristics correspond to circuits for which the phase angle does not vary rapidly with frequency and to magnetrons with limited d-c current. These conditions are analyzed and it is found that, as the anode potential is raised, $(\phi_a - \phi_{at})$ remains substantially constant so that the frequency of oscillation is almost directly proportional to the anode potential (through the threshold equation). If $\frac{B}{B_o} >> 1$ this proportionality is very near exact.

In order to calculate this current induced in the anode segments it is necessary to estimate the space-charge density in the spokes. Two assumptions are made: the spoke density is assumed to be the average density modified by the ratio of the total volume in the interaction space to the volume occupied by the spokes; the potential distribution determining the average density is assumed to be square-law (this gives a constant charge density). With these assumptions

$$\frac{\beta N}{2\pi} \rho_s = \rho_o \left[1 + \frac{4 \epsilon_o (\phi_a - \phi_{at})}{\rho_o r_c^2 (R_a^2 - R_n^2)} \right] \qquad (3.17)$$

ρ_s = space-charge density in spokes (coulombs/m3).

$\rho_o = 2 \epsilon_o \frac{m}{e} \omega_n \left(\frac{Be}{m} - \omega_n\right)$.

$R_a = r_a/r_c$.

$R_n = r_n/r_c$ $\quad r_n$ = radius where electrons reach synchronism angular velocity (ω_n).

Application of the theory of induced currents to the magnetron geometry, using the picture just described, yields finally for magnitude of the current in the external circuit

$$Ig = \frac{K_1}{\frac{\frac{\pi}{2}+\theta}{\cos\theta} \frac{K_1}{K_2} \frac{\cos 2\theta}{Y_T}} \tag{3.18}$$

$$K_1 = \frac{8}{\sqrt{2}} \pi L r_c^2 f \rho_o F(\alpha, N, R_a R_n) \text{ amperes}$$

$$K_2 = \frac{\rho_o r_c^2 (R_a^2 - R_n^2)}{4\sqrt{2K}\,\epsilon_o} \text{ volts}$$

$$F(\alpha,N,R_a,R_n) = \frac{\sin\frac{N}{2}\alpha}{\frac{N}{2}\alpha} \frac{1}{R_a^{\frac{N}{2}} - R_a^{-\frac{N}{2}}} \left[\frac{R_a^{2+\frac{N}{2}}}{2+\frac{N}{2}} - \frac{R_a^{2-\frac{N}{2}}}{2-\frac{N}{2}} - \frac{R_n^{2+\frac{N}{2}}}{2+\frac{N}{2}} + \frac{R_n^{2-\frac{N}{2}}}{2-\frac{N}{2}} \right],$$

α = angular width of gap between anode segments.

L = length of magnetron cathode.

The potentials have been eliminated from this expression by making use of (3.15), (3.16), and

$$\phi_{r\text{-}f} = \frac{Ig}{|Y_T|} \tag{3.19}$$

$|Y_T|$ = absolute value of circuit admittance as seen between alternate anode sets connected in parallel.

The power in the load is given by

$$P_L = \frac{G_L}{|Y_T|^2} \left(\frac{K_1}{\frac{\frac{\pi}{2}+\theta}{\cos\theta} \frac{K_1}{K_2} \frac{\cos 2\theta}{Y_T}} \right) \tag{3.20}$$

The d-c anode potential is given by

$$\phi_a - \phi_{at} = \frac{K\sqrt{2}}{|Y_T|} \frac{K_1}{\frac{\frac{\pi}{2} + \theta}{\cos\theta} \frac{K_1}{K_2} \frac{\cos 2\theta}{|Y_T|}} \cos 2\theta \quad . \tag{3.21}$$

These equations have been applied to the particular case of the simple resonant circuit and a non-resonant circuit to calculate typical frequency-pushing characteristics and voltage-tuning characteristics. The results agree well with experiment. A number of sets of experimental data have been analyzed and compared with the theory. The effect of cathode temperature on the magnetron behavior has been studied experimentally but very little theoretical explanation is offered.

A general conclusion, resulting from the study, which is a useful rule of thumb in predicting frequency-pushing behavior is the following. The magnetron operating with a high Q resonant system (10 or greater) and under space-charge-limited conditions may be expected to begin appreciable power generation at approximately 1/10 maximum power at $f_o \times \frac{2}{Q_L}$ megacycles below resonance. f_o is the resonance frequency in megacycles. The range of operation is from this point to between $\frac{f_o}{2Q_L}$ megacycles below resonance and f_o.

4. The Propagation of Electromagnetic Waves in a Magnetron-Type Space Charge (G. R. Brewer)

The study of the propagation of electromagnetic waves in a magnetron-type space charge started on Contract No. W-36-039 sc-35561 was completed in this period and the results of this study have been published as Technical Report No. 8.

This analysis was carried out in order to provide information on the properties of a magnetron space-charge cloud as it affects the

magnetron resonant circuit. It was an extension of the work first reported on by H. W. Welch, Jr., in Technical Report No. 1 and is specifically an attempt to determine the effective index of refraction of the space-charge region as experienced by an electromagnetic wave propagating into or through this region. A knowledge of the index of refraction, and thus the dielectric constant, as a function of the frequency of the wave and the magnetic field, will enable the calculation of the reactive (and in some cases also resistive) effects of the space charge on the microwave circuit. Welch treats this problem under the assumption that the space-charge swarm moved with constant linear velocity independent of position. The present work is an extension and refinement on the previous treatment in that the variation of electron velocity with position in the magnetron is considered.

The results of this analysis are presented in a form enabling predictions to be made of the effects of the space-charge cloud on an r-f circuit. From this information, one could design structures for frequency modulation, amplitude modulation, etc., of a microwave signal, using this type of space charge.

The complete solution of the interaction of the waves in a multicavity magnetron and space charge was considered too complicated to yield results with any degree of generality. Therefore, the radial and tangential components of the actual fields in the magnetron were used separately in the analysis, each component giving rise to a different direction of propagation, tangential or radial. In the use of space-charge clouds for frequency modulation, the characteristics for propagation in the direction parallel to the magnetic field were desired so this problem was also solved. Using these simplified types of fields, solutions were obtained for both the plane and cylindrical magnetrons structures.

The following cases are analyzed using small-signal, non-relativitic approximations:

1. Plane magnetron

   a. Propagation of a plane electromagnetic wave in a direction parallel to the applied magnetic field.

   b. Propagation of a plane electromagnetic wave in a direction perpendicular to the applied magnetic field and normal to the anode and cathode.

   c. Propagation of a plane electromagnetic wave of phase-velocity~slow compared to that of light in a direction perpendicular to the applied magnetic field and parallel to the electron drift motion.

2. Cylindrical magnetron

   a. Propagation of a TEM-type electromagnetic wave in a cylindrical space charge in a direction parallel to an axially applied magnetic field.

   b. Radial propagation of a cylindrical electromagnetic wave in a cylindrical space charge.

The Euler hydrodynamical equation,

$$\frac{\partial v}{\partial t} + (v.\nabla) = - \frac{e}{m} [E + v \times B] - \frac{\nabla p}{nm} , \qquad (4.1)$$

which is derivable[1] directly from the Boltzmann transport equation, are used to find the equations of motion for this problem of electron wave interaction.

In this equation,

v = electron velocity.

E = total electric field.

B = steady magnetic field.

---

1 Chapman and Cowling, The Mathematical Theory of Non-uniform Gases, Cambridge, 1939, Chapter 3.

n = number of electrons per unit volume.

ρ = electron gas pressure.

A term was introduced into this equation, in the form of frictional force proportional to the electron velocity, which includes the effect of collisions between the electrons and gas particles in the space charge. It is shown that the pressure gradient ($\nabla\rho$) term does not affect the final result, so that this may be ignored. The equation of motion of the electrons in the space charge subject to the electric field of the propagating wave and the applied magnetic field is then:

$$\frac{\partial v}{\partial t} + (v.\nabla)\, v + gv = -\frac{e}{m}\left[E + v \times B\right] \quad . \tag{4.2}$$

From this equation the electron velocity, and therefore the current, are obtained in terms of the applied fields. Substitution of the current relations into the Maxwell field equations enables the determination of the complex index of refraction of the space-charge medium. It has been shown that the effect of the electron motion is equivalent to the electric energy storage in the medium in addition to the usual energy storage in free space, given by $E^2\epsilon_o/2$. Thus, the space charge can be considered, in so far as the wave propagation is concerned, as a dielectric whose relative dielectric constant is a function of the ratio ω/ω_c between the wave frequency (ω) and the magnetic field $B = (\frac{m}{e})\,\omega_c$.

It is found that the effective dielectric constant of the space charge can assume values which are positive and greater or less than unity, and also negative values. The interpretation of the latter value involves an analogy to a conducting material in which the wave is attenuated upon entering.

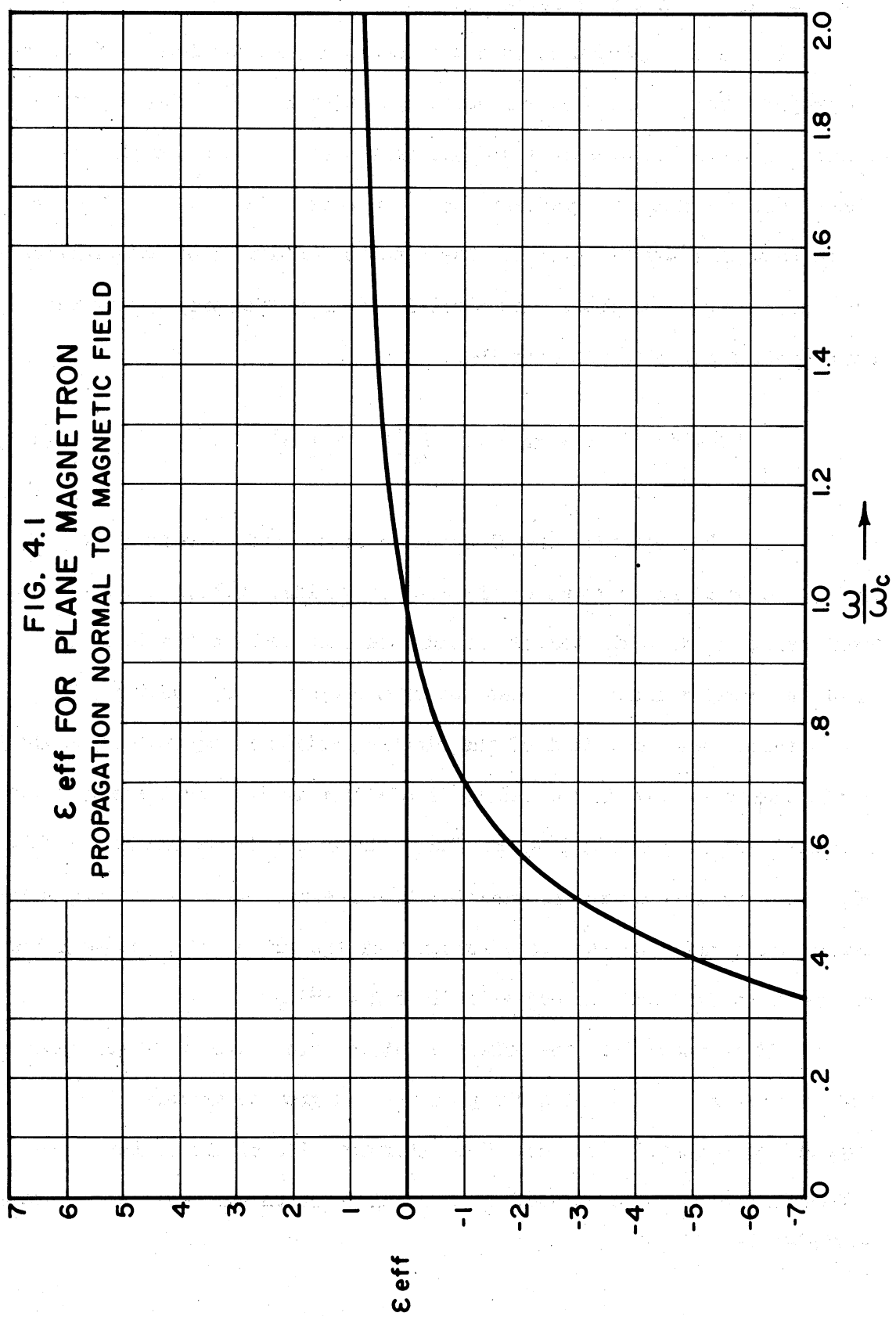
FIG. 4.1
ε eff FOR PLANE MAGNETRON
PROPAGATION NORMAL TO MAGNETIC FIELD
ε eff
7
6
5
4
3
2
1
0
-1
-2
-3
-4
-5
-6
-7
0
.2
.4
.6
.8
1.0
1.2
1.4
1.6
1.8
2.0
ω/ωc

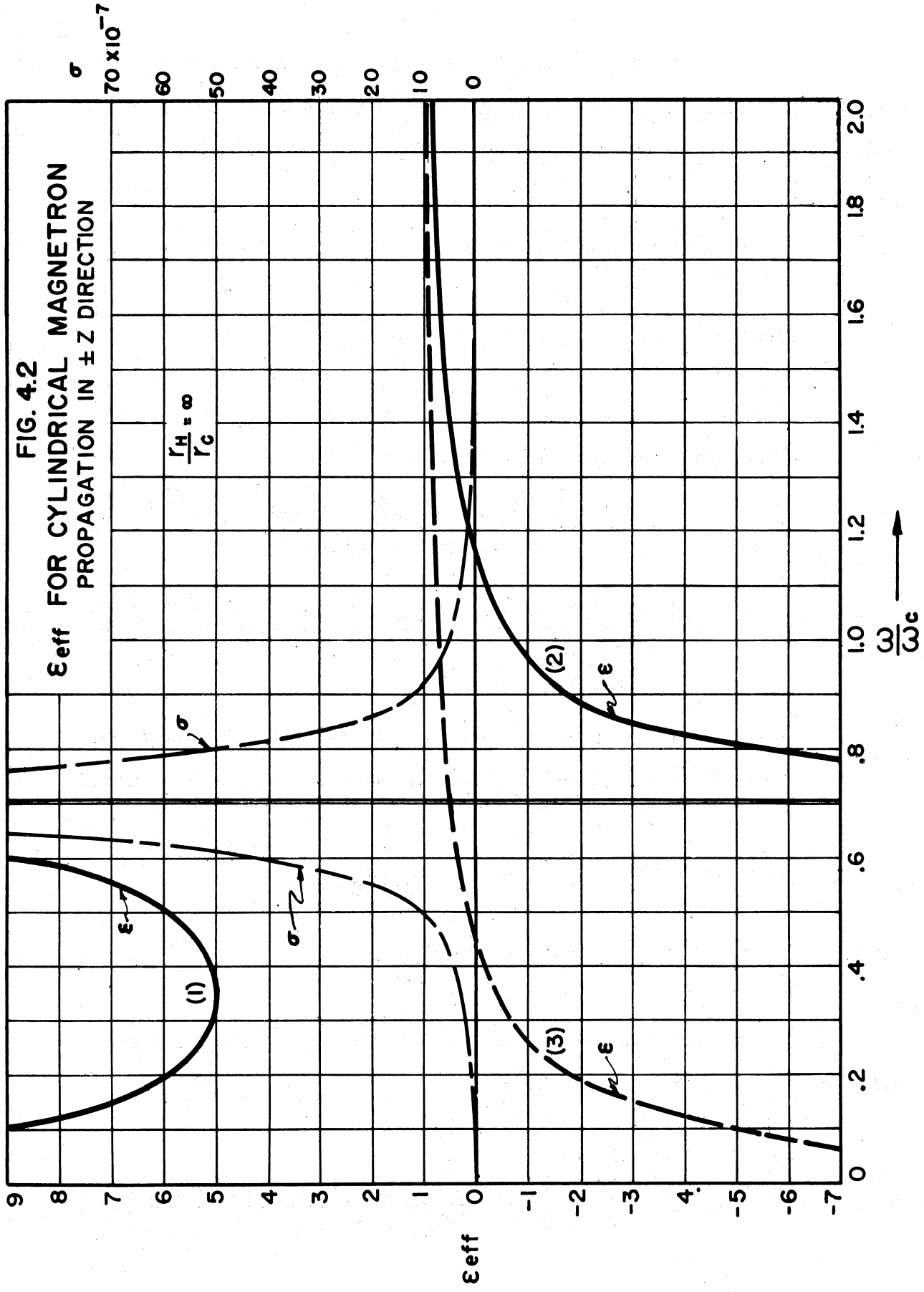
FIG. 4.2
εeff FOR CYLINDRICAL MAGNETRON
PROPAGATION IN ± Z DIRECTION
σ
70 x10⁻⁷
60
50
40
30
20
10
0
rH/rc = ∞
σ
σ
ε
(1)
(2)
ε
(3)
ε
9
8
7
6
5
4
3
2
1
0
-1
-2
-3
-4
-5
-6
-7
εeff
0
.2
.4
.6
.8
1.0
1.2
1.4
1.6
1.8
2.0
ω/ωc

The results of the analysis are expressed in the following equations for the effective dielectric constant and conductivity of the space charge (The Hull-Brillouin equation for the space-charge density has been used).

a. Propagation of a plane wave in the direction of the applied magnetic field.

Plane magnetron: $$\varepsilon_{eff} = 1 - \frac{1}{(\frac{\omega}{\omega_c})^2} \tag{4.3}$$

Cylindrical magnetron (r_c = cathode radius)

$$\varepsilon_{eff} = \frac{1 + (1 + r_c^4/r^4)\left[1 \pm (1/\sqrt{2})\,(\omega/\omega_c)\sqrt{1 - r_c^2/r^2}\right]}{1 - r_c^2/r^2 - 2(\omega/\omega_c)^2} \tag{4.4}$$

$$\sigma \cong g\,\epsilon_o \frac{(\omega_c^2/2)\left[(\omega_c^2/2)\,(1 - r_c^2/r^2) + \omega^2\right] \pm (\omega\omega_c^3/\sqrt{2})\sqrt{1 - r_c^2/r^2}}{\left[(\omega_c^2/2)\,(1 - r_c^2/r^2) - \omega^2\right]^2} \tag{4.5}$$

The above relation are plotted in Figs. 4.1 and 4.2 for $r_c/r \ll 1$.

b. Propagation of a plane or cylindrical wave in the direction normal to the anode and cathode.

Plane magnetron: $$\varepsilon_{eff} = 1 - \frac{1}{(\omega/\omega_c)^2} \tag{4.6}$$

$$\sigma = \frac{g\,\epsilon_o}{(\omega/\omega_c)^2} \tag{4.7}$$

The above equations are seen to be the same as those for the plane magnetron in the case a, above.

Cylindrical magnetron:

$$\varepsilon_{eff} \cong 1 - \frac{\omega_c^2}{2\omega^2}\left(1 + \frac{r_c^4}{r^4}\right)\left[\frac{\omega^2 - (\omega_c^2/2)\,(1 + r_c^4/r^4)}{\omega^2 - (\omega_c^2/2)\,(2 + r_c^4/r^4 - r_c^2/r^2)}\right] \tag{4.8}$$

These relations are plotted in Fig. 4.3 for $r_c/r \ll 1$.

The effective dielectric constant of a magnetron space charge as presented in the above curves are determined exactly (for the small-signal case) for the plane magnetron and the cylindrical magnetron with vanishingly small filament. Since neither of these structures are used in practice it is desirable to determine the dielectric properties of the space charge as a function of the radius of cathode and space charge. Unfortunately the complete solution is laborious so an interpretation was made based on limiting solutions already obtained and on a knowledge of the variation of the space-charge density and angular velocity as a function of r. From qualitative considerations curves presenting the above variations as a function of r are given which are considered to be reasonably valid.

c. Propagation in the direction parallel to the steady electron motion: Plane magnetron.

The propagation of electromagnetic waves in a direction parallel to the steady electron velocity in a plane magnetron having a "slow wave" anode was studied with the aim of contributing information leading to the design of a magnetron amplifier.

A basic differential equation representing the electric field in the space-charge region is arrived at presupposing only that the velocity of the wave in the space charge is small compared with the velocity of light.

$$\left[\ell - \frac{1}{\ell}\right] \frac{\partial^2 E_x}{\partial \ell^2} + \frac{2}{\ell^2} \frac{\partial E_x}{\partial \ell} - \left[\frac{2}{\ell^3} - \frac{1}{\ell} + \ell\right] E_x = 0 \quad . \tag{4.9}$$

where

$$\ell = \omega/\omega_o \left[1 + \frac{\gamma \omega_{cY}}{i\omega}\right. \tag{4.10}$$

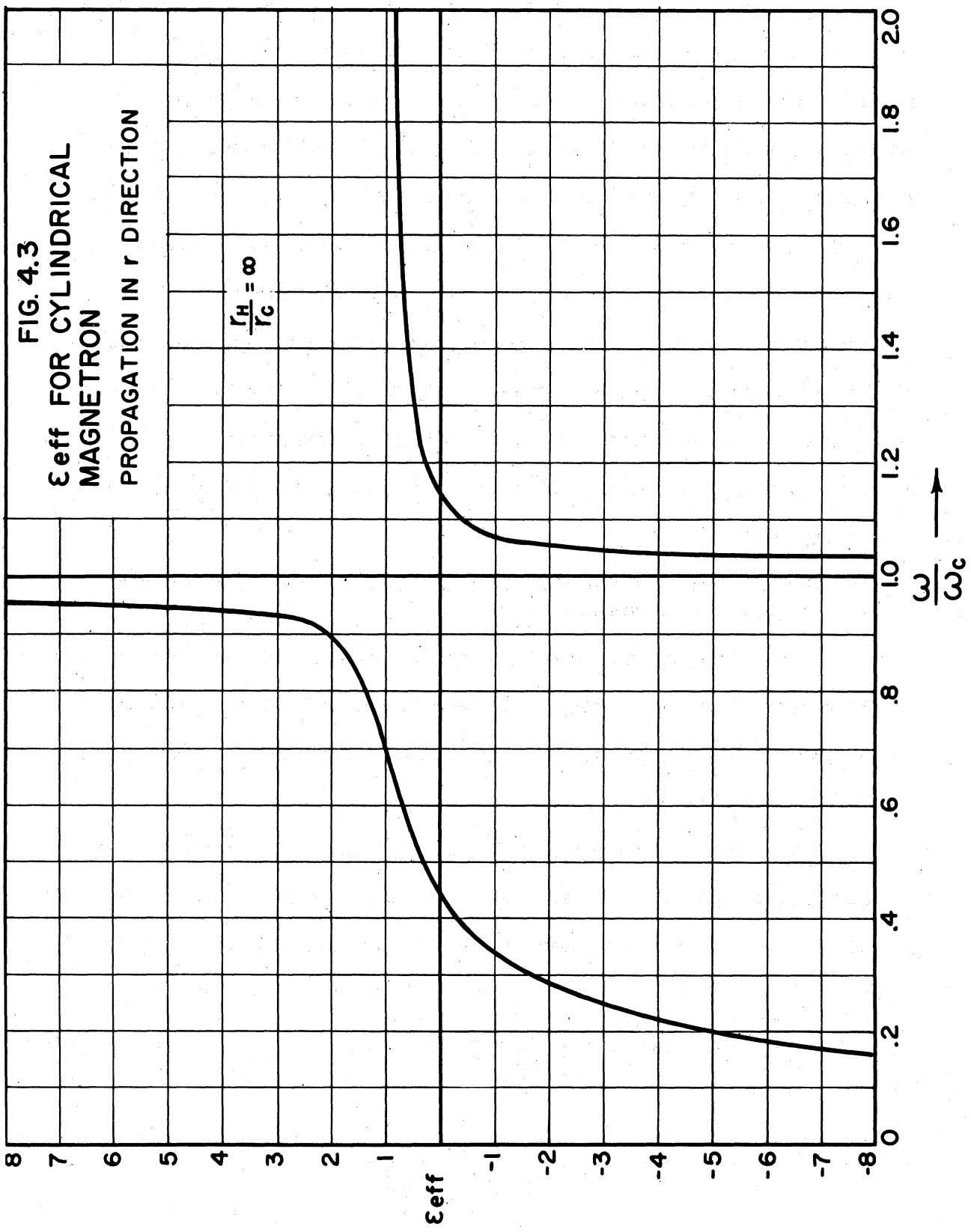
FIG. 4.3
εeff FOR CYLINDRICAL MAGNETRON
PROPAGATION IN r DIRECTION
$\frac{r_H}{r_c} = \infty$
εeff
8 7 6 5 4 3 2 1 -1 -2 -3 -4 -5 -6 -7 -8
0 .2 .4 .6 .8 1.0 1.2 1.4 1.6 1.8 2.0
$\frac{\omega}{\omega_c}$ ⟶

The intensity interaction effects the place for velocities near synchronism, therefore a solution was obtained for small values of ℓ

$$\frac{E_x}{a_2} = -\frac{\omega}{\omega_c}\ell\left[1+\frac{1}{2}\ell^2 + 0.21\ell^4 + 0.129\ell^6 + 0.0966\ell^8 + \ldots.\right]$$

$$+\ell^2\left[1 + \frac{1}{2}\ell^2 + 0.275\ell^4 + 0.191\ell^6 + \ldots.\right] \qquad (4.11)$$

The electric field E_x in the space charge is plotted in Fig. 4.4 vs. the real part of ℓ from which certain qualitative information concerning the space charge can be obtained.

The cathode of the magnetron is represented by the right hand intersection with the abscissa of the curve corresponding to the particular value of ω/ω_c under consideration. The intersection at ℓ = o corresponds to synchronism between the layer of electrons at that value of y and the travelling electromagnetic wave. It is seen that this synchronous layer of electrons becomes an infinite admittance sheet in the space charge. The portion of the curves to the right of ℓ = o represents the field on the region in which the electrons are moving slower than the wave and the part to the left of ℓ = o the region in which the electrons are moving faster than the wave. It appears that the interaction space in a magnetron is divided into two regions by this admittance sheet; the region between the cathode and the infinite admittance sheet and the region between this sheet and the anode. As the electrons are caused to increase in velocity (e.g., by increasing the magnetic field) this sheet will be displaced toward the anode.

Using the series expression derived above for the x-directed electric field in the space-charge region, together with $-\gamma E_y = \frac{\partial E_x}{\partial y}$ the x-directed field can be determined.

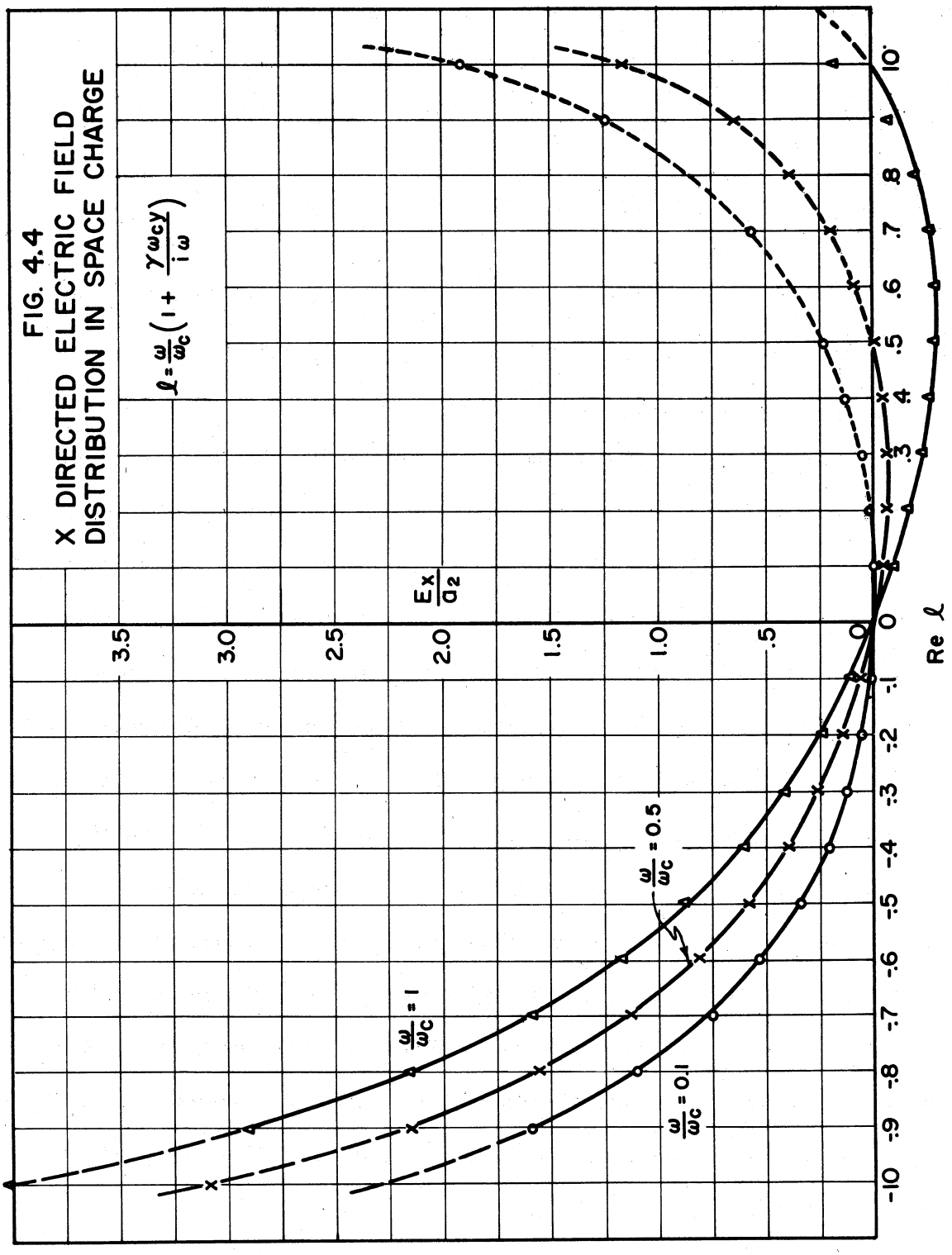
FIG. 4.4
X DIRECTED ELECTRIC FIELD
DISTRIBUTION IN SPACE CHARGE
$\ell = \frac{\omega}{\omega_c}\left(1 + \frac{\gamma\omega_{cy}}{i\omega}\right)$
$\frac{Ex}{d_2}$
3.5
3.0
2.5
2.0
1.5
1.0
.5
0
$\frac{\omega}{\omega_c} = 1$
$\frac{\omega}{\omega_c} = 0.5$
$\frac{\omega}{\omega_c} = 0.1$
-10 -9 -8 -7 -6 -5 -4 -3 -2 -1 0 .1 .2 .3 .4 .5 .6 .7 .8 .9 1.0
Re ℓ

$$E_y = \frac{1}{\gamma}\frac{\partial E_x}{\partial y} = i\frac{\partial E_x}{\partial \ell}$$

$$= ia_2\left[-\frac{\omega}{\omega_c}\left[1 + \frac{3}{2}\ell^2 + 1.05\,\ell^4 + 0.9\,\ell^6 + 0.87\ell^8 + \ldots.\right]\right. \quad (4.12)$$

$$\left. + \left[2\ell + 2\ell^3 + 1.65\,\ell^5 + 1.53\ell^7 + 1.47\ell^9 + \ldots.\right]\right]$$

This series converges slowly so values were not obtained above $\ell = 0.9$. The curves representing this series solution are shown in Fig. 4.5. It is seen that the y-directed electric field also appears to increase without limit near $\ell = \pm 1$.

A plot of the susceptance of the electron stream as seen by the anode was made employing an approximation and restricting the consideration to values of electron velocity near the synchronism condition, that is, by limiting ℓ to small values ($\ell < 0.4$).

Fig. 4.6 shows the manner of variation of Im Ye (h) for the simple case of no time average energy exchange between electrons and fields. These curves show the existence of the zero reactance sheet at $\ell = 0$ mentioned previously. They also show that the space charge appears inductive to the anode circuit for $\ell > \frac{1}{2}\frac{\omega}{\omega_c}$ and capacitive for $\ell < \frac{1}{2}\frac{\omega}{\omega_c}$. Electrons with velocity greater than that of the travelling wave appear capacitive, but not so much as the synchronous electrons. As the space charge expands due to an increase of the d-c anode voltage, the boundary of the cloud appears inductive for $\ell > \omega/2\,\omega_c$ and then capacitive.

The equation, presented in Technical Report No. 8, representing the electronic admittance indicates that the magnetron space charge is capable of delivering energy to the fields of an anode structure of the proper characteristics. A definite answer to the question of amplification

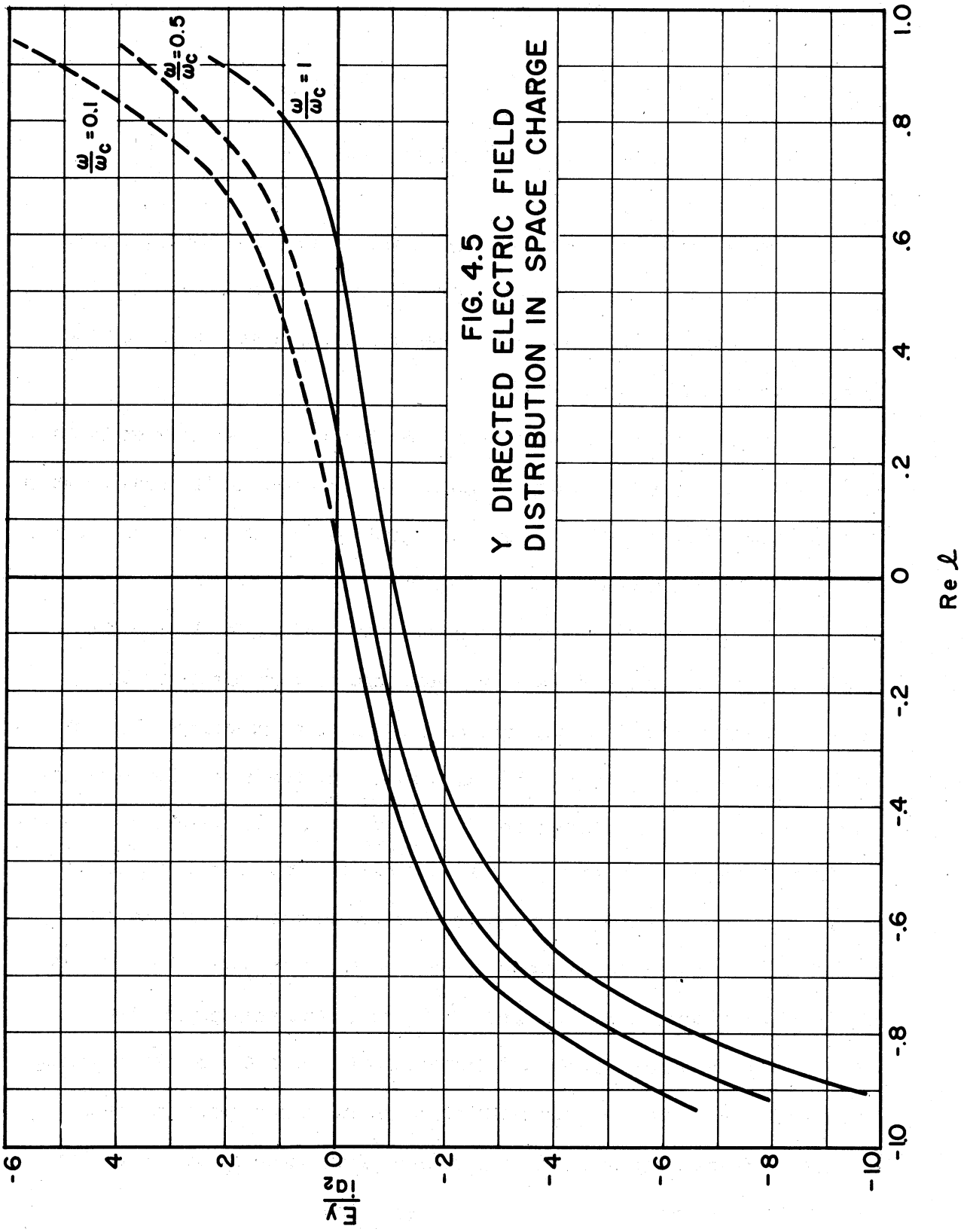
FIG. 4.5
Y DIRECTED ELECTRIC FIELD
DISTRIBUTION IN SPACE CHARGE
ω/ωc = 0.1
ω/ωc = 0.5
ω/ωc = 1
Ey/iα2
Re ℓ
-6
4
2
0
-2
-4
-6
-8
-10
1.0
.8
.6
.4
.2
0
-.2
-.4
-.6
-.8
-10

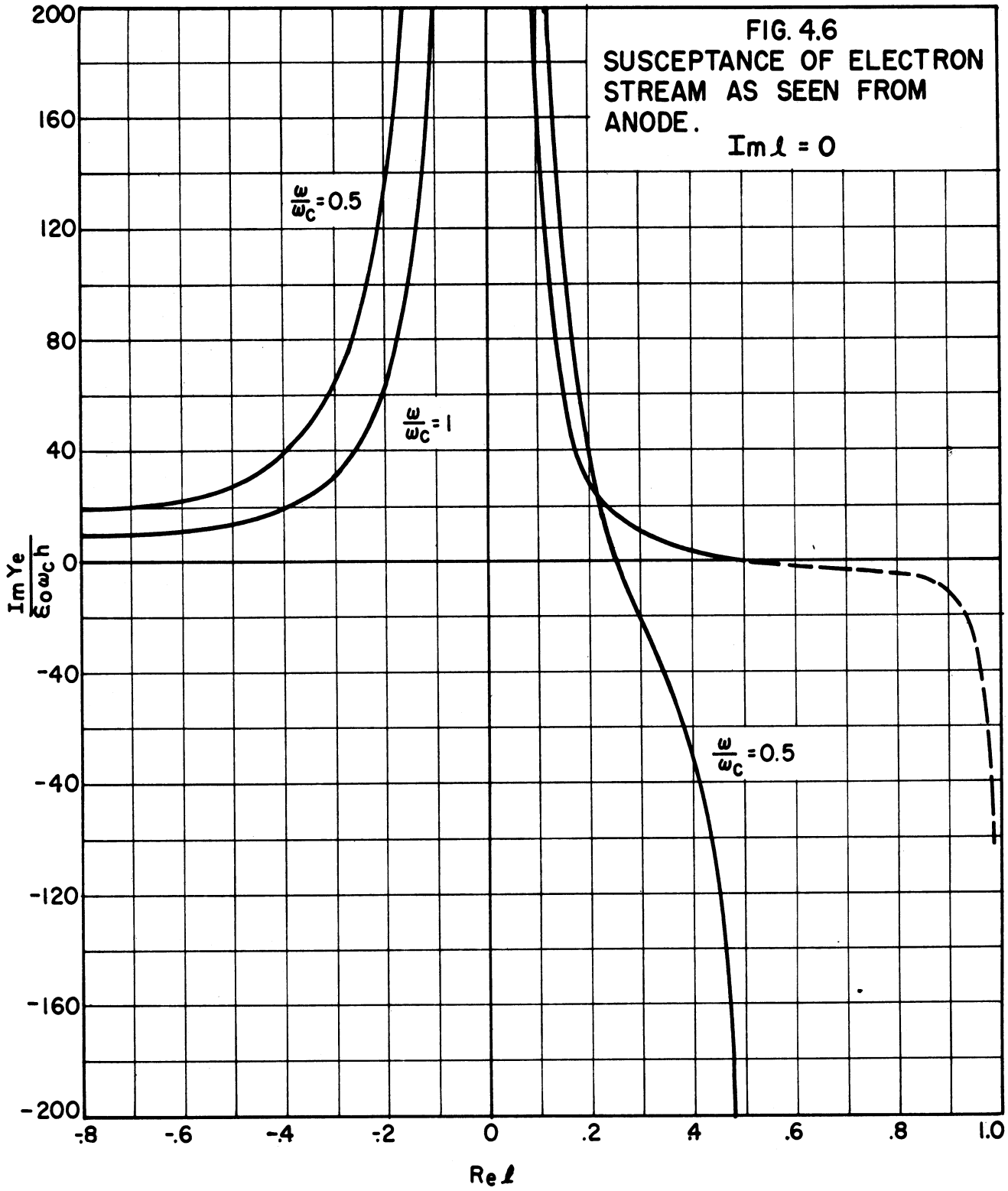
FIG. 4.6
SUSCEPTANCE OF ELECTRON STREAM AS SEEN FROM ANODE.
Im ℓ = 0
ω/ωc = 0.5
ω/ωc = 1
ω/ωc = 0.5
Im Ye / ε0 ωc h
Re ℓ
200
160
120
80
40
0
-40
-40
-120
-160
-200
-.8
-.6
-.4
-.2
0
.2
.4
.6
.8
1.0

can be obtained only from a complete solution of the boundary conditions imposed by the confining circuit.[1]

Experimental Results

Three experiments, described in Technical Report No. 8, were made in an effort to determine the validity of the analytical expressions determined for the dielectric properties of the magnetron space charge. The results of these experiments appear to confirm certain critical parts of the theory.

5. Space-Charge Equilibrium in a Magnetron - A Statistical Approach (G. Hok)

The results of the study of space-charge equilibrium in a magnetron using statistical methods was presented in Technical Report No. 10.

As an initial state for the oscillating magnetron, the non-conducting (or approximately non-conducting) condition of a d-c magnetron has a considerable interest and has received appreciable attention, both of a theoretical and experimental nature. Nontheless, a satisfactory agreement has not been reached about the shape of the electron orbits and the detailed distribution of potential and electron density in such a space charge.

The solutions presented necessarily rest on postulates and assumptions that consititute idealizations of the real conditions. So does, of course, all physical theory, but in this case well known factors have been neglected with the justification that their effect to be so small that the approximate solution resulting will be close enough to be of value. Furthermore, the mathematical difficulties of a more rigorous approach appeared prohibitive.

It has been the purpose of this study to reconsider the conventional simplifications on which these solutions are based, to discuss

---

1 Macfarline and Hay found that amplification along the stream was possible, but it is believed that the boundary conditions they used are open to question.

whether or not they introduce appreciable errors, and to investigate the feasibility of a solution from a more realistic set of assumptions. Since the space charge is essentially a gas formed by discrete electrons, classical statistical mechanics offered a logical approach to a fresh study of the problem.

The conditions to be satisfied for thermal equilibrium in a magnetron were considered; if the cathode of the magnetron is at a constant temperature and no current flows to the anode, no energy is received or lost by the swarm of electrons in the tube. When a minute current flows, on the other hand, the problem becomes a transport problem and a solution is obtained from the thermal equilibrium by applying a small perturbation to the distribution function for the electrons. As the current is increased further, the diffusion of electrons through the space charge from the cathode gradually changes to a steady flow of the whole space charge to the anode. The intermediate conditions, with severely distorted distribution function but no coherent flow pattern, offer the greatest mathematical difficulties. Unfortunately, there are reasons to believe that this is the actual state of affairs in a cutoff magnetron.

Fig. 5.1 indicates the space-charge distribution arrived at for thermal equilibrium. It obviously does not resemble the distribution in a cutoff magnetron, since it demands emission of electrons from the anode with the same temperature as those emitted from the cathode but with considerably higher density. However, this equilibrium has a certain interest since the difference between this distribution and the actual distribution in any particular volume element in real space dictates the amount of diffusion that takes place in that element. A steady state

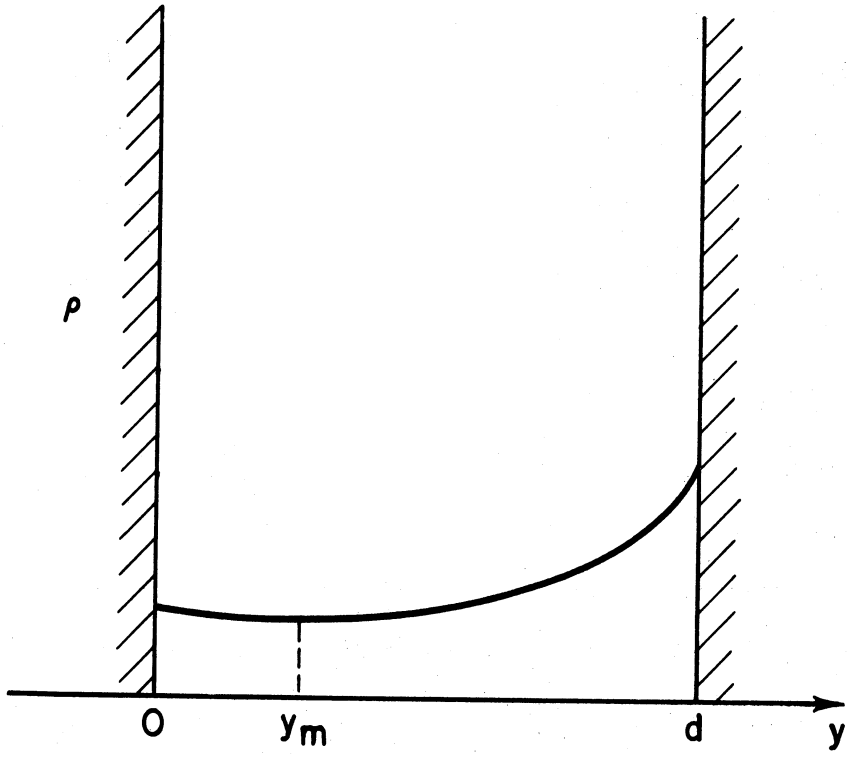

FIG. 5.1
SPACE-CHARGE DISTRIBUTION
AT THERMAL EQUILIBRIUM

is reached when the diffusion into every energy state is equal to the diffusion out of the same energy state. If the minimum point of the curve (y_m) is negative, it would then represent temperature-limited conditions.

If one considers the representation of electron energy states as points and orbits in phase space it is only necessary to consider the space p_x, p_y, and y. (p_x, p_y, and p_z are momentum space.) The energy state of an electron is characterized by its energy and two of the components of its momentum, p_x and p_z, these three quantities being constants of motion, as long as energy and momentum are conserved. On the other hand, the component p_y and the potential energy vary during the motion.

The accessibility criterion is obtained from:

$$2m\,W = p_x^2 + p_{yo}^2 + p_z^2 = (p_x + eBy)^2 + p_y^2 + p_z^2 - 2m\,eE$$

or

$$p_y^2 = p_{yo}^2 + 2m\,eE - e^2B^2y^2 - 2p_x\,eBy$$

where p_y and p_{yo} have to be real quantities.

Fig. 5.2 shows a sketch of the boundary surface between the accessible and inaccessible part of p_x-p_y-y-space. It is, of course, only qualitative since E(y) is not known but related to the space-charge distribution by Poisson's law.

The region accessible from the cathode is the space to the right of the solid line while the region accessible from the anode is to the left of the dashed line. The region inaccessible from the cathode has a shape of a distorted cone with its apex on the axis $p_y = 0$ but in

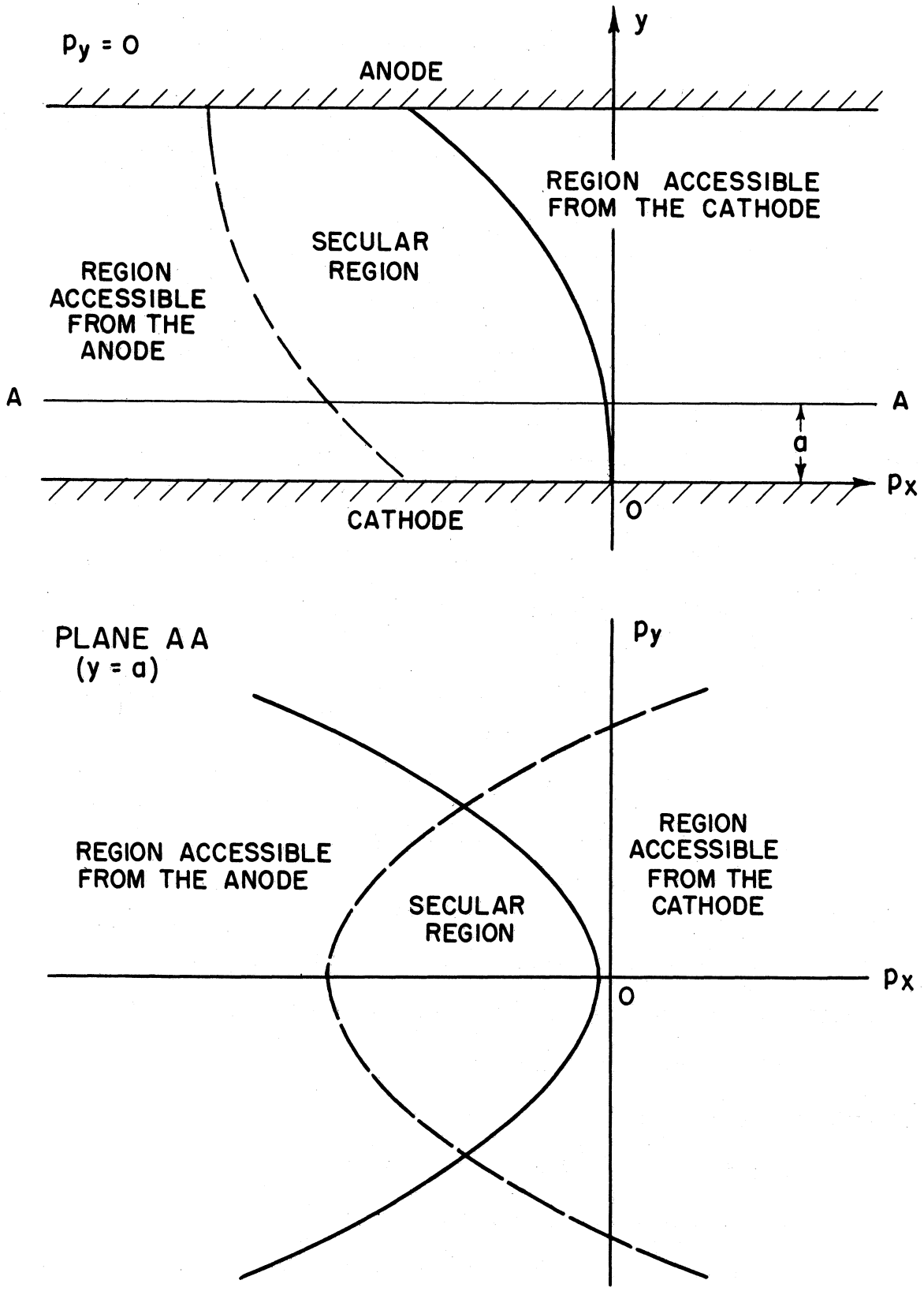

FIG. 5.2
REGIONS IN PHASE SPACE ACCESSIBLE TO ELECTRONS WHOSE ORBITS INTERSECT THE ANODE OR CATHODE PLANE.

general not at $p_x = 0$. The axis $p_y = 0$ to the left of the apex is a generatrix of the surface. It should be pointed out that the fact that the inaccessible region reaches the axis does not mean that electrons with $p_y = 0$ and p_x in this range can not escape from the cathode. They do, but only tangentially to the p_x-p_y-plane.

The boundary for interception of the electrons by the anode is indicated by the dashed line. Any electron to the left of this surface will be removed by impact on the anode. The space-charge density can therefore be considered zero to the left of this boundary except where this region overlaps with the region accessible from the cathode.

The volume between the two boundaries contains all possible energy states whose electron orbits reach neither the anode nor the cathode. This volume is referred to as the secular region since the life of an electron energy state in this region is very long compared with the period of the cyclic motion of the electron. It should be noted that:

1. Only an infinitesimal change in momentum is required for an electron to cross the boundary into this volume.
2. The electron population of this volume will continue to increase until the current flowing to the anode through the opposite boundary equals the current entering the volume from the cathode-accessible region.
3. Whether the discrete electron-electron interaction is weak or strong determines primarily the time required to reach a steady state but not necessarily the final space-charge distribution.

The above is important for it indicates that electron-electron interaction, no matter how weak, is an important factor in determining the space charge distribution and should not be neglected. The effect of the interaction, however weak, is cumulative.

By inspecting the single-stream space-charge distribution described by Brillouin[1] and the double-stream space-charge distribution described by Slater,[2] Page and Adams,[3] and others in phase space it becomes apparent that these distributions are initial conditions only and do not describe a steady state.

Fig. 5.3 shows the Brillouin single-stream distribution in phase space. This is limited to the line AB and within this range is independent of y. At first sight this distribution may appear to be a possible equilibrium state at 0°K temperature. However, it would be strange indeed if all electrons occupied the same point in momentum space, although lower energy states certainly are possible. The above state could possibly be metastable, lacking a process whereby the unoccupied energy states could be populated. However, such a process does exist. The electric field at the edge of the space-charge cloud necessarily fluctuates in magnitude and direction in time and space since the space charge is formed by discrete electrons whose velocity varies with y. A diffusion will therefore take place both out into the unoccupied space and towards the cathode. The energy required for this random motion is supplied by the d-c electric field.

The double-stream distribution is represented by an approximately elliptic line charge in phase space (Fig. 5.4). In real space the space-

1 L. Brillouin, "Electronic Theory of the Plane Magnetron," Advances in Electronics, Vol. 3, p. 85, 1951.

L. Brillouin and F. Bloch, "Electronic Theory of the Cylindrical Magnetron," Advances in Electronics, Vol. 3, p. 145, 1951.

2 J. C. Slater, Microwave Electronics, New York, 1950.

3 L. Page and N. J. Adams, "Space Charge in a Plane Magnetron," Phys. R., Vol. 69, p. 492, May 1946.

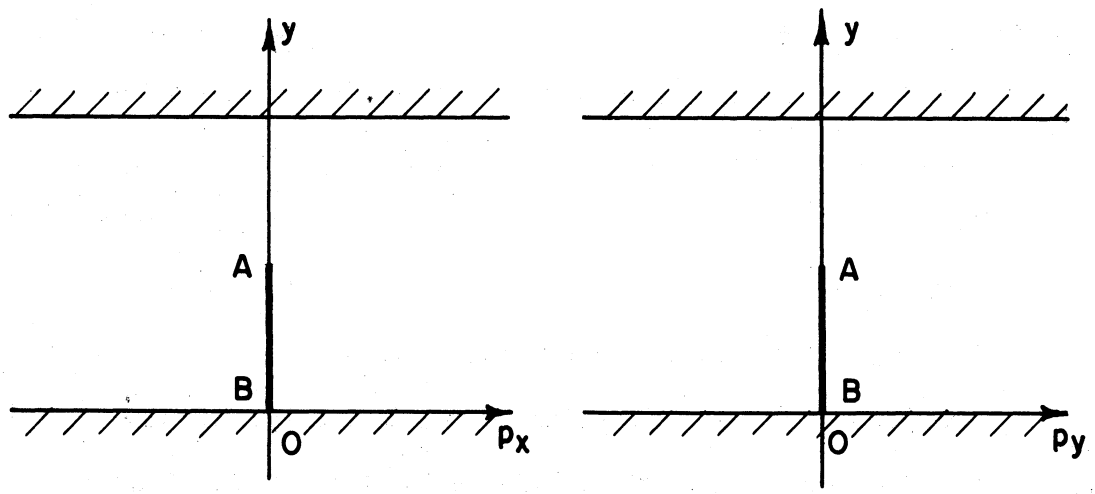

FIG. 5.3
BRILLOUIN DISTRIBUTION IN PHASE SPACE

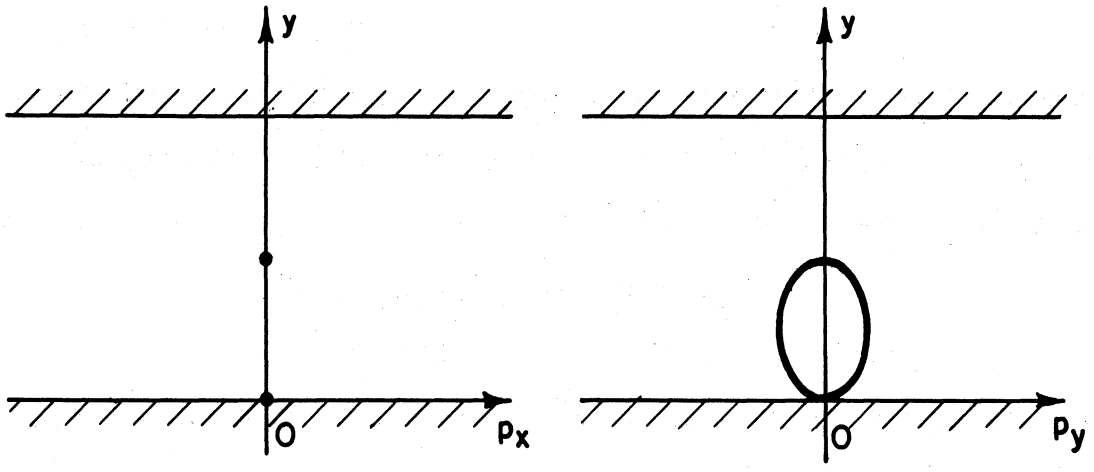

FIG. 5.4
DOUBLE-STREAM DISTRIBUTION IN PHASE SPACE

charge density at the cathode and at the edge of the swarm is infinite; a finite minimum is located at an intermediate plane. This is also at 0°K temperature distribution, since all the electrons have the same energy although occupying a line rather than a point in momentum space. There can be no question in this case about a metastable state since the electron orbits intersect with considerable relative velocity so that exchange of energy and momentum is inevitable.

Twiss[1] has considered the modification in the initial space-charge distribution produced by the initial velocities of the electrons. His solution avoids the discontinuities and singularities of the two distributions mentioned above, but is otherwise subject to the same criticism; it is an initial state but not a steady state.

An attempt was made to arrive at a qualitative understanding of the way in which a steady-state space-charge distribution is reached by considering it as a diffusion problem. Technical Report No. 10 discusses such complicating circumstances as the relationships governing the transfer of momentum between the electrons, the irregular actual distribution density because of the initially abrupt variation at the accessibility boundaries, and the distorted distribution density function caused by increased electron temperature as the electrons diffuse to the higher potential part of the space charge.

Figs. 5.5 and 5.6 present qualitatively the difference between space-charge-limited and temperature-limited distributions in phase space. As in Fig. 5.2 the area to the left of the solid line indicates the region

---

1 R. Q. Twiss, On the Steady-State and Noise Properties of Linear and Cylindrical Magnetrons, Doctoral Thesis, M.I.T., 1949.

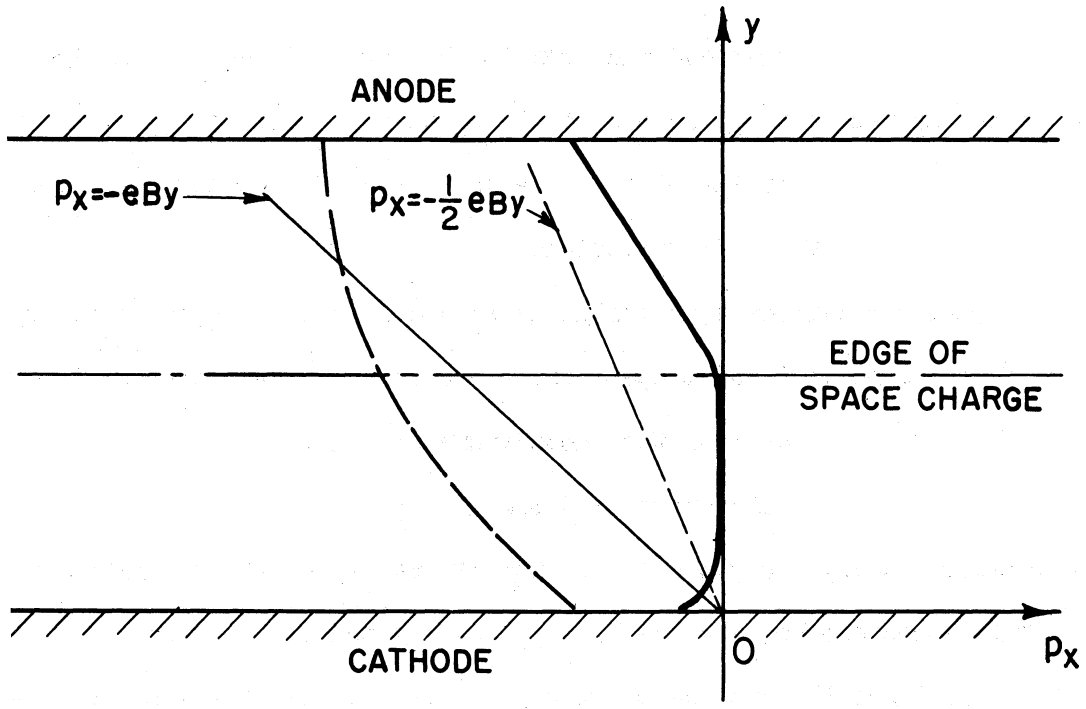

FIG. 5.5
SPACE-CHARGE-LIMITED CONDITIONS

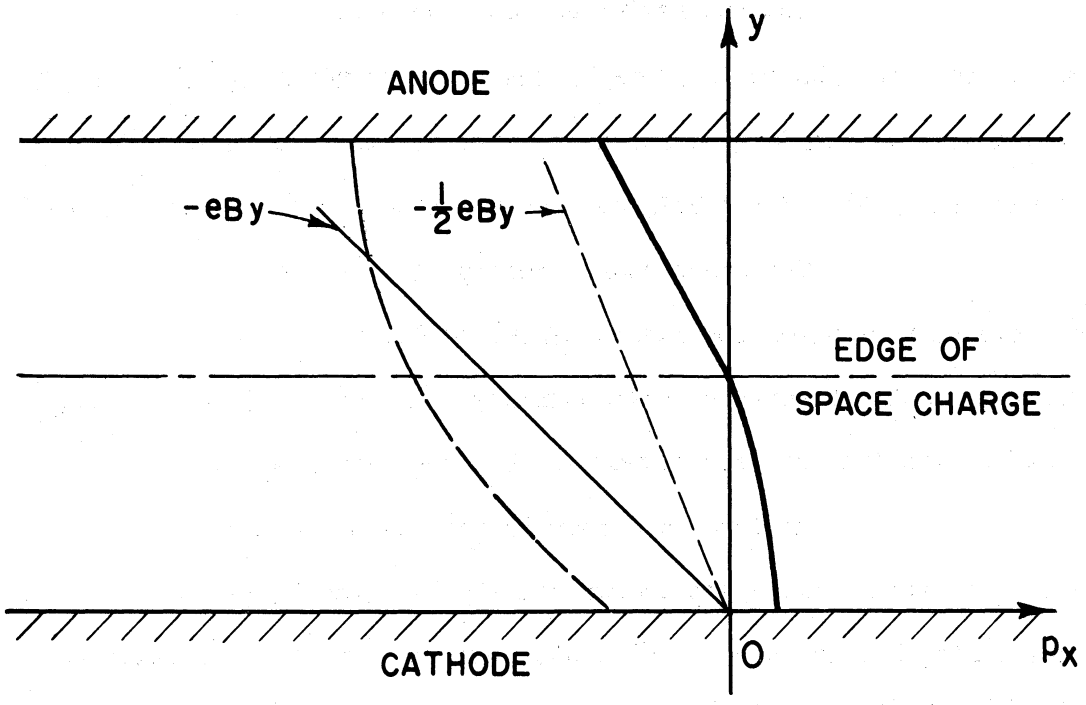

FIG. 5.6
TEMPERATURE-LIMITED CONDITIONS

accessible from the anode and the area to the right of the dotted line indicates the region accessible from the cathode. The lines $p_x = -eBy$ and $p_x = -\frac{1}{2}eBy$ are indicated to serve as a guide for constructing the center of gravity of the distribution.

At the cathode with its large mass and thermal capacity it is natural to assume that the temperature and distribution of the emitted electrons are independent of the temperature and distribution of the returning electrons. The energy and momentum of the electron cloud is not conserved here, therefore the center of gravity of the distribution must fall somewhere between the line $p_x = -eBy$ and $p_x = 0$.

Between the cathode and the potential minimum the inaccessible part of the phase space is likely to be small and not include dense regions of the distribution. The potential and space-charge density then falls off until roughly the Brillouin density is reached.

In real space the region between the potential minimum and the edge of the space charge is probably the most interesting. In phase space the cathode side boundary of the secular volume is probably not much different from that of the Brillouin solution and is likely to run parallel to the y-axis. The space-charge density in the secular volume is less than that required for ideal thermal equilibrium since the net number of electrons entering this boundary from the right should equal the number leaving the left boundary. The space-charge density required for steady-state conditions is closer to the right boundary than to the one on the left. This space-charge density is evidentally very difficult to calculate, but it should be pointed out that it is by no means negligible as far as calculation of space-charge distribution in real space is concerned.

Electrons move into the positive y-direction and gain kinetic energy from the electric field. They also move towards the high energy fringes of a distribution that, if it were complete, would have a much higher space-charge density than at the cathode.

The high-energy electrons will be much closer to the center of gravity of the actual distorted distribution than to the center of gravity of the Maxwell-Boltzmann distribution, therefore the average energy or "temperature" of the actual distribution will be much higher than at the cathode.

The mathematical difficulties discourage any attempt to predict numerically the space-charge distribution in a cutoff magnetron. Experimental methods must therefore be used. The work at the University of Michigan discussed elsewhere in this report being carried out by Mr. W. Peterson on the "trajectron" shows great promise as a method for determining the space-charge distribution. The Columbia Radiation Laboratory is also attacking this problem experimentally employing a beam of helium ions.

III. EXPERIMENTAL RESULTS

6. Model 9 Low-Power Insertion Magnetron (J. S. Needle)

The Model 9 magnetron consists of a short hermetically-sealed section of coaxial transmission line which contains a multi-anode structure consisting of six-equally-spaced vanes extending radially from the inner wall of an outer coaxial cylinder into six longitudinal slots in an inner coaxial cylinder. The cathode is located symmetrically within the inner coaxial cylinder at the position of the multi-anode structure. This sealed-off tube is used to excite a TEM mode in an external coaxial circuit. An assembly drawing for one model of the insertion magnetron is given in the Appendix (Dwg. B10,009 B).

Design parameters for the insertion magnetron are as follows:

λ = 10 cm.

$n\lambda$ = 60

$n = \frac{N}{2} = 6$

r_a = 0.317 cm

r_c = 0.190 cm

$\frac{r_c}{r_a}$ = 0.6

E_o = 280 volts

E = 1400 volts

B_o = 554 gauss

B = 1662 gauss

$\frac{B}{B_o}$ = 3

The experimental program for the insertion magnetron was carried out with the following objectives in mind.

a. To determine the feasibility of operating the insertion tube as a mechanically-tunable magnetron over a wide range of frequencies.

b. To find out whether or not wide range voltage tuning could be attained with this tube and its associated circuitry, and to determine the limiting factors in this type of operation.

c. To determine the effect of loading on upper-mode-boundary current and on frequency pushing.

d. To obtain design experience for the construction of higher-power and higher-frequency ceramic seal tubes of similar geometry.

The presentation of the experimental results is divided into three parts; namely, high Q, intermediate Q, and low Q operation. The Q referred to here is the external Q which is defined as follows:

$$Q_{ext} = 2\pi \frac{\text{energy stored in circuit}}{\text{energy dissipated in the load per cycle}} . \qquad (6.1)$$

In practice it is found that an order of magnitude relation between the space-charge effects on the frequency of oscillation is given by

$$\frac{\omega - \omega_o}{\omega_o} \cong \frac{1}{2Q_L} \qquad (6.2)$$

where Q_L is the loaded Q of the circuit. Q_L is defined by the relation

$$Q_L = 2\pi \frac{\text{energy stored in circuit}}{\text{energy dissipated in the load and cavity per cycle}} . \qquad (6.3)$$

The relation between the external Q and the loaded Q is given by

$$\frac{1}{Q_{ext}} = \frac{1}{Q_L} - \frac{1}{Q_o} \qquad (6.4)$$

where Q_o is the internal Q defined as follows:

$$Q_o = 2\pi \frac{\text{energy stored in circuit}}{\text{energy dissipated in the cavity per cycle}} . \qquad (6.5)$$

In the material which follows we have made the tacit assumption that

$$Q_o > Q_L \quad \text{and} \quad Q_{ext} = Q_L \ , \tag{6.6}$$

for both the high and intermediate-Q regions of operation. The error rising from this assumption is not serious since Eq 6.2 is an order of magnitude relation.

We can now state the three ranges of external Q in terms of the space-charge effects on frequency as follows:

High Q_{ext} -- less than 1/28 frequency pushing,

Intermediate Q_{ext} -- between 1/2% and 5% frequency pushing,

Low Q_{ext} -- greater than 5% frequency pushing.

The terms high-Q and intermediate Q operation, as employed here, imply that the frequency of magnetron operation is determined primarily by the properties of the circuit. The term low Q operation, on the other hand, implies that the frequency of magnetron operation is substantially independent of the circuit and depends primarily on the anode potential and magnetic field. These two types of magneton operation appear to overlap at values of loaded Q of the order of 5 to 10.

The coaxial cavities employed for high Q operation of the insertion magnetron have been designated No. 1 and No.3, and are depicted in the Appendix, Dwgs. B2050 and B2053, respectively. Cavity No. 1 was subsequently modified to provide movable shorting slugs for tuning. In addition, a series of tapped holes were provided for facilitating changes in the coupling probe position of the cavity.

The first operating test on the insertion magnetron was made using tube No. 39 in cavity No. 1, which was non-tunable at the time of this test. The tube was operated with a 15 microsecond pulse having a repetition rate of 60 pulses per second. Oscillation was observed at 10.7 cm, which corresponds to the 1/2-wavelength TEM coaxial-cavity mode. Oscillation was also observed at approximately 30 cm corresponding to the 3/2-wavelength coaxial mode. The anode segments for both of the above cavity modes operate in the π-mode. The anode potential corresponding to the 10.7 cm mode was approximately 900 volts with a magnetic flux density of 1280 gauss.

An experiment was performed to determine the minimum wavelength attainable as well as a tuning curve for the tunable version of cavity No. 1. In this experiment the Model 9B, No. 43 (oxide-coated cathode) was operated under pulsed conditions. The conditions for this experiment are listed below.

I_{fil} = 2.25 amperes.

B = 1200 gauss.

ℓ_1 = 0.2 cm (distance of output probe from one tuner slug).

ℓ_2 = 1.2 cm (distance from right edge of vanes to output probe).

ℓ_3 = (variable distance from movable tuner slug face to left edge of vanes).

The results of this experiment are given in Fig. 6.1 together with a theoretical tuning curve.[1] The agreement between the calculated and experimental plots should not necessarily be considered as a verification of the theory, since the computations do not include the effects

---

1 See J. S. Needle, "The Insertion Magnetron: A New External Cavity Magnetron for Low-Power Electronically-Tunable Operation in the 10 to 20-cm Wavelength Range," Technical Report No. 11, Electron Tube Laboratory, University of Michigan, Ann Arbor, August 1951.

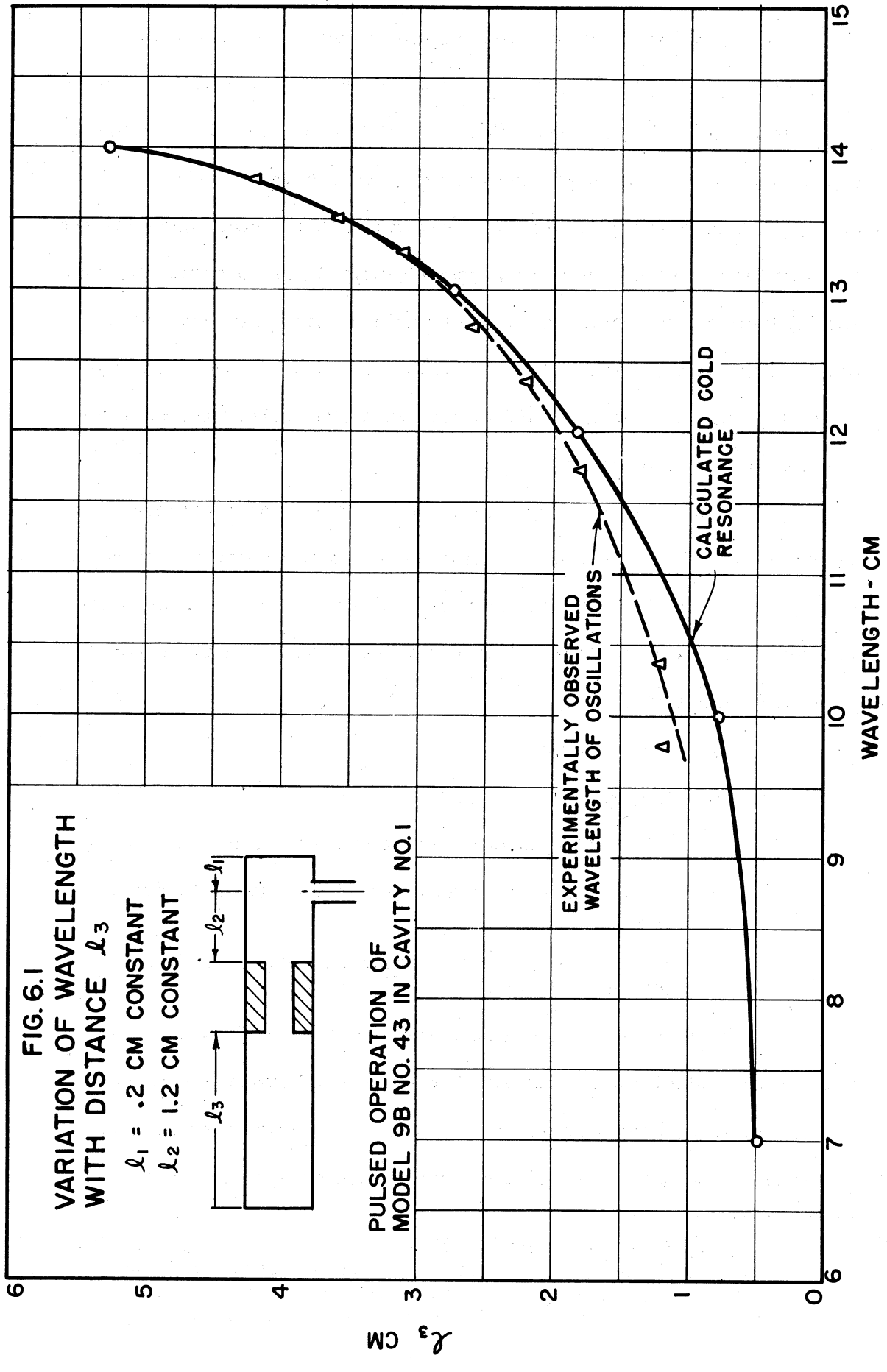
FIG. 6.1
VARIATION OF WAVELENGTH WITH DISTANCE ℓ_3
ℓ_1 = .2 CM CONSTANT
ℓ_2 = 1.2 CM CONSTANT
ℓ_3
ℓ_2
ℓ_1
PULSED OPERATION OF MODEL 9B NO. 43 IN CAVITY NO. 1
EXPERIMENTALLY OBSERVED WAVELENGTH OF OSCILLATIONS
CALCULATED COLD RESONANCE
λ_3 CM
WAVELENGTH - CM
0
1
2
3
4
5
6
7
8
9
10
11
12
13
14
15

of the cathode circuit or the glass seals. However, it is reasonable to conclude that the general shape of the experimental tuning curve is predictable from the theory for this unsymmetrical case.

Cavity No. 3 was constructed in order to obtain further information regarding the mechanical tunability of the insertion magnetron. One of the important aspects of wide-range tuning is the degree of variation of upper-mode-boundary current with frequency. Figs. 6.2 and 6.3 give the results of two experiments which were conducted to determine the upper-mode-boundary current as a function of tuner position. The conditions for this experiment using the same "ℓ" notations as in the previous case were:

Pulsed operation of Model 9B No. 43

ℓ_1 = 0.318 cm

ℓ_2 = 1.082 cm

ℓ_3 = variable

I_{fil} = 2.0 amps.

B = 1650 gauss.

The significant results of this experiment are apparent from Figs. 6.2 and 6.3. Here we observe that when an external cathode bypass causes an increase in operating wavelength, the upper-mode-boundary current is reduced: whereas, if this shift is toward lower wavelengths, the upper-mode-boundary current is increased with respect to that obtained in the absence of the external cathode bypass. It is important to realize that the cathode circuit consists of a section of coaxial transmission line inside the evacuated envelope in addition to any external circuit components. The foregoing results demonstrate the feasibility of operating the insertion magnetron in a mechanically-tunable

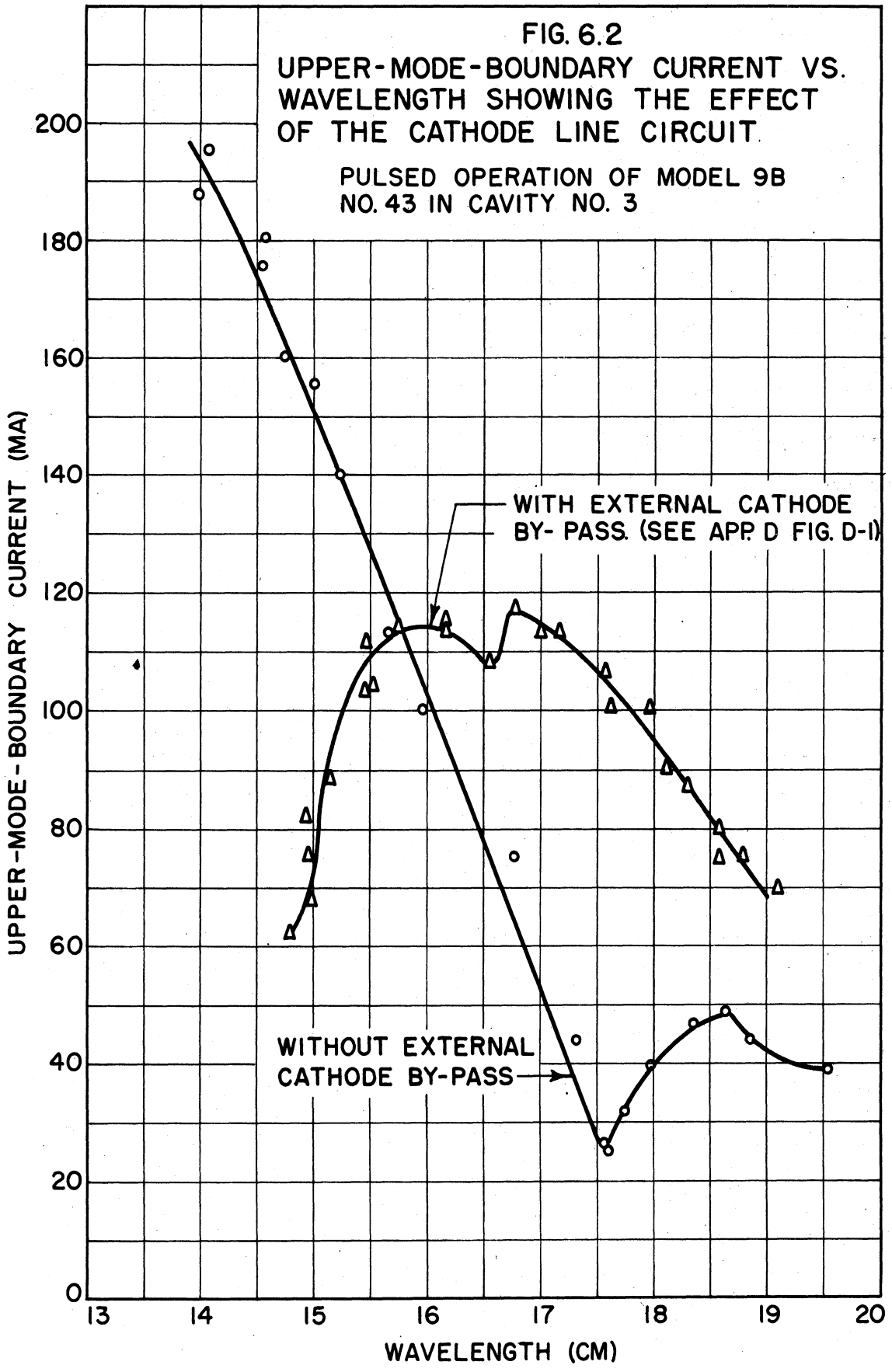
FIG. 6.2
UPPER-MODE-BOUNDARY CURRENT VS. WAVELENGTH SHOWING THE EFFECT OF THE CATHODE LINE CIRCUIT.
PULSED OPERATION OF MODEL 9B NO. 43 IN CAVITY NO. 3
WITH EXTERNAL CATHODE BY-PASS. (SEE APP. D FIG. D-1)
WITHOUT EXTERNAL CATHODE BY-PASS
UPPER-MODE-BOUNDARY CURRENT (MA)
WAVELENGTH (CM)
0
20
40
60
80
100
120
140
160
180
200
13
14
15
16
17
18
19
20

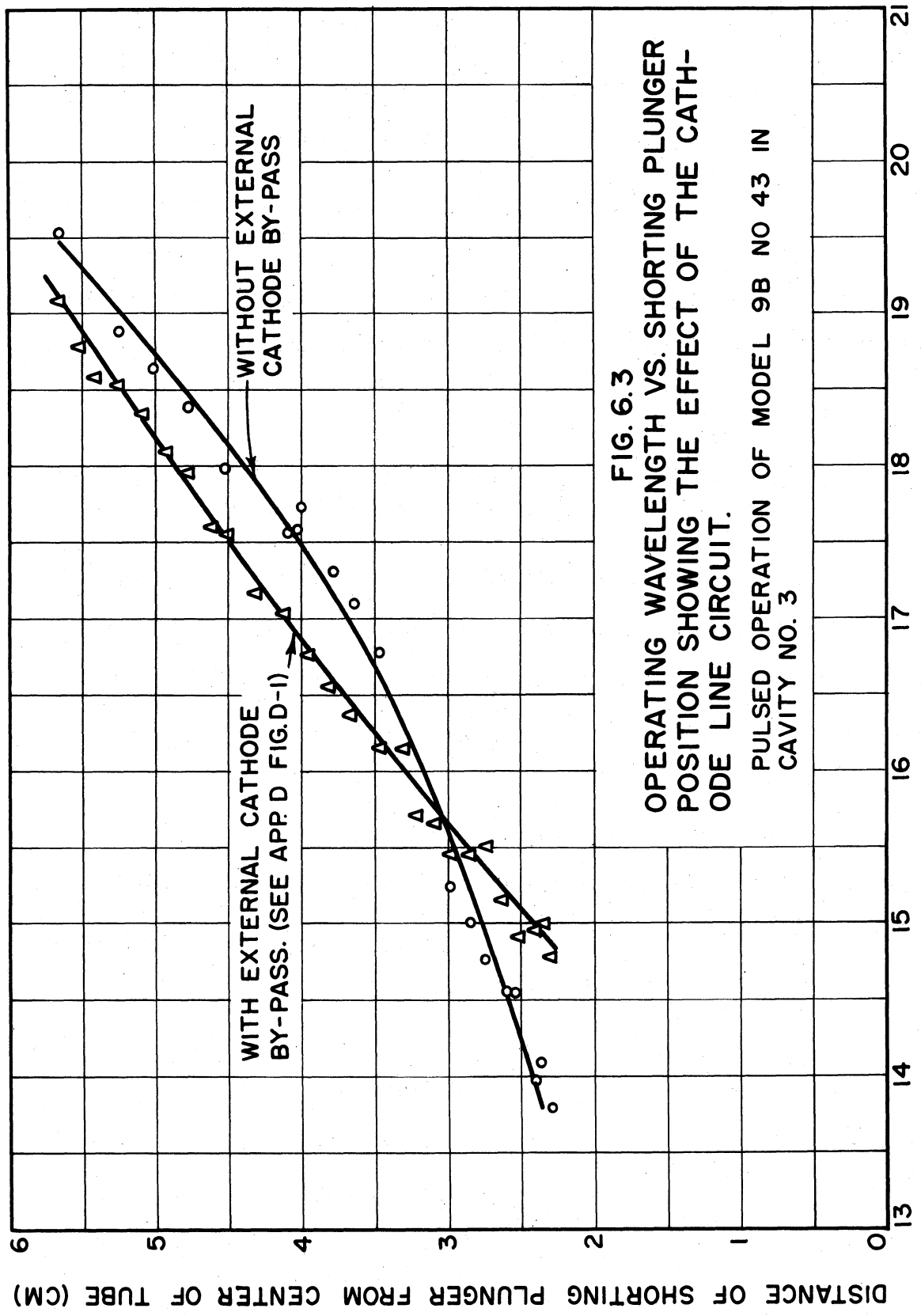

FIG. 6.3
OPERATING WAVELENGTH VS. SHORTING PLUNGER POSITION SHOWING THE EFFECT OF THE CATHODE LINE CIRCUIT.

cavity over a wide wavelength range with a reasonable upper-mode-boundary current. The conditions in this experiment were not necessarily those which would result in optimum upper-mode-boundary current for a given bandwidth. It should therefore be possible to improve the mode boundary versus bandwidth characteristics by further study of cathode-circuit effects.

The c-w power output available from the insertion structure has been as high as three watts with high Q operation. The following data are typical for high Q, c-w performance.

E_b (volts)	I_b (ma.)	I_{fil} (amps.)	B (gauss)	λ (cm)	P_o (watts)
800	20	2.0	1770	20.090	3.0

This information was obtained using the Model 9A No. 39 tube with the arrangement of apparatus shown in Fig. 6.4. The shorted-stub tuner was adjusted to obtain maximum power output. Observation of the signal on a spectrum analyzer indicated a noise level approximately 20 db below the signal level.

Model 9C No. 48 (see Appendix, Dwg. B10,009C) was pulse-tested in cavity No. 3. This tube employs an oxide-coated cathode and may be used with an external cathode bypass. All attempts to obtain tunable output with this tube and cavity failed. Very low power was detected at a wavelenth near 7 cm irrespective of the position of the movable short. This is indicative of resonance in the vane-mode oscillation. The term "vane mode" signifies a mode of oscillation characteristic of the vane-type magnetron and is encountered with the vane-and-bar geometry when the phase difference between r-f potentials of adjacent vane-anode segment

is π-radians. This is not the only phase difference which is associated with the vane magnetron type of operation, but it is the most common one. Within the limits imposed by this tube structure, changing the vane-mode resonance wavelength can be accomplished by changing the radial length of the vanes or the angular displacement between vanes.

6.1. Intermediate Q Operation

An external circuit was designed for low Q operation, but was modified to perform the following experiment, in which the external Q may be varied from approximately 10 to 100. An assembly drawing of cavity No. 2 is given in the Appendix, Dwg. B2052.

A sketch showing the modified version of cavity No. 2, employed in the following experiment, is shown in Fig. 6.4. Listed below are the conditions of the experiment.

Model 9A, No. 39 Tube

Pulsed operation.

Wavelength measured at both the high and low current ends of the volt-ampere characteristic for each position "d" of the tunable shorting stub.

Upper-mode-boundary current measured for each position "d" of the tunable shorting stub.

I_{fil} = 2.15 amperes -- constant.

B = 1850 gauss -- constant.

Note: This insertion tube uses an oxide-coated cathode. A cathode-line choke and bypass is contained inside the vacuum envelope.

Fig. 6.5 shows the results of this experiment. It is interesting to observe that the pushing (increase of frequency with increase in plate

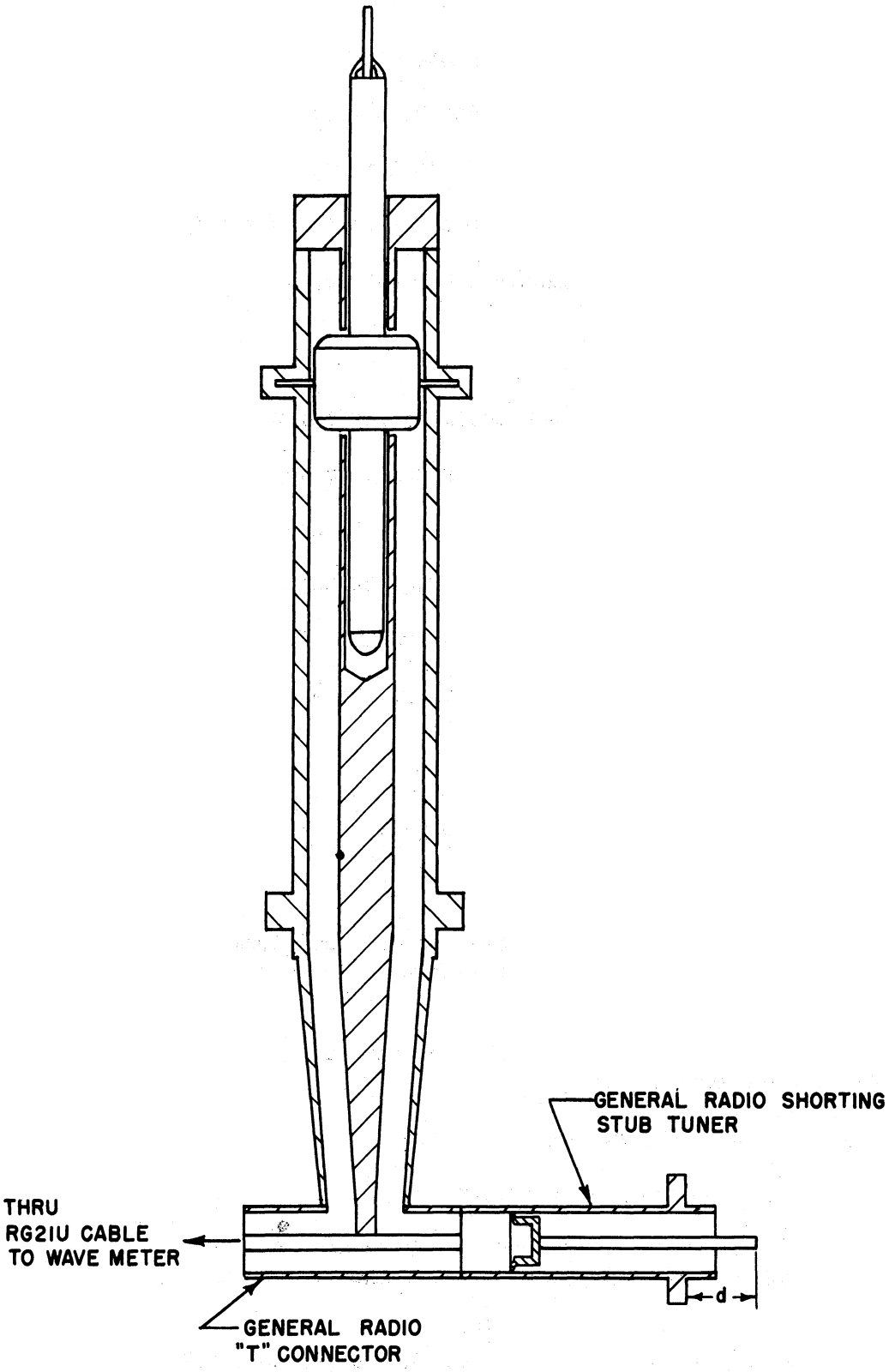

FIG. 6.4
ARRANGEMENT USED TO STUDY THE EFFECT OF THE LOAD ON UPPER-MODE-BOUNDARY CURRENT AND FREQUENCY PUSHING.

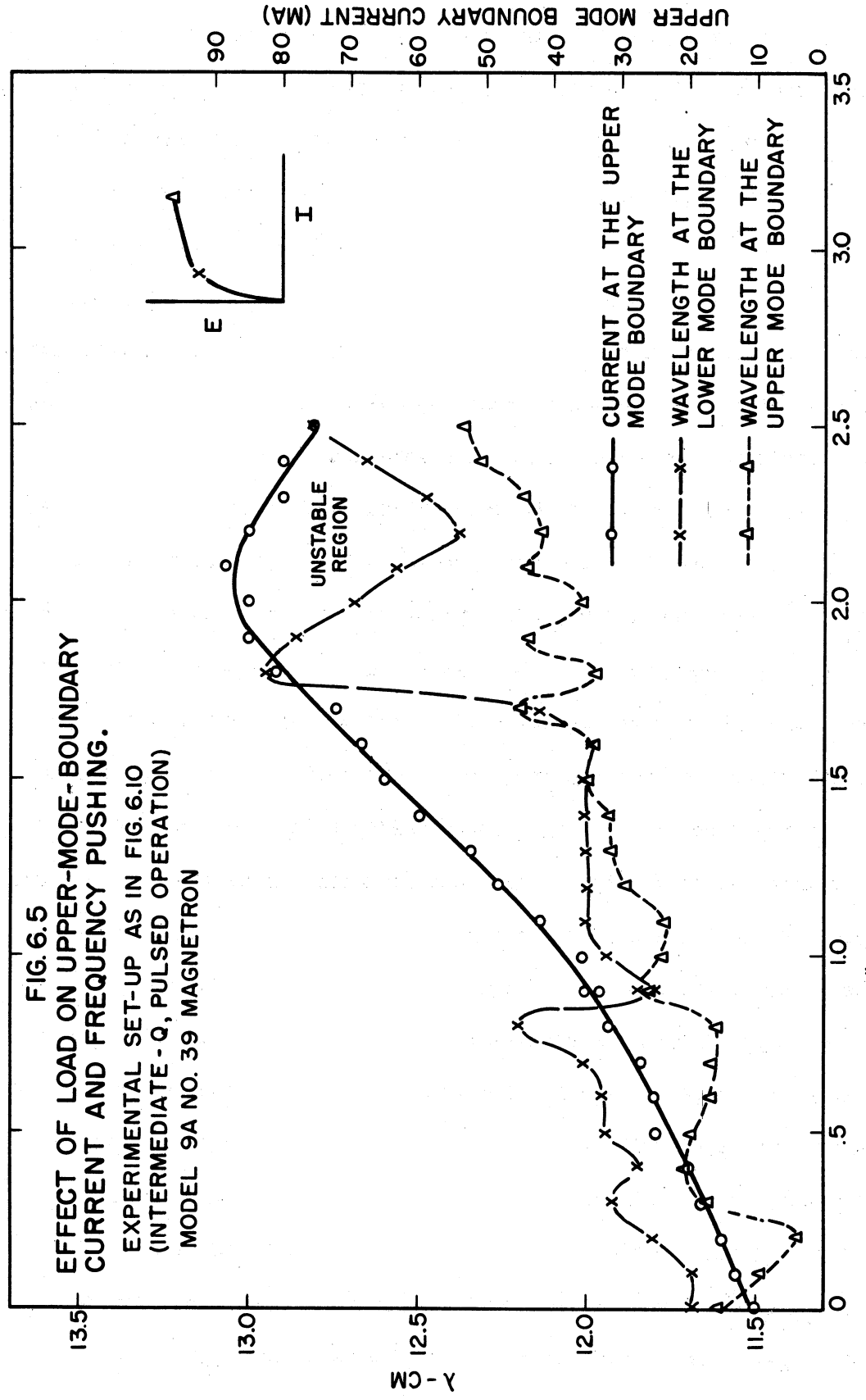
FIG. 6.5
EFFECT OF LOAD ON UPPER-MODE-BOUNDARY CURRENT AND FREQUENCY PUSHING.
EXPERIMENTAL SET-UP AS IN FIG. 6.10 (INTERMEDIATE-Q, PULSED OPERATION)
MODEL 9A NO. 39 MAGNETRON
λ - CM
"d" SHORTING STUB TUNER POSITION (CM)
UPPER MODE BOUNDARY CURRENT (MA)
CURRENT AT THE UPPER MODE BOUNDARY
WAVELENGTH AT THE LOWER MODE BOUNDARY
WAVELENGTH AT THE UPPER MODE BOUNDARY
UNSTABLE REGION
E
I

current), is positive for "d" less than 0.9 cm, negative at 0.9 cm, positive from "d" = 0.9 cm to 1.5 cm, and zero for "d" = 1.5 to 1.6 cm.

Calculations of the shunt susceptance and shunt conductance between adjacent anode segments as a function of wavelength were made for some of the values of "d" used in the experiment above. These calculations are based on the assumption of a lossless cavity and do not take cathode-line effects into account. The output circuit is assumed to be terminated in its characteristic impedance, i.e., 50 ohms. Values used for the vane-to-bar capacitance, and vane inductance were 2.0 $\mu\mu$f and 100 $\mu\mu$h, respectively. The results of the calculations are shown graphically in Fig. 6.6. If the wavelengths corresponding to the computed values of zero shunt susceptance are plotted against the distance "d," one obtains the solid curve shown in Fig. 6.7a. It is interesting to note that the computed curve is in close agreement with the average of the curve for wavelength versus "d" for the maximum current readings. The variations present in the experimental curve could easily be the result of an improperly matched, long output line. Assuming this to be true, we observe upon study of both the computed shunt susceptance curves in Fig. 6.6 and the experimental results in Fig. 6.5, that the tube reaches the wavelength corresponding to the maximum current when the circuit susceptance tends to become capacitive. Furthermore, if the magnetron is oscillating at some wavelength, say 11.8 cm, corresponding to the region of negative pushing, a small increase in "d" tends to make the circuit capacitive for this wavelength. This can be seen with the aid of Fig. 6.6. It appears, from these observations, that the magnetron "prefers" to operate with the circuit inductive and therefore changes to a longer

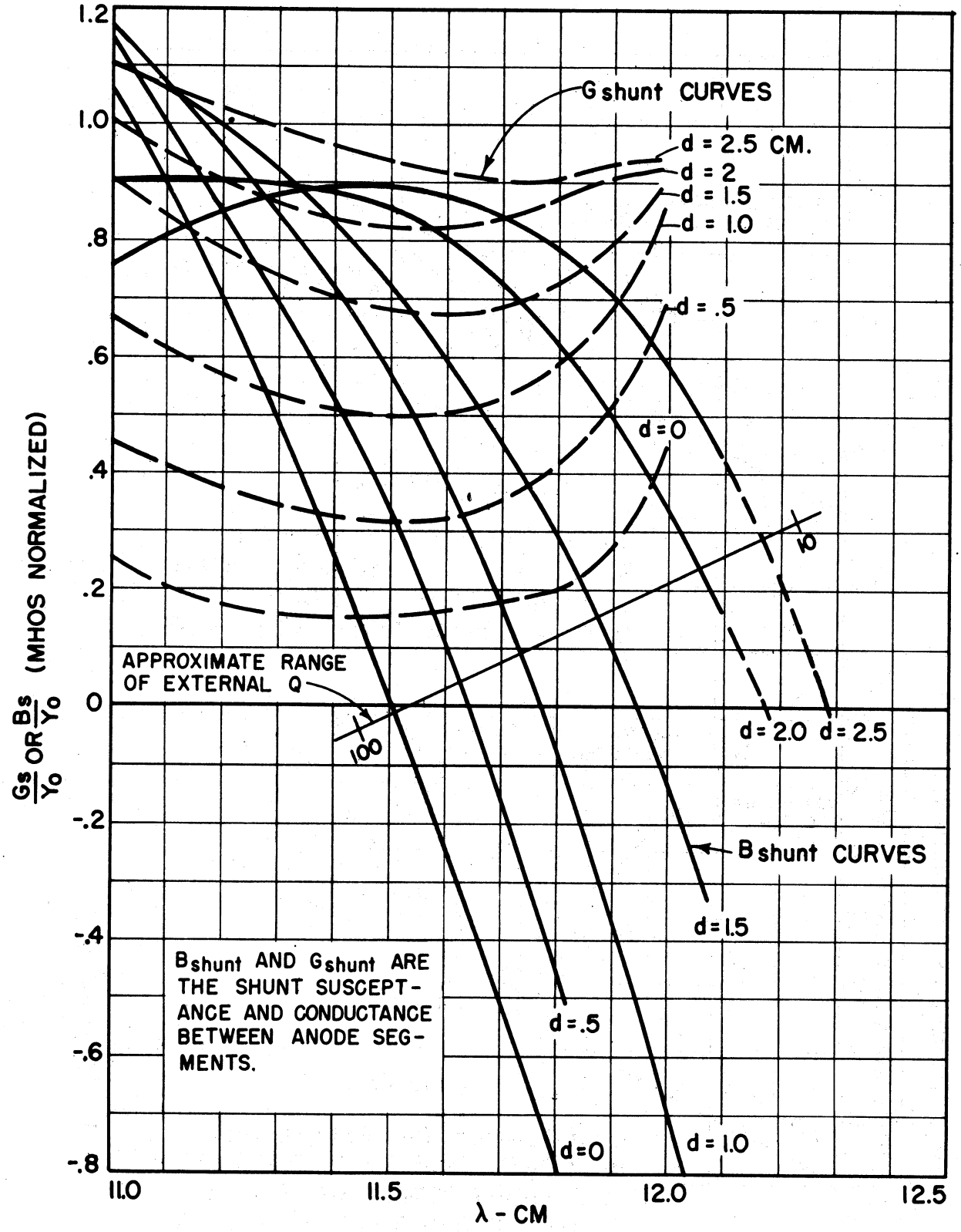

FIG. 6.6

NORMALIZED G_{shunt} AND B_{shunt} VS. WAVELENGTH WITH "d" AS A PARAMETER FOR CAVITY NO. 2 WITH REACTANCE TUNER. Y_o = .02 MHOS

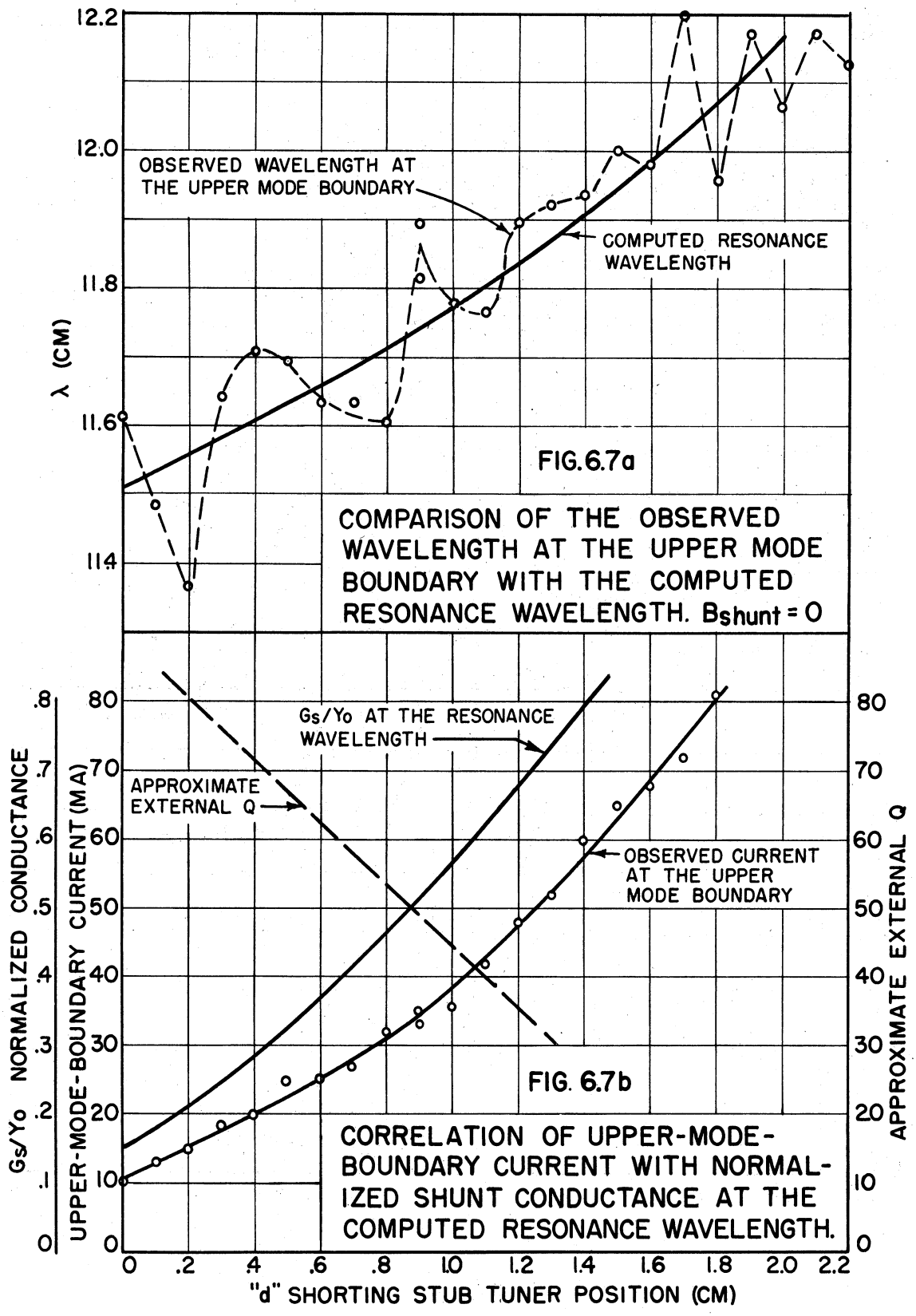
12.2
12.0
11.8
11.6
11.4
λ (CM)
OBSERVED WAVELENGTH AT THE UPPER MODE BOUNDARY
COMPUTED RESONANCE WAVELENGTH
FIG. 6.7a
COMPARISON OF THE OBSERVED WAVELENGTH AT THE UPPER MODE BOUNDARY WITH THE COMPUTED RESONANCE WAVELENGTH. Bshunt = 0
Gs/Yo AT THE RESONANCE WAVELENGTH
APPROXIMATE EXTERNAL Q
OBSERVED CURRENT AT THE UPPER MODE BOUNDARY
FIG. 6.7b
CORRELATION OF UPPER-MODE-BOUNDARY CURRENT WITH NORMALIZED SHUNT CONDUCTANCE AT THE COMPUTED RESONANCE WAVELENGTH.
Gs/Yo NORMALIZED CONDUCTANCE
UPPER-MODE-BOUNDARY CURRENT (MA)
APPROXIMATE EXTERNAL Q
0 .1 .2 .3 .4 .5 .6 .7 .8
0 10 20 30 40 50 60 70 80
0 .2 .4 .6 .8 1.0 1.2 1.4 1.6 1.8 2.0 2.2
"d" SHORTING STUB TUNER POSITION (CM)

wavelength at which the inductive susceptance predominates. It is perhaps premature to conclude that the above speculation is correct without further experimental and theoretical study.

One further point should be mentioned with regard to the experimental data presented above. If one plots the computed circuit conductance for the wavelengths and "d" positions corresponding to the point of upper-mode-boundary current the results indicate a direct correlation between this current and the computed shunt conductance. This is readily apparent from Fig. 6.7b. This correlation is in contradiction to that which is generally observed for magnetron oscillators having Q's of the order of 10 or larger. One possible explanation of the correlation found here may be inferred from the computed curves given in Fig. 6.5. A study of the manner in which the conductance varies with wavelength along a constant "d" line shows that the magnitude of the conductance decreases as the wavelength of operation decreases toward the upper-mode-boundary wavelength. This differs from the more generally observed cases in which the conductance is relatively constant over the range of frequency pushing. Hence if one considers the magnetron as a constant-current generator operating into a constant conductance, the r-f voltage across the tank and the r-f power output would increase rapidly as the resonance frequency of the tank circuit is approached. If, however, the circuit conductance decreases with an increase in frequency, the power output would tend to rise more slowly than it would for the constant-conductance load. This would take place in spite of a rapid rise in r-f voltage which would in turn result in stronger (radial field) phase-focussing action. Under these conditions, the radial r-f field phase-focussing action may be sufficient to prevent loss of

synchronism (between the space-charge spokes and the r-f potential travelling wave) until the region is reached in which the conductance no longer decreases with increasing frequency.

6.2. Low Q Magnetron Operation

The first steps taken in attempting to attain low Q voltage-tunable operation were directed toward the reduction of the Q of the circuits by means of lossy materials. Uskon cloth,* steel wool, and a sand-and-carbon mixture were some of the materials used in the initial phases of the investigation. All of these lossy materials were successful insofar as it was possible to attain a voltage-tunable signal from the insertion structure by using them. A typical arrangement employing a sand-and-carbon mixture as an absorption medium is shown in Fig. 6.8. With this arrangement it was possible to obtain c-w ouput from 11.8 to 20.3 cm for the Model 9B No. 43 magnetron. The magnetic field used was 1200 gauss and the filament current was 1.67 amperes. Anode voltages were in the neighborhood of 1000 volts with plate currents reaching a maximum of 6 ma at the low wavelength end of the voltage-tunable range. No extensive data were taken with this apparatus primarily because the output as viewed on a spectrum analyzer indicated a tunable, broad, noisy signal with a bandwidth greater than the maximum bandwidth of the analyzer, which in this case was 40 megacycles. The power output of the broad noise signal varied considerably over the tuning range, and was estimated to be of the order of 100 milliwatts at most.

Cavity No. 2 was designed to permit low-Q operation with a minimum of unusable absorbed power. The output from this coaxial circuit

---

* This is cloth impregnated with carbon.

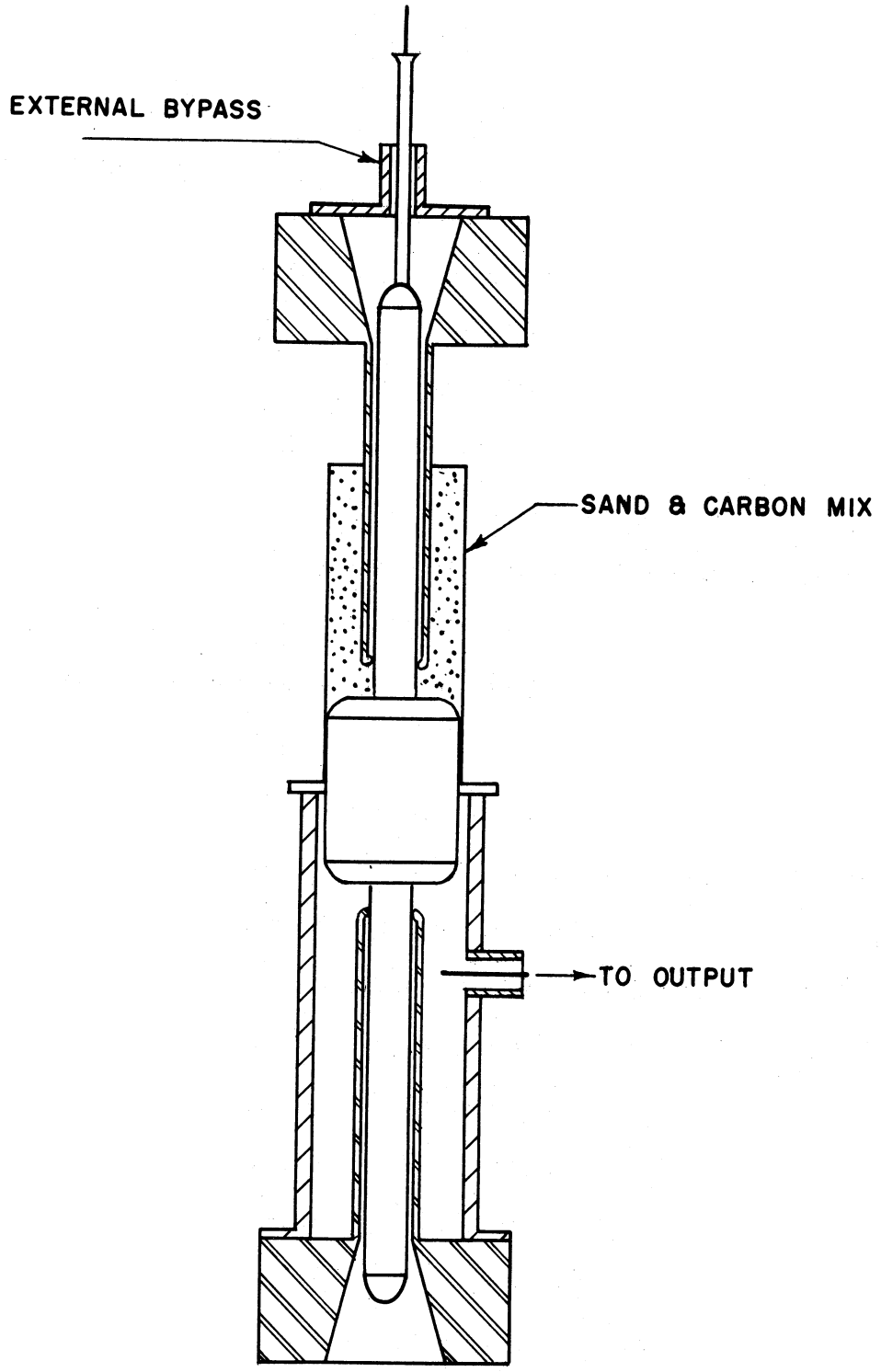

FIG. 6.8

SKETCH OF EXPERIMENTAL SET UP FOR LOW Q OPERATION USING CAVITY NO. 1

MODEL 9B NO.43 MAGNETRON

was initially terminated in its characteristic impedance of 50 ohms. Under this condition the external Q of the system, which is given approximately by $\omega_o C_A/G_{sh}$, is of the order of one or two. Although low Q operation was attained with this direct termination into 50 ohms, the power output was too small to be measured accurately on a power bridge. It was possible, however, to measure relative output and wavelength by using a high-gain amplifier to amplify the output from a crystal detector.

The modifications made on cavity No. 2 to increase the power output are shown in Fig. 6.9. The purpose of the carbon iris was to increase the resistive component of the impedance "seen" by the electrons. This was only partially accomplished, since the effect of the iris was also reactive. The aquadag coating indicated inside the upper portion of the coaxial structure was employed to decrease the Q of this section of the line. Calculations assuming a short circuit at the upper face of the carbon iris gave a cavity resonance wavelength of 13.5 cm. The arrangements shown in Fig. 6.9 was employed in order to obtain the volt-ampere characteristics and power output for two different filament temperatures. The experimental results are given in Fig. 6.10 for the Model 9A No. 39 magnetron. Here the magnetic flux density was 1760 gauss for both sets of curves. The signal output as viewed on a spectrum analyzer was still broad and noisy, so that frequency measurements are not too meaningful. However, it is interesting to note that the frequency of the broad noise signal decreased with increasing cathode temperature. The sharp peak in power output is directly related to the resonant properties of the coaxial circuit employed here.

A volt-ampere characteristic for the Model 9B No. 43 insertion tube is shown in Fig. 6.11. The external circuit employed to obtain this

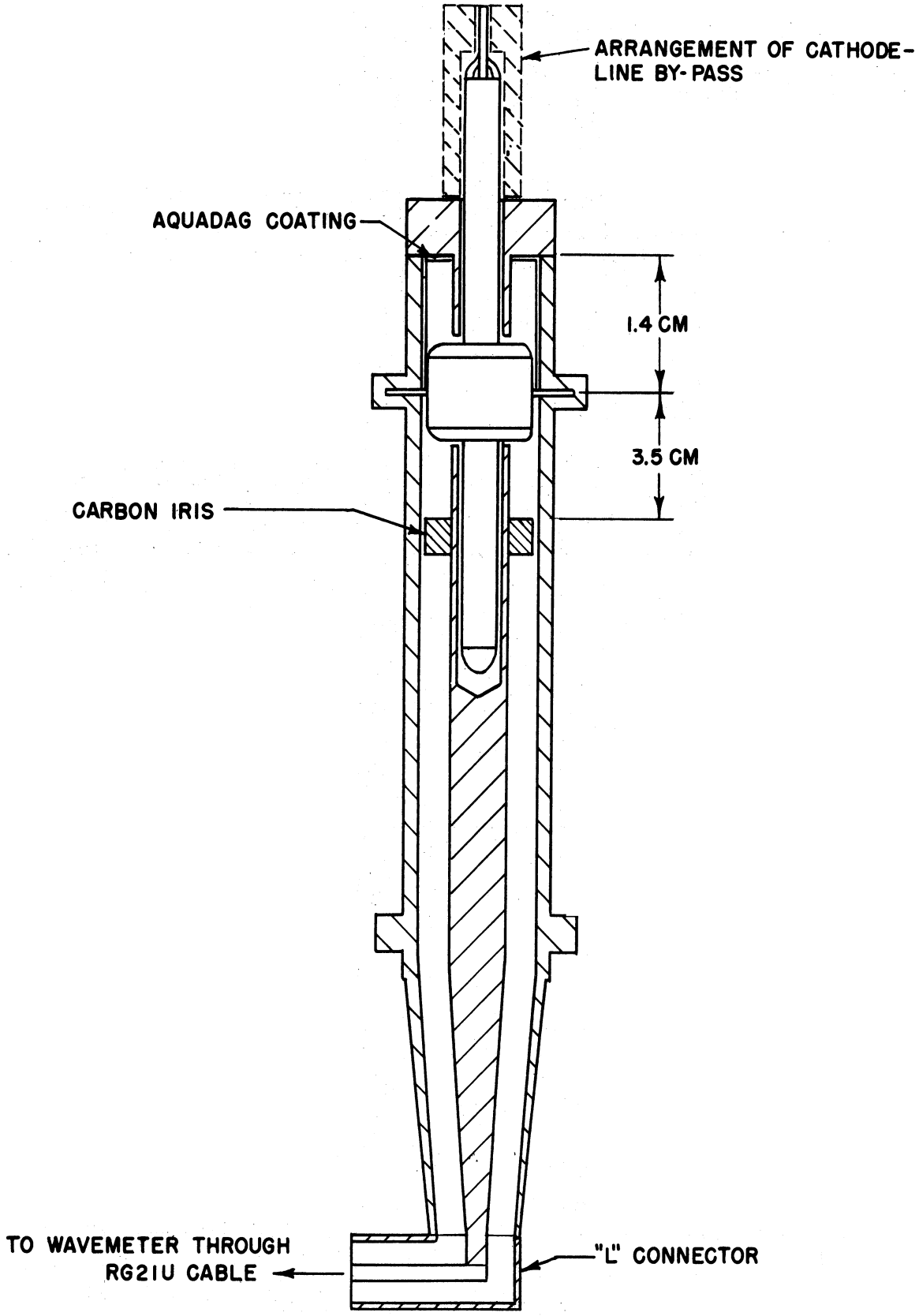

FIG. 6.9
SKETCH OF EXPERIMENTAL SET UP FOR LOW Q
OPERATION IN CAVITY NO. 2

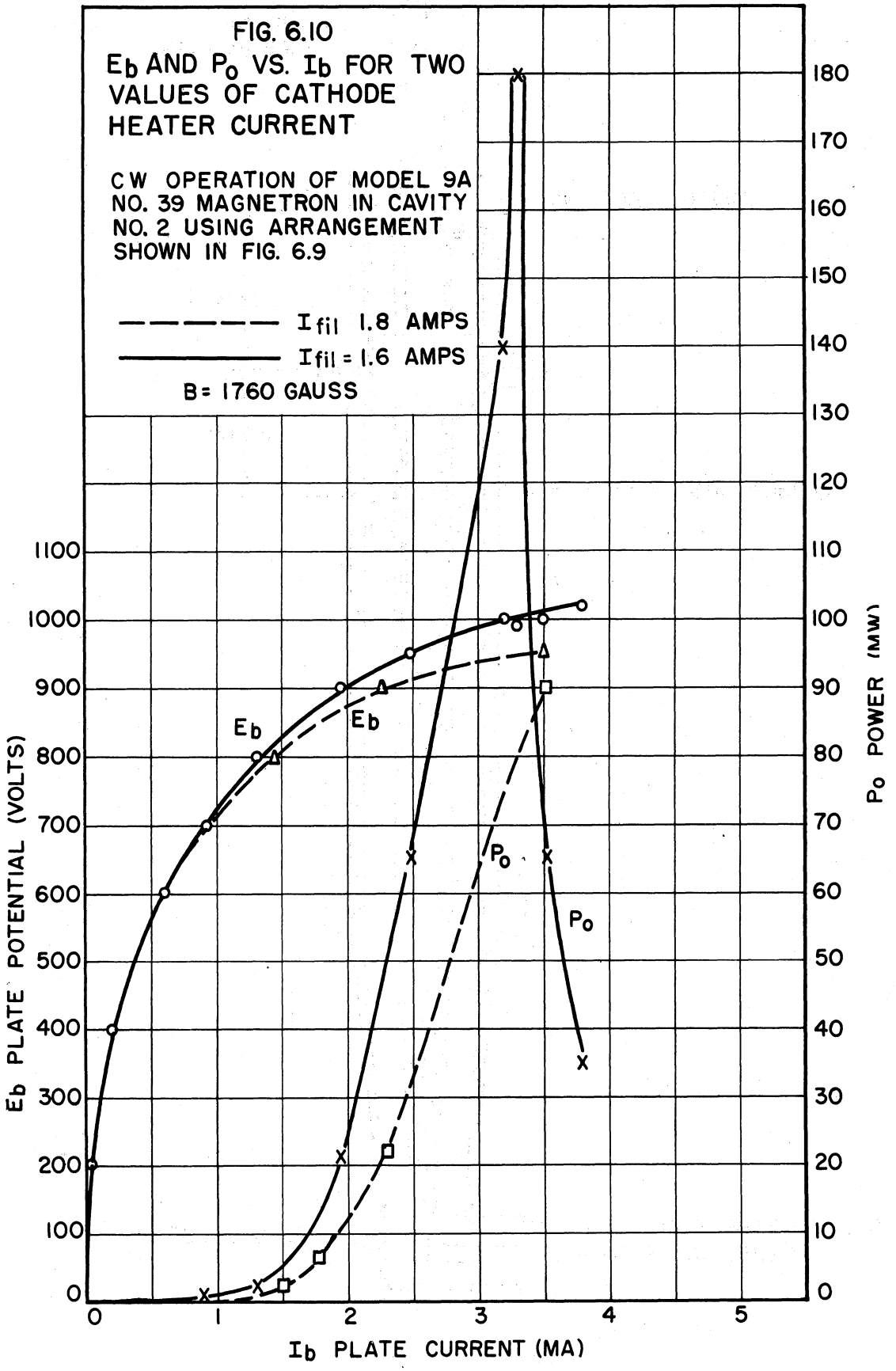
FIG. 6.10
Eb AND Po VS. Ib FOR TWO VALUES OF CATHODE HEATER CURRENT
CW OPERATION OF MODEL 9A NO. 39 MAGNETRON IN CAVITY NO. 2 USING ARRANGEMENT SHOWN IN FIG. 6.9
Ifil 1.8 AMPS
Ifil = 1.6 AMPS
B = 1760 GAUSS
Eb
Eb
Po
Po
Eb PLATE POTENTIAL (VOLTS)
Po POWER (MW)
Ib PLATE CURRENT (MA)
0
100
200
300
400
500
600
700
800
900
1000
1100
0
10
20
30
40
50
60
70
80
90
100
110
120
130
140
150
160
170
180
0
1
2
3
4
5

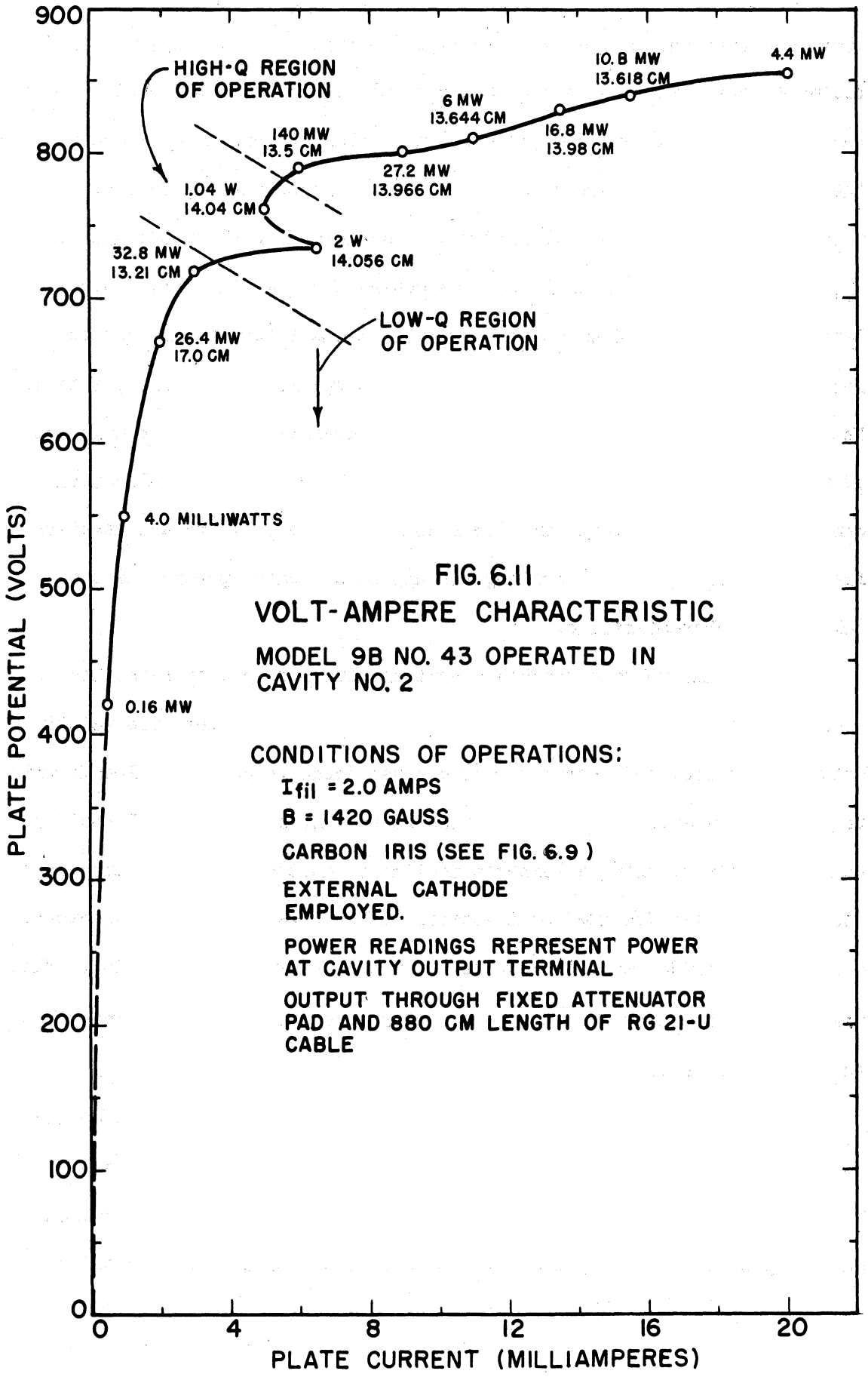

FIG. 6.11

VOLT-AMPERE CHARACTERISTIC

MODEL 9B NO. 43 OPERATED IN CAVITY NO. 2

CONDITIONS OF OPERATIONS:

I_{fil} = 2.0 AMPS

B = 1420 GAUSS

CARBON IRIS (SEE FIG. 6.9)

EXTERNAL CATHODE EMPLOYED.

POWER READINGS REPRESENT POWER AT CAVITY OUTPUT TERMINAL

OUTPUT THROUGH FIXED ATTENUATOR PAD AND 880 CM LENGTH OF RG 21-U CABLE

curve was the same as indicated in Fig. 6.9 except for the absence of the aquadag coating, and the presence of an external cathode bypass. The magnetic field was 1550 gauss and the filament current 2.0 amperes. The wavelengths and power outputs indicated on the volt-ampere characteristic represent measured values for a broad noisy signal except near the high-Q resonance region of 14 cm. We observe here a significant wavelength shift from 17.0 cm to 13.21 cm with a small increase in output power. The wavelengths corresponding to the two lowest voltage points on the volt-ampere characteristic were not measureable with the arrangement of apparatus employed to obtain these data. No reasonable explanation can be presented, at this time, to account for the positive and negative frequency pushing indicated along the upper horizontal portion of the volt-ampere characteristic.

In the voltage-tunable operation attained by Wilbur and his group at the General Electric Company below 1000 megacycles, the relation between frequency and operating voltage was found to coincide closely with the Hartree relation. This group also found that a clean signal could be generated only by using a temperature-limited emitter. Either pure tungsten or specially designed oxide-coated cathodes were found satisfactory. Conventional oxide cathodes resulted in unstable or noisy operation. This also turned out to be the case in the microwave range using the insertion tube described here.

An experiment employing the Model 9B No. 49 insertion tube was conducted to investigate the effect of a tungsten cathode on voltage-tunable output. Model 9B No. 49 employs a pure tungsten helical cathode and was provided with an external bypass in the cathode line for this

experiment. The cathode supply consisted of storage batteries and the anode potential was obtained from a series of minimax batteries. Dwg. B2052 in the Appendix shows the external circuit employed to obtain the clean signal voltage-tuning data given in Table 6.I below.

TABLE 6.1

E_b (volts)	I_b (microamps)	I_{fil} (amps)	λ (cm)	B (gauss)
740	80	6.76	18.210	1520
850	80	6.8	14.628	1520
940	160	7.0	12.492	1520
1080	500	7.1	11.34	1520

In this experiment it was found necessary to adjust the cathode current for each anode voltage in order to maintain a clean signal. The frequency was sensitive to cathode current, decreasing with increasing current. Fig. 6.12 shows a plot of the frequency versus anode potential from Table 6.1. Note the close correspondence between the experimental date and the curve computed from the Hartree equation for a magnetic field of 1400 gauss. It should be pointed out that the measured flux density (1520 gauss) given in Table 6.1 is considered to be somewhat in error. The output available in the form of a clean voltage-tunable signal varied between 10 and 30 microwatts over the measured frequency range.

A different approach to the study of voltage-tunable operation made use of the arrangement shown in Fig. 6.13. The block diagram shown in this figure illustrates how the insertion-tube magnetron was used as a

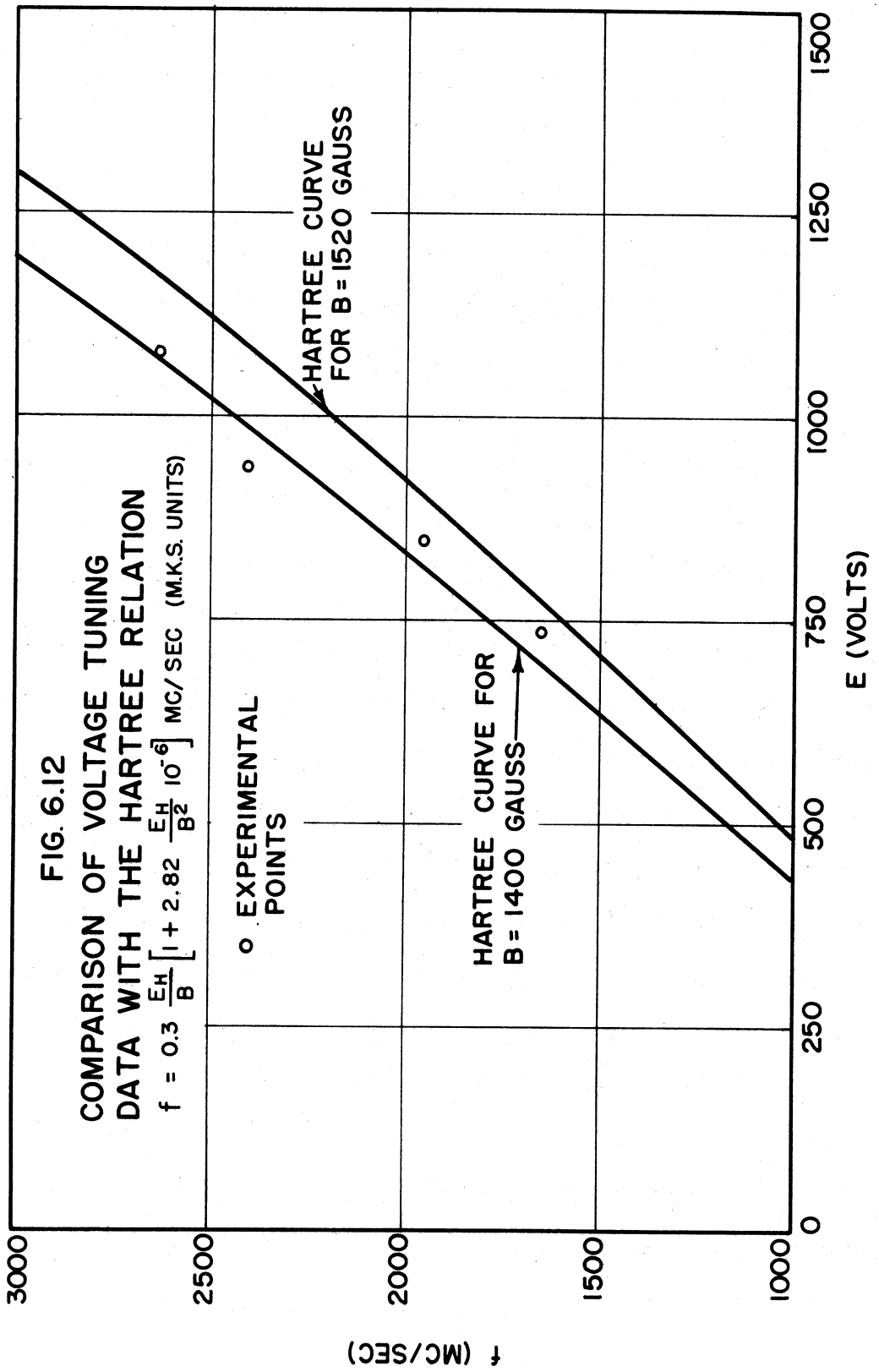
FIG. 6.12
COMPARISON OF VOLTAGE TUNING DATA WITH THE HARTREE RELATION
$f = 0.3 \frac{E_H}{B}\left[1 + 2.82 \frac{E_H}{B^2} 10^{-6}\right]$ MC/SEC (M.K.S. UNITS)
o EXPERIMENTAL POINTS
HARTREE CURVE FOR B = 1400 GAUSS
HARTREE CURVE FOR B = 1520 GAUSS
f (MC/SEC)
3000
2500
2000
1500
1000
0
250
500
750
1000
1250
1500
E (VOLTS)

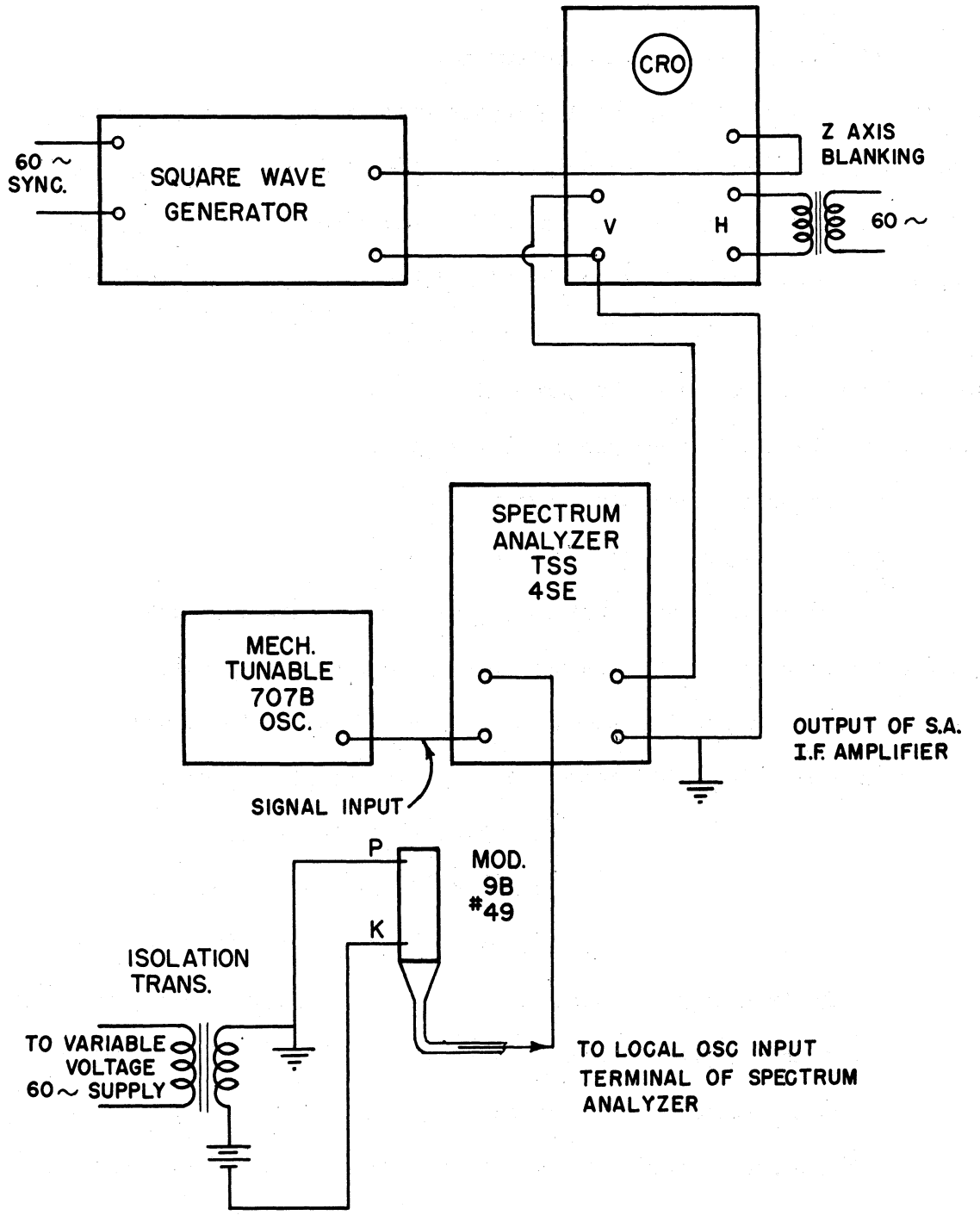

FIG. 6.13

EXPERIMENTAL SET UP USING INSERTION TUBE AS LOCAL OSCILLATOR FOR SPECTRUM ANALYZER.

local oscillator for an s-band spectrum analyzer. The frequency of the insertion magnetron is swept at a 60-cycle rate with a sine-wave source in series with the anode d-c supply. Since the horizontal sweep of the cathode-ray oscillograph is obtained with the same 60-cycle supply, the frequency of the voltage-tunable insertion tube is proportional to the horizontal deflection on the CRO. Z-axis blanking was employed to remove the signal output from the screen during the return trace of the 60-cycle sweep. With this arrangement it was possible to measure the total width of the frequency-modulated magnetron output by mechanically tuning a reflex klystron signal generator through the frequency range of the magnetron local oscillator. Frequency measurements were obtained from the klystron signal source for different settings of the mechanically-tunable klystron cavity. Fig. 6.14a shows the results of one of the tests made with the apparatus described above. In this figure two separate oscillograph traces are presented, each of which shows the amplitude of the intermediate-frequency amplifier output as a function of local-oscillator sweep voltage (or frequency). The upper trace was photographed with a 2042 mc/sec klystron signal-generator frequency. The lower trace shows the results with a 1690 mc/sec external-signal input. The above frequencies correspond to the positions lying midway between the vertical pips shown in the upper and lower traces, respectively. The frequency difference between two adjacent vertical pips corresponds to 40 mc, which is twice the intermediate frequency of the spectrum analyzer. The total voltage-tuned frequency difference obtained from the local oscillator for this particular test was therefore 2062-1670 or 392 mc/sec.

The conditions under which the magnetron was operated are listed below.

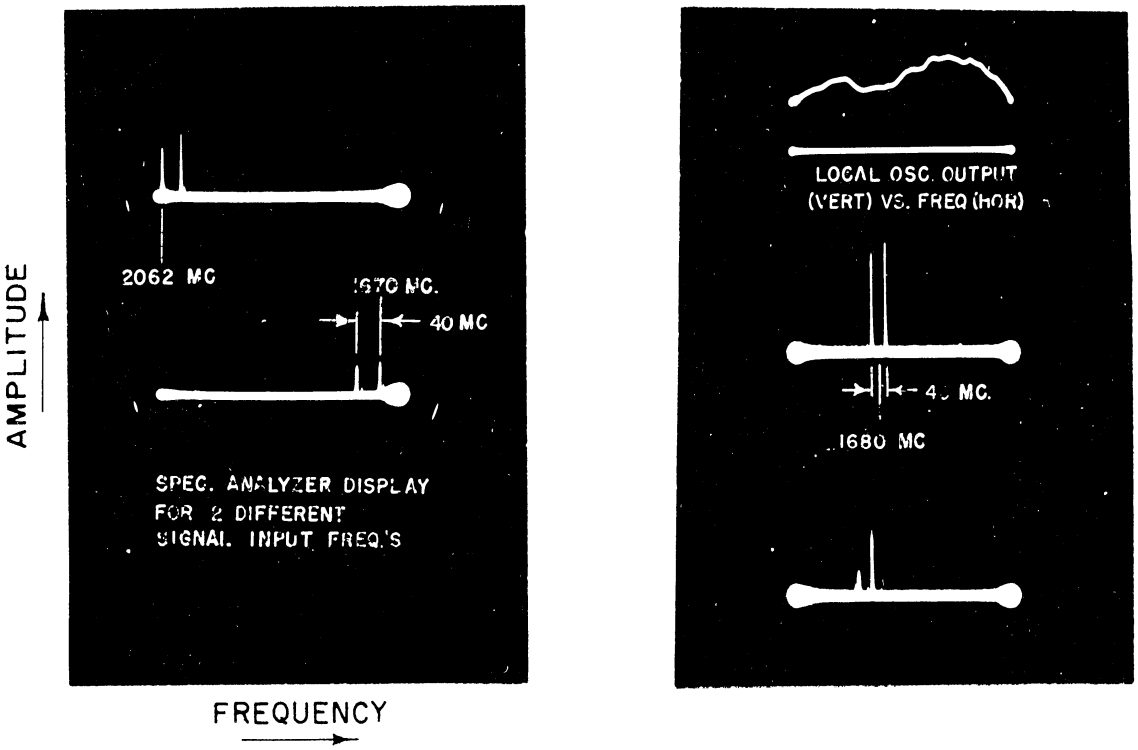

(a) (b)

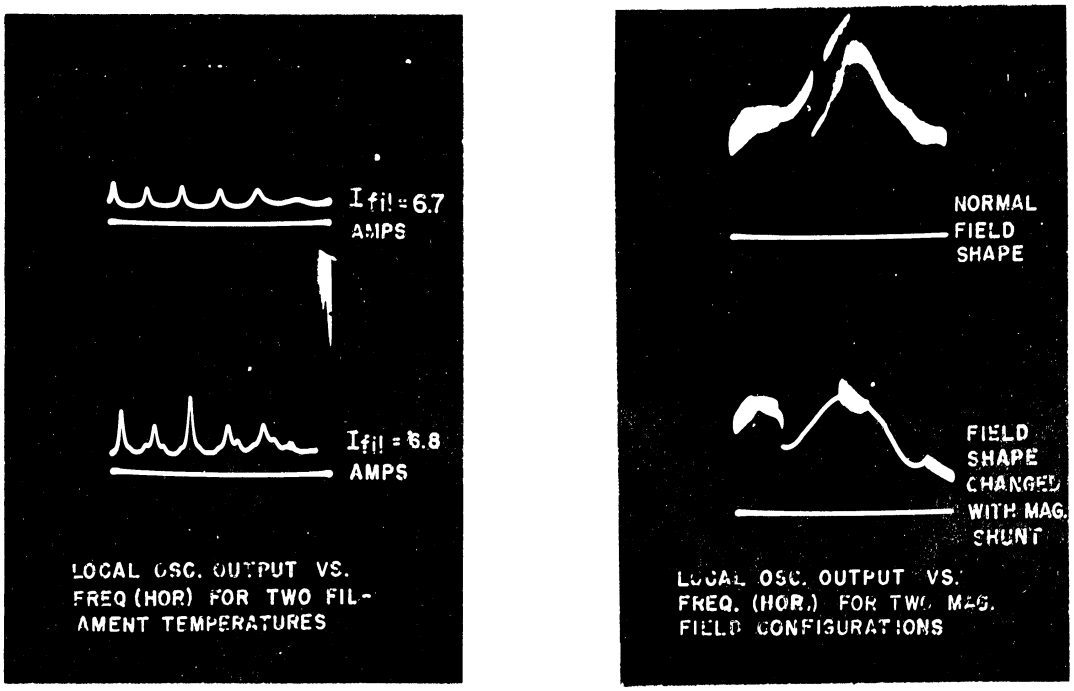

(c) (d)

FIG. 6.14

OSCILLOGRAPH TRACES OBTAINED WITH THE EXPERIMENTAL ARRANGEMENT SHOWN IN FIG. 6.13

Model 9B No. 49 Tube

This tube uses a pure tungsten helix cathode.

Cathode bypass used.

Cavity No. 2 through GR "L" connector and one 37-in. section of RG-21U GR cable to spectrum analyzer.

E_b = 860 volts.

E_{ac} = 226 volts peak to peak (60-cycle modulating voltage).

A polystyrene disk partially coated with aquadag was placed inside the cavity 3 inches below the center of the tube.

I_b = 75 μ amps. (average).

I_{fil} = 6.7 amps.

B = 1580 gauss.

Fig. 6.14b depicts the output of the voltage-tunable local oscillator versus frequency in the uppermost trace. The frequencies corresponding to the two tall pips in the center trace are 1680 $\pm$ 20 mc/sec. The conditions used to obtain this picture are the same as given immediately above except for the following:

E_b = 845 volts

E_{ac} = 390 volts (peak to peak)

I_b = 10 μ amps. (average)

I_{fil} = 6.3 volts

B = 1695 gauss

Note: The output from the magnetron was taken through a GR "L" connector and one 37-in. section of GR RG-21U cable to a crystal detector. The output of the crystal detector is displayed in the top trace.

The oscillogram given in Fig. 6.14c was obtained with the same circuit conditions as for the preceding test except that here a cathode bypass was not employed. The voltages, currents and magnetic field for this case were:

E_b = 860 volts

E_{ac} = 226 volts (peak to peak)

I_b = 75μ amps. (average)

B = 1580 gauss

I_{fil} = 6.7 amps.
(top trace)

I_{fil} = 6.8 amps.
(bottom trace)

These oscillograms portray the effect of a long line on the power output versus frequency of a tunable magnetron. The top trace is essentially the impedance of a transmission line as a function of frequency when the line is many wavelengths long. The lower trace shows the effect of a slight increase in the temperature of the cathode. We observe that in the lower trace, the output versus frequency no longer resembles the response expected with a constant-current generator. Here we find a clue to the properties of voltage-tunable operation in magnetrons. Since the anode voltage determines the frequency of the r-f output, and if the top oscillogram in Fig. 6.14c represents the output obtained with an r-f constant-current generator, then it is reasonable to ascribe the r-f constant-current properties of the magnetron mainly to the temperature-limited operation of the cathode.

An attempt to determine the effect of magnetic-field distribution in the interaction space on the noise output of the insertion tube,

resulted in the oscillogram shown in Fig. 6.14d. The traces represent the output through a crystal detector versus frequency for two magnetic-field conditions. Listed below are the conditions of the experiment.

Model 9B No. 49 Tube

Cavity No. 2 - with a carbon iris 3.5 cm from the nearest vane edge. The carbon iris O.D. was 0.600-in. wide and .250-in. long.

Output - Through GR "L" connector and a 10DB GR fixed attenuator pad to crystal rectifier and then to the oscillograph.

Magnetic field -
Top trace - Normal operation.

Bottom trace - Magnetic-field distribution changed with an external iron bar.

E_b = 700 volts

E_{ac} = 382 volts (peak to peak) 60-cycle modulation

I_b = 450 μ amps. (average)

I_{fil} = 7.1 amps.

B = 1420 gauss

Although the exact magnetic-field distributions are not known for this experiment, the field distribution which gave the results shown in the bottom trace of Fig. 6.14d is presumed to be asymmetric with respect to the anode axis. The study of the field distribution is complicated by the presence of the vane-anode Kovar cylinder which forms a magnetic shunt.

6.4. Conclusions

The results of the experiments employing the insertion magnetron in a mechanically-tunable high Q resonator definitely indicate that that mechanically-tunable magnetron operation in the 10 to 20 centimeter

wavelength range with power output of the order of one-half or more watts is attainable. The problems which still require attention are: (a) the improvement of the signal to noise ratio (b) the development of more easily tunable high-Q resonators for this tube structure. Since the signal-to-noise ratio is to a great extent a function of the Q of the resonator, it can be improved by employing more adequate circuitry.

This investigation has further shown that with a combination of very low Q and critical emission limited cathode operation it is possible to obtain a "clean" voltage-tunable power output of the order of 10 to 30 microwatts from 1600 to 2600 megacycles per second. This frequency range is attainable only if the cathode temperature is adjusted for minimum noise output at intervals along the tuning range. If the cathode temperature is not adjusted along the tuning range the clean-signal output is voltage tunable over approximately 300 megacycles.

The limitations in voltage-tunable operation with the present magnetron structure are: (a) low-power output and (b) the critical nature of the cathode temperature required for clean-signal output. At this time it appears reasonable to ascribe both of the above limitations at least in part ot the properties of the cathode. In addition it should be apparent that a low Q circuit which results in a high impedance between adjacent anodes will increase power output as well as reduce noise. Further study of cathode requirements for low-Q operation is necessary if higher power clean-signal voltage-tunable operation is to be attained.

The potentialities of the insertion magnetron as a tool for the study of mode boundary and pushing have been demonstrated by the results

obtained thus far. The effects of the cathode circuit on upper-mode-boundary current are of particular significance for high-Q mechanically-tunable operation and the results obtained are very encouraging.

Experience gained in the design, construction, and operation of the insertion tube will be extremely valuable for the development of higher power, higher frequency tubes of similar design. It appears feasible, at this time, to extend the upper frequency high-Q operation of this tube structure to approximately 6000 megacycles per second.

7. Model 8 Double-Anode Set Interdigital Magnetron (J. R. Black)

The geometry of the resonant structure of the Model 8 magnetron provides a flexible structure for designing magnetrons for various uses. This is due to the fact that the r-f. field distribution within this structure is such that it may easily be affected by external means.

Initially, an effort is being made to adapt the Model 8 structure to an f-m magnetron, as shown in Fig. 7.1b. One set of anodes with its associated cathode will form the magnetron oscillator section, while the other set of anodes with its associated cathode will form a reactance tube employing a magnetron-type space charge as the variable reactance.

To determine the characteristics of the Model 8 structure a high-power tube, as shown in Fig. 7.1a, is being studied. This arrangement employs two oscillator anode sets with their associated cathodes operating in a push-pull type operation. It is believed that over 1000 watts c-w will be obtained from this structure operating at 2300 mc.

An easily tunable magnetron could be built, as shown in Fig. 7.1c. One set of interdigital anodes would form the magnetron oscillator while a mechanically-variable condenser would be placed at the other voltage-

FIG. 7.1

POSSIBLE TYPES OF MAGNETRONS EMPLOYING THE MODEL 8 RESONANT SYSTEM

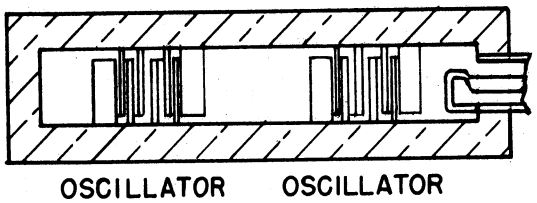

A

HIGH POWER MAGNETRON

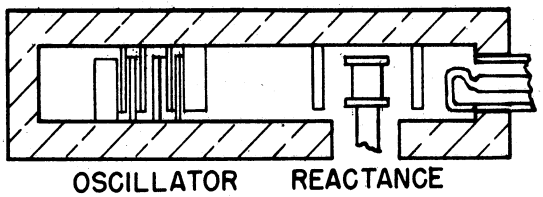

B

F-M MAGNETRON

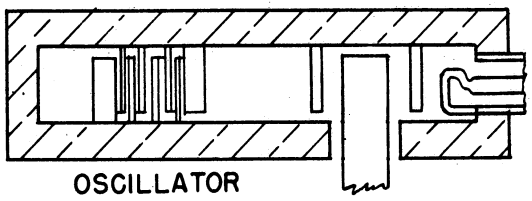

C

TUNABLE MAGNETRON

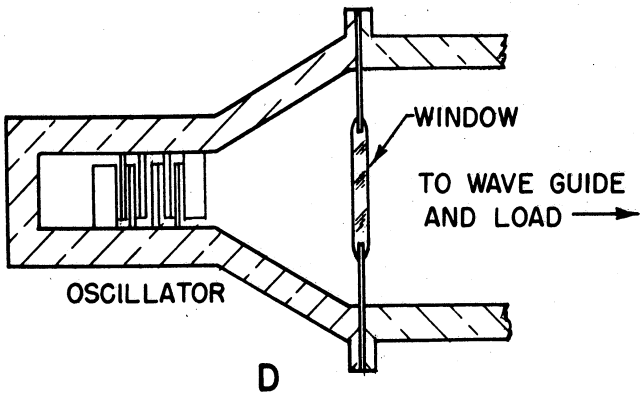

D

VOLTAGE TUNABLE MAGNETRON

maxima position. A simple cup-and-rod variable condenser on cold tests indicated a tuning range in the order of 1.5 to 1.

A fourth type of use for this structure is indicated in Fig. 7.1d. This system is a means of loading down a magnetron structure having no resonant circuit for use as a voltage-tunable magnetron having an out-power in the order of hundreds of watts. One-half of the Model 8 structure would be used feeding directly into a waveguide through a window. See Section 6 of this report for further discussion of voltage tuning.

Originally, development was started on a high-power double-anode set magnetron. It was felt that such a structure would lead to results immediately applicable to the development of an f-m magnetron. Earlier on a previous contract Model 8 No. 36 was constructed employing oxide cathodes which operated in the full wavelength mode of 18.4 cm.

A new tube was constructed having tapered anode fingers to reduce the anode capacity. This was designated as Model 8B. Carburized thoriated tungsten cathodes were used with this tube each of which produced four amperes of diode emission current. The design factors for Model 8B are as follows:

$N = 16$

$r_a = .450$ cm

$r_c = .269$ cm

$B_o = 320$ gauss

$E_o = 175$ volts

cavity = 2.12 x 4.24 cm

$h = 1.016$ cm cavity height

$\lambda = 13.2$ cm

A photograph of this tube is given in Fig. 7.2 and the assembly drawing appears in the Appendix. Due to a shifting of jigs during brazing the anodes were not inserted their full depth in the tube causing the resonate wavelength to shift from the desired 13.2 cm to 12.3 cm.

Model 8B operated in two different modes, neither of which was the desired cavity λ mode. They were the cavity 2 λ mode at λ = 8.5 cm (f = 3530 mc) and a parasitic mode of λ = 14.9 cm (f = 2012 mc). The parasitic mode was associated with the coaxial lines formed by the cathodes, the pole pices and the cathode chokes.

Fig. 7.3 shows three pulsed-performance oscillograms of the Model 8B. The upper curve shows the voltage-current diagram for the No. 1 cathode only, the center curve is the No. 2 cathode performance diagram. The lower curve of Fig. 7.3 shows the peformance curve for both cathodes operating together.

It is of interest that the maximum-current boundary for the 14.9 cm wavelength mode with both cathodes operating was considerably greater than the total of the maximum-current boundaries for the cathodes operating individually. With both cathodes operating together the maximum-current boundary is 290 ma, as compared to 155 ma when the cathodes are operated individually. This is a factor of about 1.9 to 1 and indicates that space charge, as far as the mode boundary is concerned, likes to work into a high impedance.

In order to investigate the role played by the cathode chokes in this structure it was deemed desirable to construct a tunable version of the rectangular tube. This was designated as Model 8C. An assembly drawing for this structure is given in the Appendix. The Model 8C No. 63

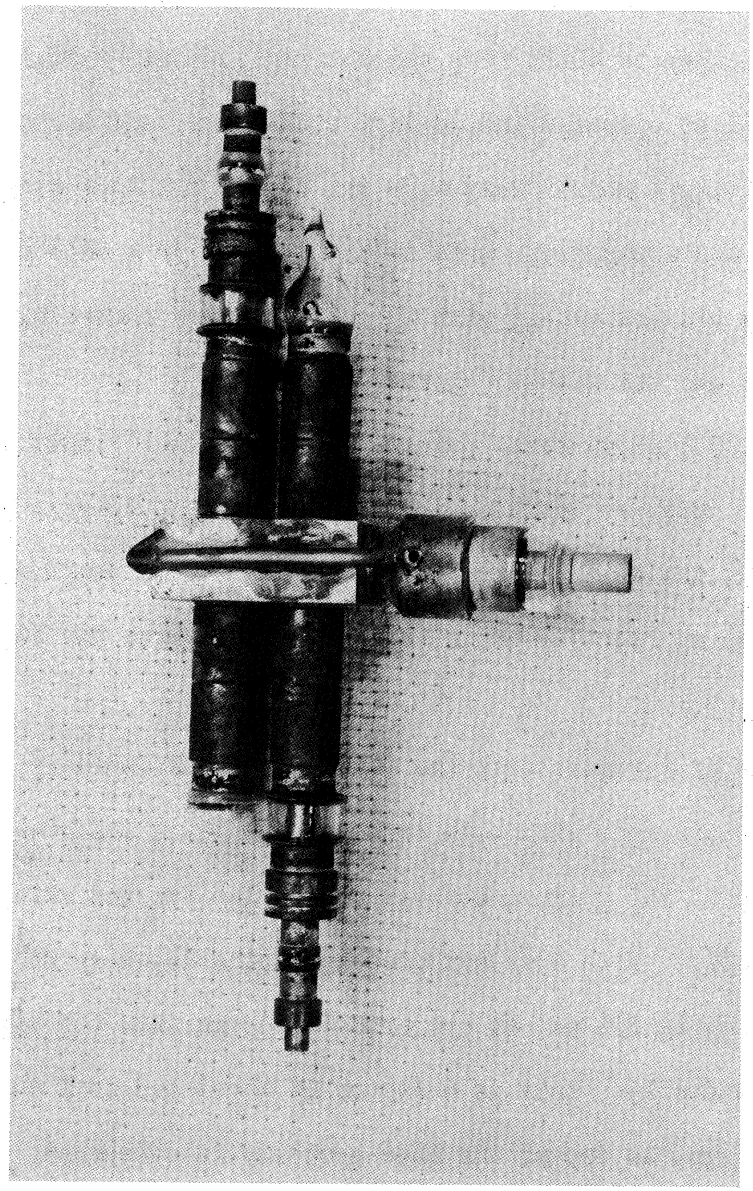

FIG. 7.2
PHOTOGRAPH OF MODEL 8B

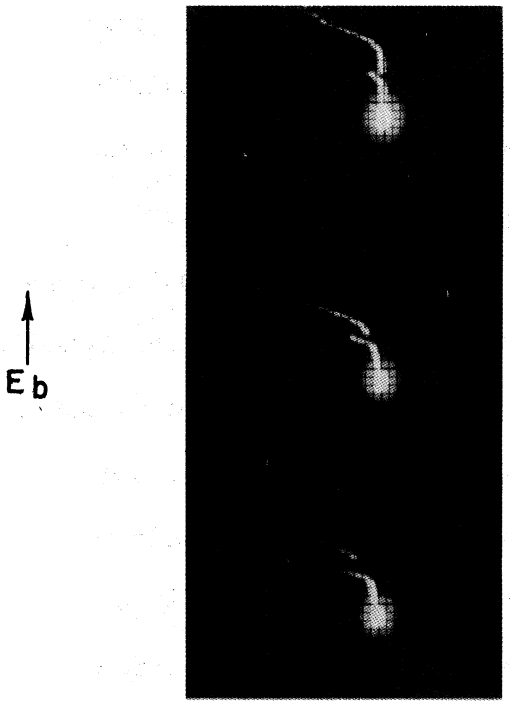

FIG. 7.3
PULSED PERFORMANCE OSCILLOGRAMS MOD. 8B
CURRENT CALIBRATION = 25 MA. PER DIVISION
VOLTAGE CALIBRATION = 330 V. PER DIVISION

employed an old cavity which was machined but never used. The dimensions of this cavity were 3 x 6 cm by 1.02 cm high and if loaded by two sets of anodes of the Model 8B variety would resonate in the desired cavity λ mode at 16.74 cm. The Model 8C structure used one set of anodes of the Model 8B type and a variable condenser of the cup-rod type at the position normally occupied by the second anode set.

Fig. 7.4 is a tuning curve of this tube presenting λ vs d (the gap width of the variable condenser). As indicated there appear two fixed frequency modes coupled rather tightly to the tunable mode. The fixed frequency modes are associated with the cathode structure and it is believed that these can be removed from the tuning range.

The maximum mode-jump current in this tube is quite low varying between 30 and 40 ma in the tunable mode and 75 ma in the fixed modes. The low mode-jump current is believed to be due to the high anode capacitance of 6.2 $\mu\mu$f. Power output in the tunable mode varied between 20 to 35 watts with efficiencies on the order of 33 to 45 per cent. 75 watts power output was obtained in the fixed frequency mode at an efficiency of 52 per cent.

Plans for the future development of this tunable structure are as follows:

1. Determine the cause of the fixed frequency parasitic modes and eliminate them.
2. Reduce the anode capacitance to increase the mode-jump current.
3. Determine the correct choke design for the f-m version of the rectangular tube.

It should be pointed out that this type of tunable magnetron holds great promise at frequencies above 5,000 mc. The physical separation

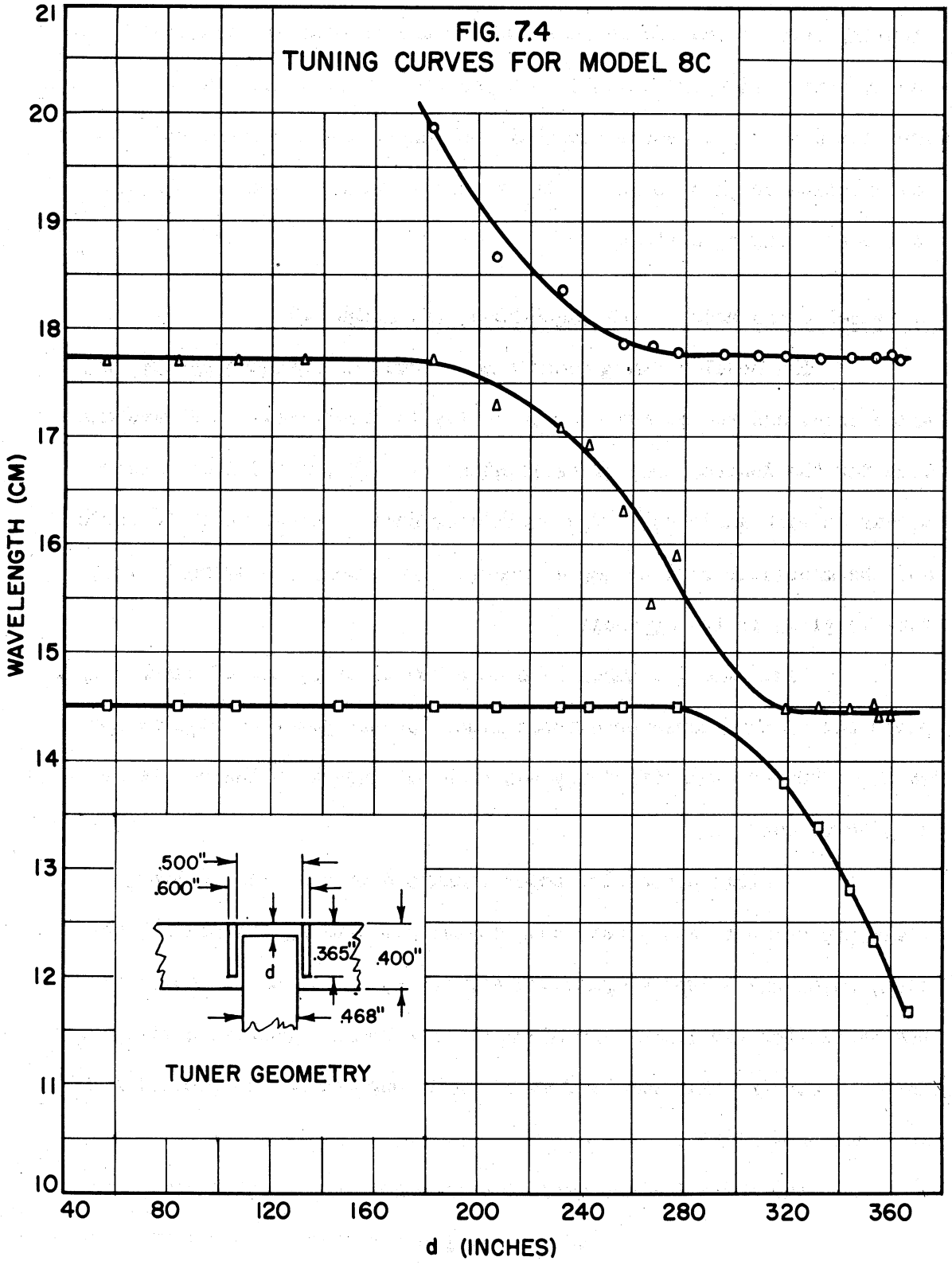
FIG. 7.4
TUNING CURVES FOR MODEL 8C
WAVELENGTH (CM)
d (INCHES)
21
20
19
18
17
16
15
14
13
12
11
10
40
80
120
160
200
240
280
320
360
.500"
.600"
.365"
.400"
d
.468"
TUNER GEOMETRY

of the tuning structure from the anode structure while maintaining tight coupling between the two is an answer to the problem of obtaining tuning ranges better than or 1.2 to 1 at these frequencies. At high frequencies the vane structures become too small to insert L and C rings while external cavities coupled to one of the resonant structures are inherently narrow-band tuning devices.

8. Model 6 and Model 7 F-M Magnetrons (S. Ruthberg)

The Model 6 f-m magnetron has a coaxial resonant system, two anode sets, and two cathodes. The cavity is electrically one wavelength long for the desired mode of oscillation (λ = 13 cm). Voltage maxima appear at each anode set. The oscillator section consists of 16 anodes and the modulator section has 4 anodes. An assembly drawing of this tube is given in the Appendix.

Eight Model 6 tubes have been constructed, all of which coupled power out of the modulator cathode line. Output power as high as 190 watts at 40 per cent efficiency has been obtained with the modulator cathode removed.

Problems concerning power leakage down the cathode line, mode-jump current, etc., have been investigated using the Model 7 magnetron, which has a less complicated structure, but which is identical to the oscillator section of the Model 6. The Model 7 coaxial cavity resonator is electrically one-half wavelength long and has no provision for frequency modulation.

The objective has been to bring the study of this structure to a point where work on it can be stopped but readily resumed at some future date. This decision was made in order to devote more time to voltage-tunable tubes.

A rather extensive study of three different tube structures has been made to determine, if possible, the cause of the erratic behavior of the Model 7. These structures are the Model 7D, with large loop area, the Model 7A, with external line on the cathode structure, and the Model 7F, a mechanically-tuned device. In addition, information on the modes of operation of Model 7E (modified vane structure) is presented. (See Appendix for drawings of these tubes.)

7E No. 45

The Model 7E magnetron has been operated c-w. This tube is identical to Model 7B but has a modified vane-and-bar structure for the purpose of equalizing the r-f voltage between the cathode and the anode segments by balancing the capacitance between the bars and cathode with that between the vanes and cathode. This geometry is given in Fig. 8.1. The cathode, used in this experiment is oxide coated, and has no filter for preventing power loss down the cathode line. Fig. 8.2 lists two representative volt-ampere characteristics. Because of back-heating difficulties, the tube was not operated at much more than 100 watts input power. Both examples given are for a magnetic-field density less than that of the cyclotron frequency but for two different cathode-heater currents. Higher heater power and stronger magnetic fields lead quickly to large back-heating. Information about the various modes found in the volt-ampere characteristics may be obtained by use of the Hartree equation and the actual starting voltage.

This is done by the following method. If k represents the number of r-f periods necessary for an electron to complete one revolution of the interaction space, its angular velocity is $2\pi f/k$, where f is the frequency of the r-f field. Then, in these terms, the Hartree equation is

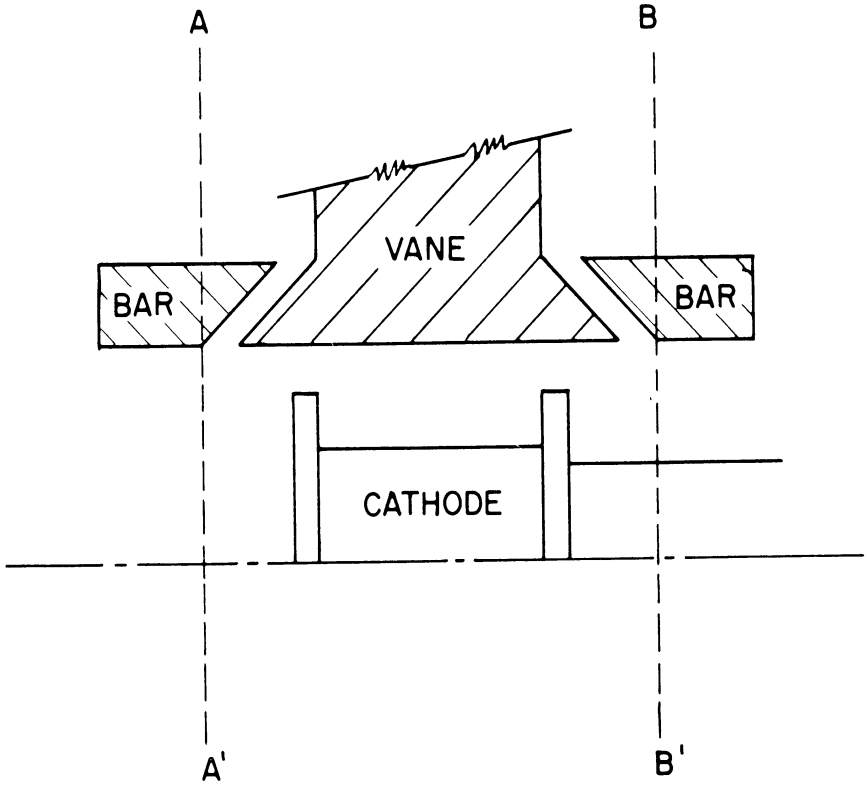

FIG. 8.1

VIEW SHOWING VANE PROTRUDING THROUGH SLOT. MODEL 7E

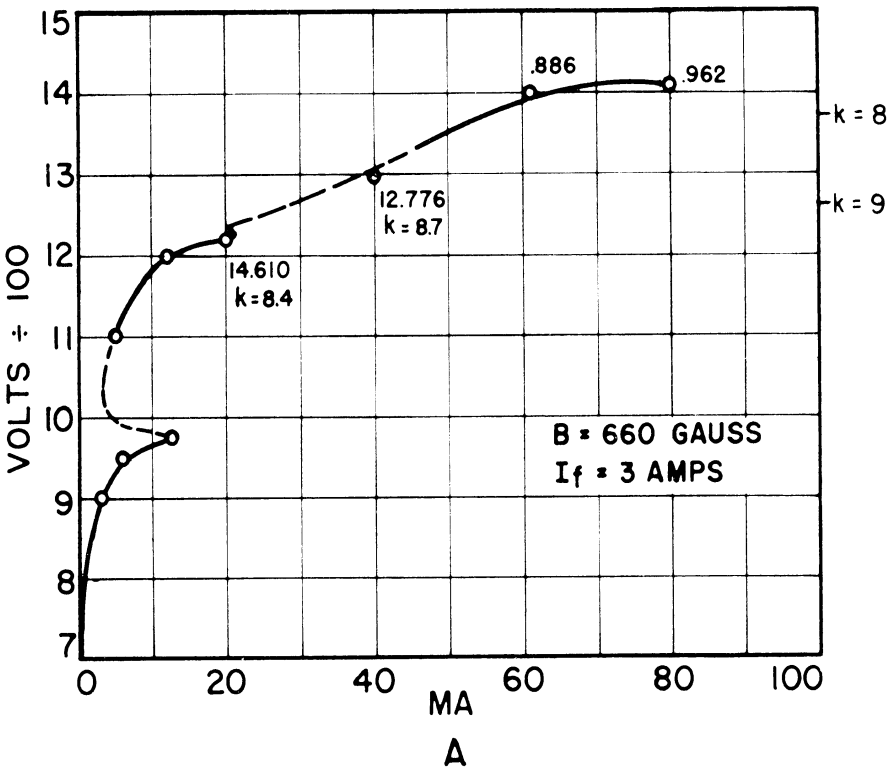

A

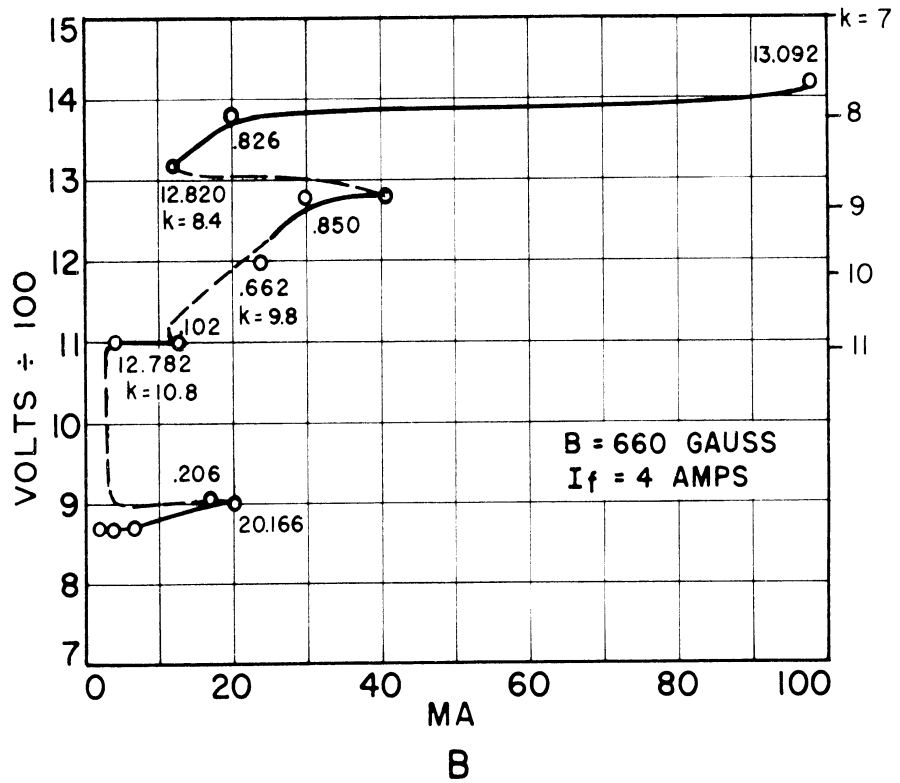

B

FIG. 8.2
VOLT AMPERE CHARACTERISTICS MODEL 7E 45

$$E = \pi(r_a^2 - r_c^2) B\frac{f}{|k|} - 4\pi^2 \frac{m}{e} r_a^2 \frac{f^2}{|k|^2} ,$$

from which the value of $|k|$ may be found. r_a, r_c, B, and f are respectable the anode radius, cathode radius, magnetic-field density, and frequency. The quantity k is related to the number of wavelengths of the r-f field in the circumference of the interaction space by

$$k = n \pm p N; \qquad p = 0, 1, 2, \ldots$$

where n is the number of waves of the r-f field around the periphery and N is the number of anode segments. n is called the mode number for the interaction space. If $p = 0$, $k = n$, which indicates the electrons move in synchronism with the traveling r-f wave. If $p \neq 0$, the number of r-f periods taken by the electrons to travel around the interaction space differs from the time taken by the r-f wave to cover the same distance. If $p > 0$, the transit time of an electron from gap-to-gap in the anode is p r-f periods greater than that of the r-f wave. If the electrons move from gap-to-gap faster than the r-f wave, they would, on the average, not give energy to the r-f field. $p < 0$ indicates the electrons are moving in the reverse direction to the r-f wave but in such a way as to convert their d-c energy to r-f. So $p \neq 0$ leads to other volt-ampere characteristics than for the case of $k = n$. These cases of $p \neq 0$ are called the Hartree harmonics. The approximate values of k found by use of Eq 8.1 have been placed on the volt-ampere curves of Fig. 8.1. The interesting range of wavelengths is in the $\lambda = 12.8$ cm region, since this seems to include the main cavity mode. For comparison, the Hartree voltage for a given choice of k is found to be greater than the actual starting voltage and is in agreement

with the usual experience of finding the starting voltages less than the Hartree voltages. These facts indicate that k = 8 for the mode appearing in the 1300 to 1400-volt range, k = 9 in the 1100 to 1300-volt range, and k = 10 in the 1100-volt range. Values of k for other volt-ampere characteristics at different magnetic fields agree with those presented.

In the desired cavity mode (TEM) $k = n = N/2 = 8$ for π-mode operation of the anode structure. The first Hartree harmonic would then appear for p = 1 at k = 24. Apparently, the tube operates in the n = 8 mode for the 1300 to 1400 volt characteristic. However, the Hartree harmonics for this mode do not explain the appearance of k = 9 or 10, and as yet no convincing argument has been devised to explain them. Preliminary investigation indicates that a TE_{m1} mode in the cavity could produce the k = 9 or 10 configuration within the interaction space, but this analysis is complicated by the vane structure. For this mode of operation modal lines in the electric field occur along diameters in the cavity. Such a cavity operation would give rise to pairs of anode potential waves in the interaction space which are the components of a wave of periodicity N/2 or 8 with an envelope whose variation is that of the field in the cavity. Thus, the pairs of waves for

$$n = 8 \pm s \qquad s = 0, 1, 2, \ldots$$

where s is the periodicity of the cavity field. Hartree harmonics can exist for each of these waves. Then k = 9 might exist as the fundamental k = n = 9 or as the first Hartree harmonic of n = 7 or k = 7 - 16. However, k = 10 demands a fundamental of n = 6. But one would expect the resonant frequency for these TE modes to be quite different from TEM; for example,

the resonant wavelength for a TE_{11} mode in a cavity of the dimensions of Model 7 would be in the neighborhood of 6 cm when the vane and coupling structures are disregarded.

7D No. 42

The performance chart of the Model 7D 42 tube given as Fig. 9.4 in Technical Report No. 6 issued in January 1951 shows large pushing at high magnetic fields. Since this would be a desirable feature for the oscillator section of the Model 6 f-m tube, this tube was re-examined in the region of high magnetic fields.

The resultant performance (Fig. 8.3) was found to be radically different from that previously obtained. (See Fig. 9.4 Technical Report No. 6.) The new performance diagram indicated erratic behavior especially in the appearance of frequency doublets. Wavelengths were measured with a coaxial wavemeter whose output fed into a crystal. The doublets were observed as a double maximum in the crystal current. Further examination of such points of operation with a spectrum analyzer showed the output to consist of many frequencies. Also, the wavelengths increased as the mode-jump current was approached, which was quite the opposite in normal operation. This tube failed before more complete data could be obtained.

Cold tests on the tube showed three resonances in the range of wavelengths from 10 to 15.5 cm. These are seen in the graph of voltage-standing-wave ratios vs wavelength, Fig. 8.4. The resonance at $\lambda = 12.96$ cm is an undercoupled case with a loaded Q of about 10. The other two are overcoupled cases. The resonance at $\lambda = 14.6$ cm is given in more detail in Fig. 8.4. Q_L for this mode is about 41. A comparison is made in this figure with the results found previously.

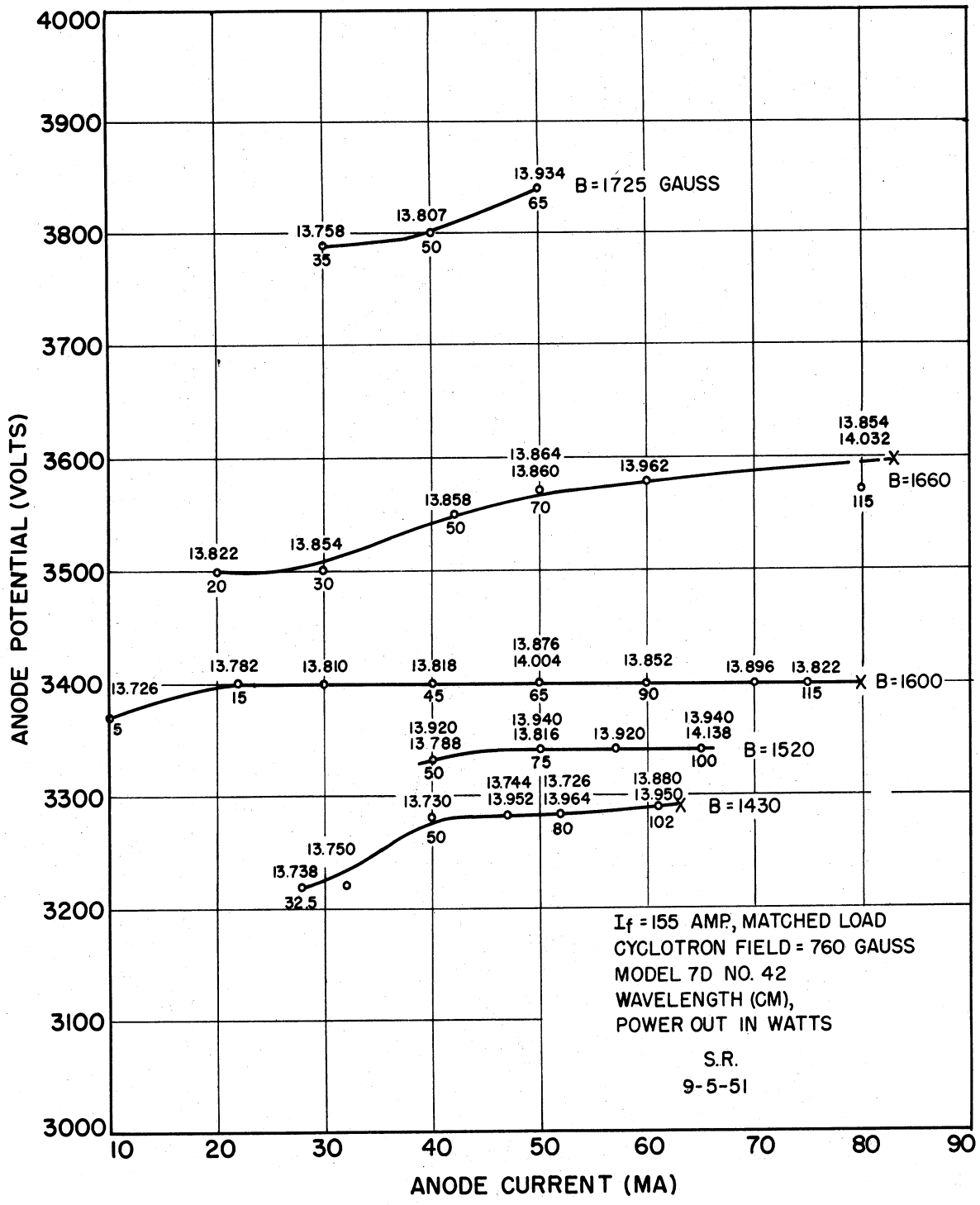

FIG. 8.3

PERFORMANCE CHART FOR COAXIAL SINGLE-CAVITY MAGNETRON

FUNDAMENTAL-CAVITY MODE

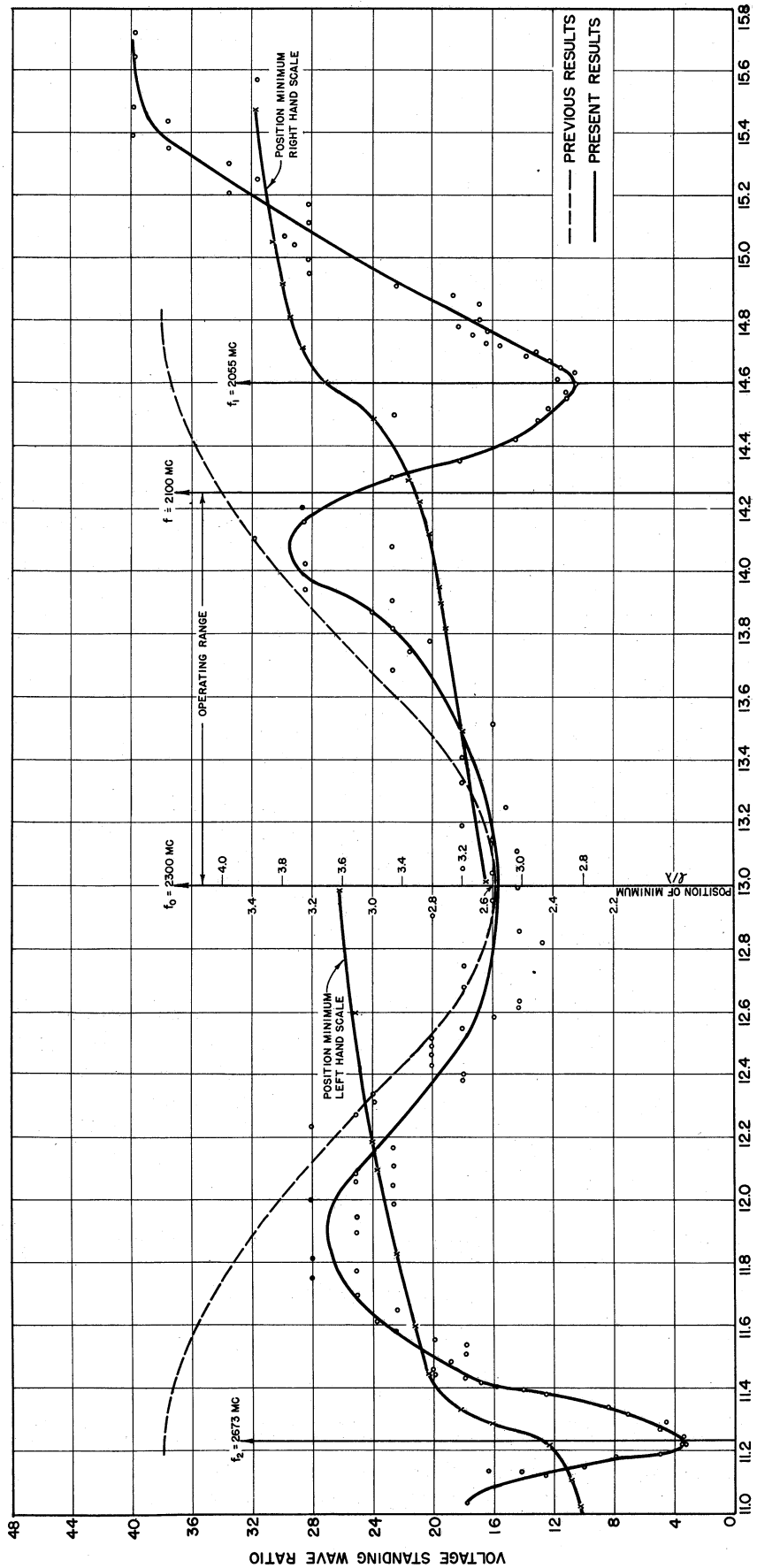

FIGURE 8.4 RESONANCE CURVE, MODEL 7D NO. 42 MAGNETRON

The large discrepancy between the past and present results indicates that some mechanical or electrical change has occurred in the tube itself so that the two sets of information are not comparable. However, due to the unusual behavior of this tube, these results have been incorporated in this report.

7A No. 33

In order to study the effects of cathode impedance on tube operation, the Model 7A No. 33 containing a small diamter cathode (anode-to-cathode ratio = 2.47) and having no choke or bypass on the stem was operated under pulsed conditions with an external coaxial-line stub tuner mounted on the cathode. Without this external tuner the tube operated strongly in the vane mode but weakly in any other mode. The external cathode-line tuner did not cause a large increase in the upper-mode-current boundary although small variations could be observed. Both 14 and 16 cm modes could be made to appear, but the 14 cm mode was intermittent. It is believed that considerably more information could be obtained using this approach by incorporating a tuner which would produce a wider range of impedances at the cathode. The d-c voltage isolation problem associated with this tube makes a wider range of impedance difficult to obtain. The problem will be studied further using a Model 9 tube. When a slotted line was coupled to the cathode in place of a stub tuner, it was noted that power could be coupled out the cathode at the vane-mode wavelength as well as the 14 and 16 cm wavelengths.

7F No. 55

A mechanically-tunable Model 7 tube designated as Model7F was constructed to aid the study of the Model 6 structure. A drawing of this

tube is presented in the Appendix. With this model the operating characteristics may be studied as a function of frequency over a range of 1 cm in the 14 cm wavelength region. The vane, bar, and cathode geometries are those of the Model 7B, which has a single output loop, and a backing ring on the vanes to reduce the vane-mode wavelength. The ratio of anode-to-cathode radius is 2.1. In addition, the cathode-line structure has been modified for better heat transfer.

The Model 7F No. 55 magnetron tuned over the wavelenth range of 14.8 to 17.1 cm. The mode-jump current was extremely low over the entire tuning range with a maximum of about 15 ma. X-rays of this tube indicated that the cathode was misaligned.

The cathode was realigned and the tube pumped down. Subsequent cold and hot tests have produced interesting results. The loaded Q of the resonant structure with cold cathode changes from 40 to 20, while the unloaded Q goes from 70 to 30, as the length of the structure is varied. These values are intermediate between those of previous Model 7 magnetrons, except the 7D, and those of the Model 9 voltage-tuned magnetrons. Data are given showing the frequency range over which the tube tunes, both as a cold resonant and a hot oscillating structure. Mode-jump current is given as a function of heater power. Further, under certain operational conditions, frequency doublets appear.

As is seen in the assembly drawing (see Appendix) one side of the coaxial cavity is contained between 2 monel metal bellows, such that the length of this side can be varied by the thrust-bearing and plunger arrangement shown. The variation in length is given arbitrarily as a distance, d, measured as indicated in the insert of Fig. 8.7.

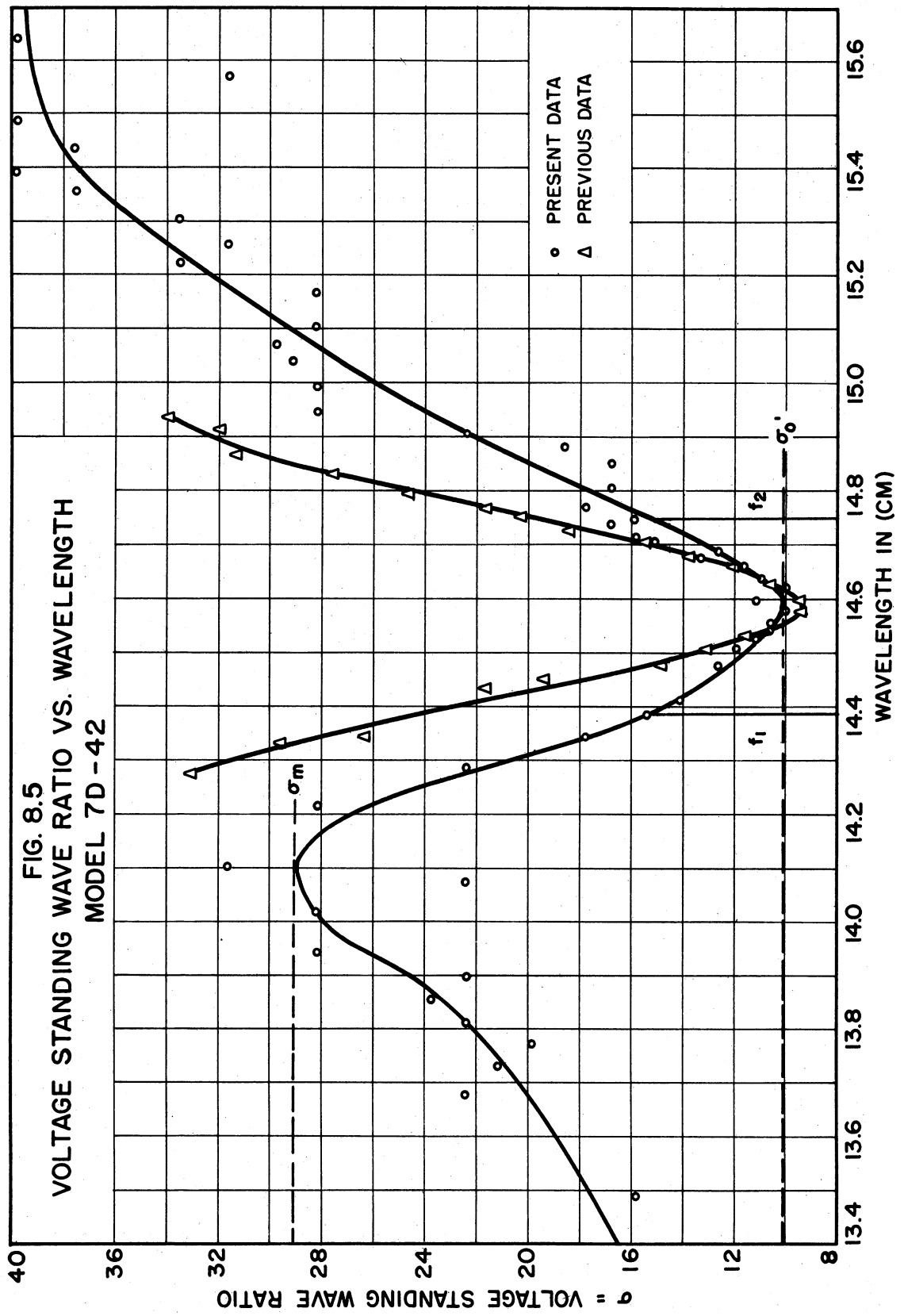
FIG. 8.5
VOLTAGE STANDING WAVE RATIO VS. WAVELENGTH
MODEL 7D-42
PRESENT DATA
PREVIOUS DATA
σ_m
σ_o'
f_1
f_2
σ = VOLTAGE STANDING WAVE RATIO
WAVELENGTH IN (CM)
40
36
32
28
24
20
16
12
8
13.4
13.6
13.8
14.0
14.2
14.4
14.6
14.8
15.0
15.2
15.4
15.6

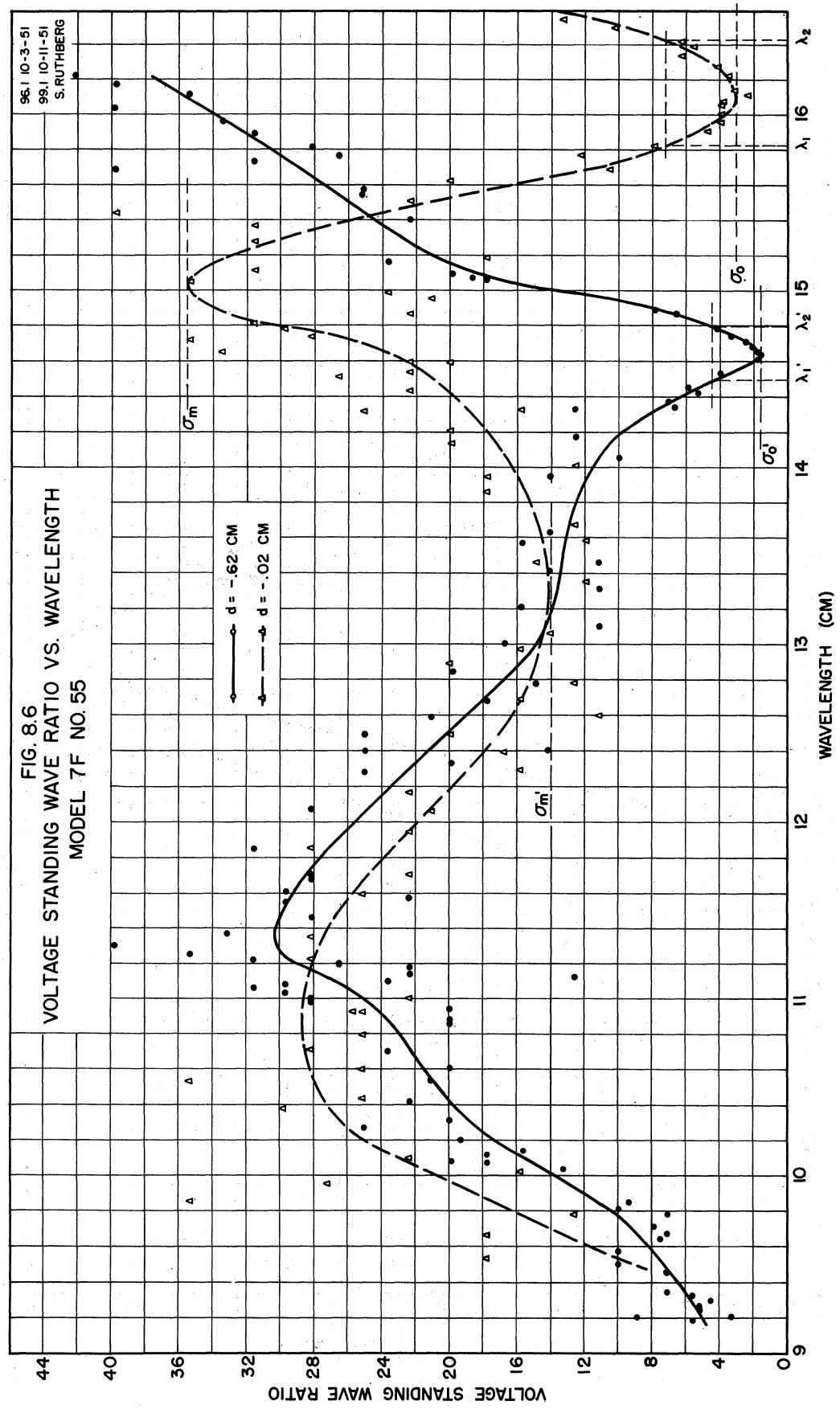
96.1 10-3-51
99.1 10-11-51
S. RUTHBERG
VOLTAGE STANDING WAVE RATIO VS. WAVELENGTH
MODEL 7F NO. 55
FIG. 8.6
d = -.62 CM
d = -.02 CM
σ_m
σ_o
σ_m'
σ_o'
λ_1
λ_2
λ_1'
λ_2'
VOLTAGE STANDING WAVE RATIO
WAVELENGTH (CM)

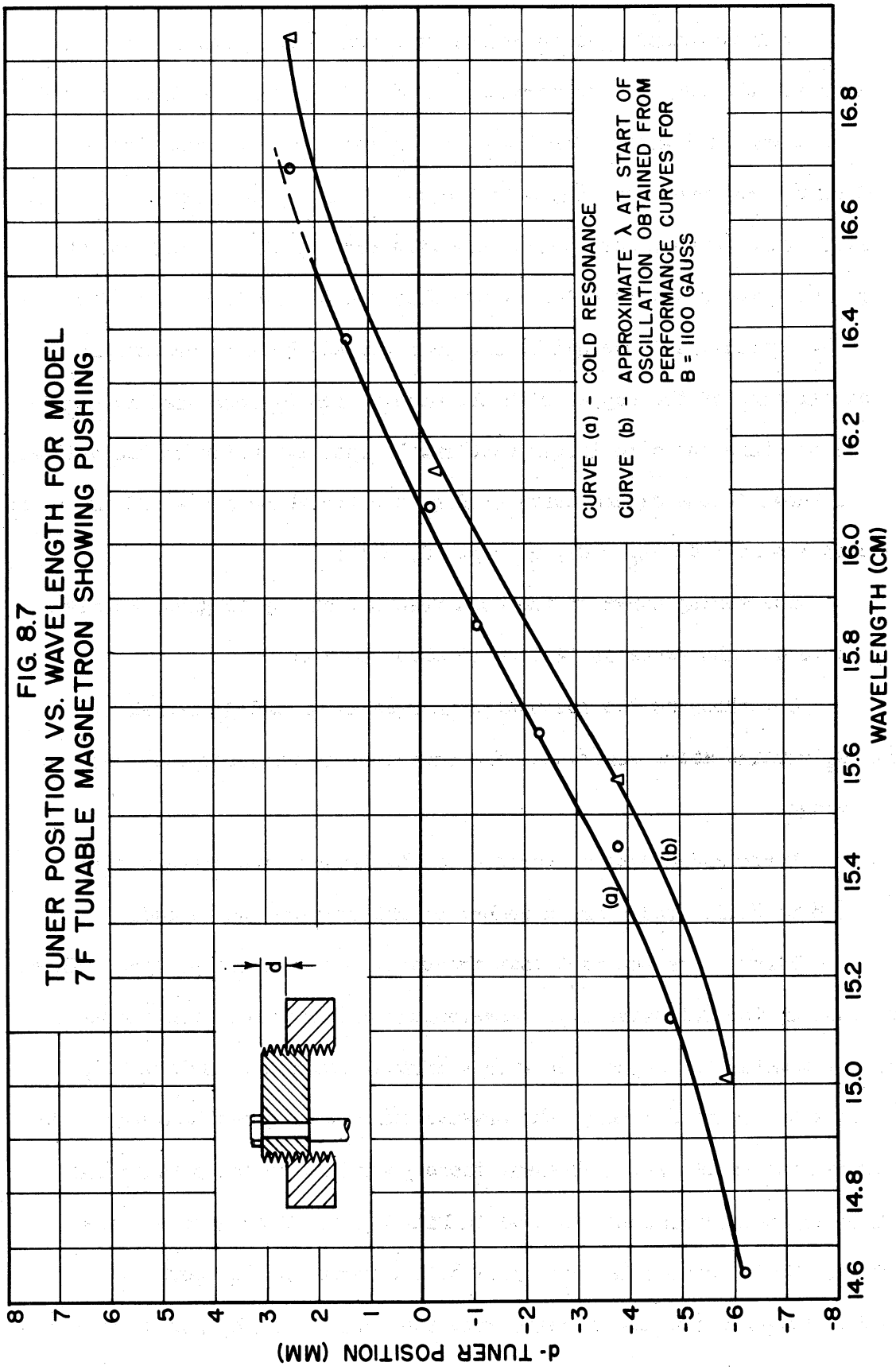
FIG. 8.7
TUNER POSITION VS. WAVELENGTH FOR MODEL 7F TUNABLE MAGNETRON SHOWING PUSHING
CURVE (a) - COLD RESONANCE
CURVE (b) - APPROXIMATE λ AT START OF OSCILLATION OBTAINED FROM PERFORMANCE CURVES FOR B = 1100 GAUSS
d
(a)
(b)
d - TUNER POSITION (MM)
WAVELENGTH (CM)
8
7
6
5
4
3
2
1
0
-1
-2
-3
-4
-5
-6
-7
-8
14.6
14.8
15.0
15.2
15.4
15.6
15.8
16.0
16.2
16.4
16.6
16.8

Voltage-standing-wave ratios as a function of wavelength, λ, obtained for the tube as the termination of a 50 Ω slotted line in cold test are given in Fig. 8.6 for d = - .62 cm and d = - .02 cm. For d = - .62 cm the resonant wavelength is λ = 14.65 cm; Q_L is about 40; Q_o, 65; Q_e, 140. This is an undercoupled case with VSWR at the minimum point being 1.6. The low internal Q is probably due to the loss in the bellows. Although, initially, these had been copper plated, brazing operations caused alloying of the copper with the monel. The Q_L decreased in magnitude as the tube tuned to larger wavelengths upon extension of the bellows. This is shown in the dashed curve of Fig. 8.6 for which d = - .02 cm, where resonant λ = 16.1 cm, Q_L = 27, Q_o = 34, Q_e = 131.

The tuning curve of the cold resonant cavity is given as Fig. 8.7, curve a. The range is 14.7 cm to about 16.7 cm.

So, then, as the resonant λ increases, Q_L and Q_o decrease, while Q_e remains about constant. The structure is undercoupled over the whole range.

Performance data at various cavity lenghts are presented in Figs. 8.8 to 8.11. There are a number of observations to be made.

First, note the fact that frequency doublets are present. These are found in the following way. Wavelengths are measured with a coaxial cavity wavemeter in conjunction with a crystal detector. Ordinarily, positions are found for which the crystal current is a maximum, where the distance between is $\lambda/2$. Represent these positions of the plunger for maximum crystal current as lines as in Fig. 8.12a. When doublets are observed, the situation is as in Fig. 8.12b, where the "dispersion" between plunger positions increase with the "order" of the position, i.e.,

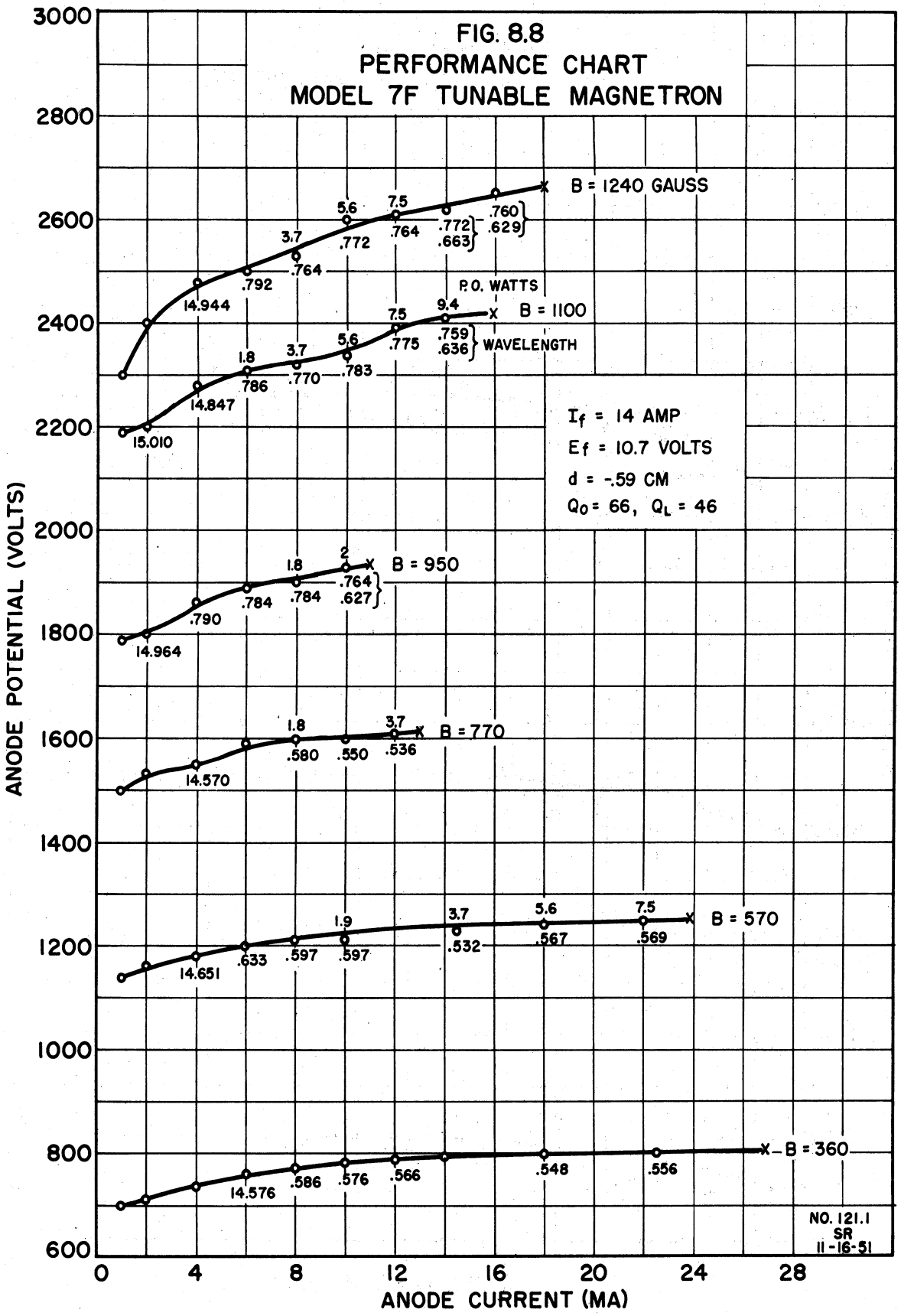
FIG. 8.8
PERFORMANCE CHART
MODEL 7F TUNABLE MAGNETRON
B = 1240 GAUSS
B = 1100
B = 950
B = 770
B = 570
B = 360
P.O. WATTS
WAVELENGTH
If = 14 AMP
Ef = 10.7 VOLTS
d = -.59 CM
Q0 = 66, QL = 46
ANODE POTENTIAL (VOLTS)
ANODE CURRENT (MA)
NO. 121.1
SR
11-16-51

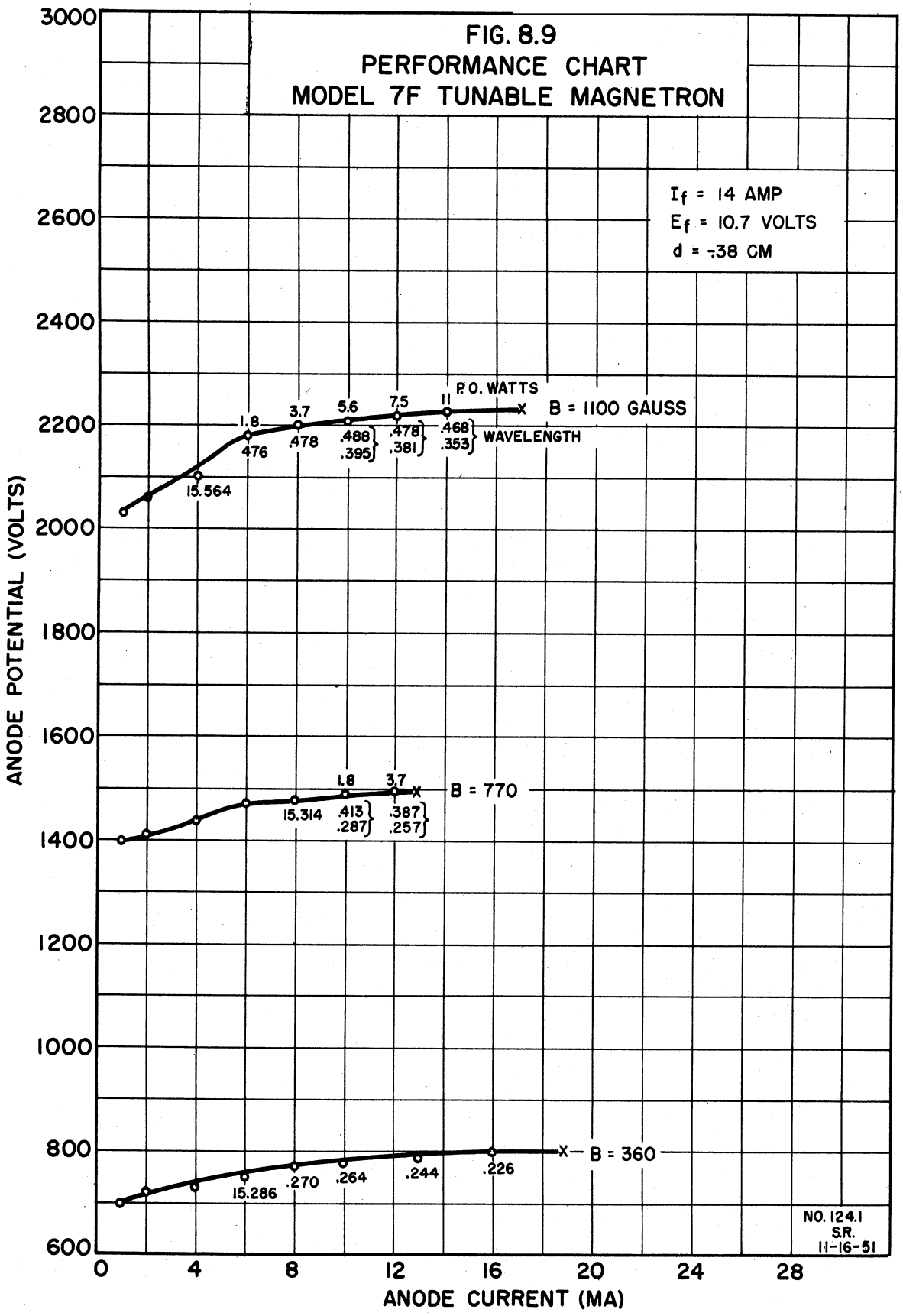
FIG. 8.9
PERFORMANCE CHART
MODEL 7F TUNABLE MAGNETRON
I_f = 14 AMP
E_f = 10.7 VOLTS
d = .38 CM
P.O. WATTS
1.8
3.7
5.6
7.5
11
B = 1100 GAUSS
476
.478
.488
.395
.478
.381
.468
.353
WAVELENGTH
15.564
1.8
3.7
B = 770
15.314
.413
.287
.387
.257
B = 360
15.286
.270
.264
.244
.226
NO. 124.1
S.R.
11-16-51
ANODE POTENTIAL (VOLTS)
ANODE CURRENT (MA)
3000
2800
2600
2400
2200
2000
1800
1600
1400
1200
1000
800
600
0
4
8
12
16
20
24
28

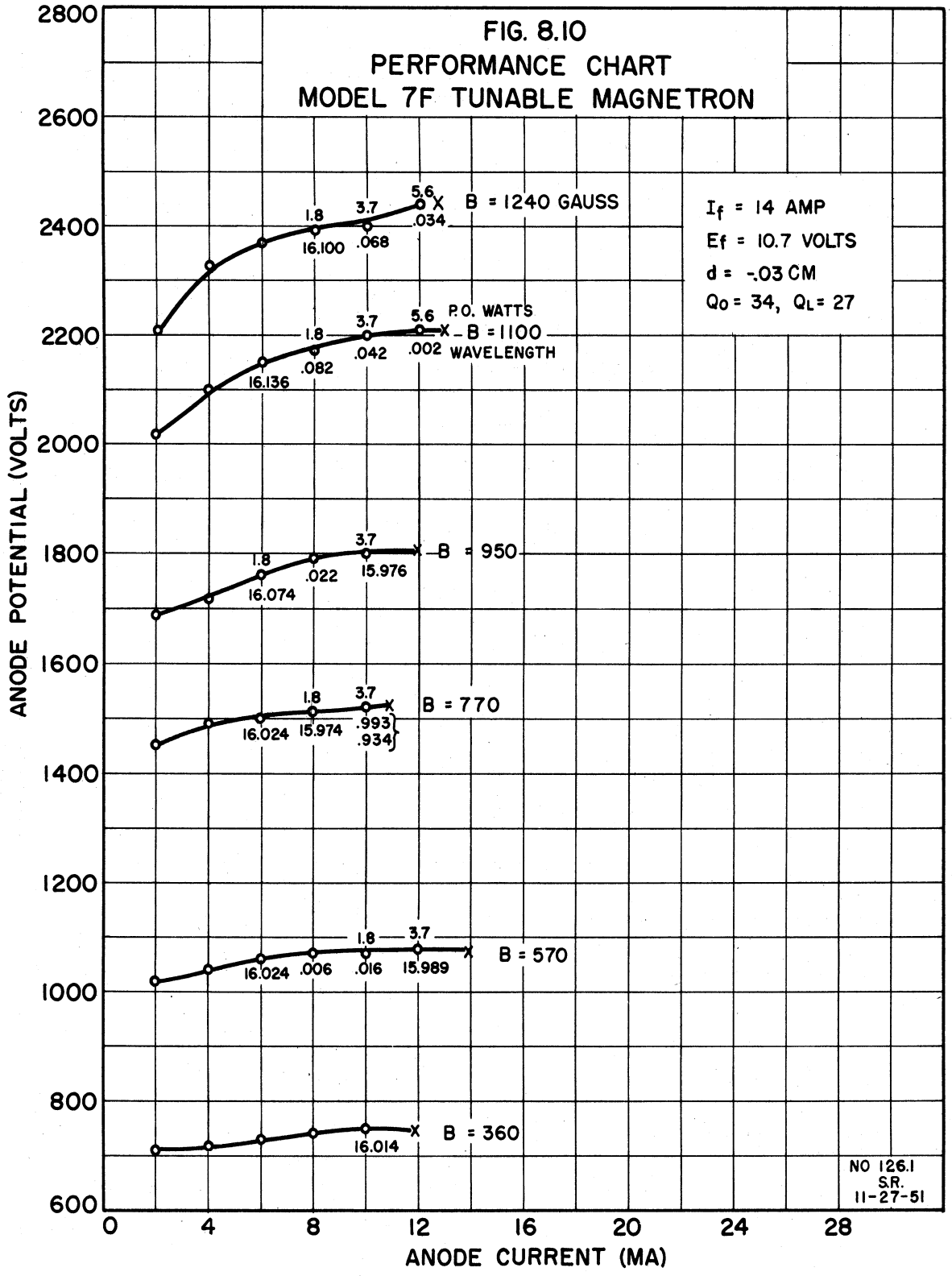
FIG. 8.10
PERFORMANCE CHART
MODEL 7F TUNABLE MAGNETRON
I_f = 14 AMP
Ef = 10.7 VOLTS
d = -.03 CM
Q_O = 34, Q_L = 27
B = 1240 GAUSS
1.8
3.7
5.6
16.100
.068
.034
P.O. WATTS
B = 1100
WAVELENGTH
16.136
.082
.042
.002
B = 950
16.074
.022
15.976
B = 770
16.024
15.974
.993
.934
B = 570
16.024
.006
.016
15.989
B = 360
16.014
NO 126.1
S.R.
11-27-51
ANODE POTENTIAL (VOLTS)
2800
2600
2400
2200
2000
1800
1600
1400
1200
1000
800
600
0
4
8
12
16
20
24
28
ANODE CURRENT (MA)

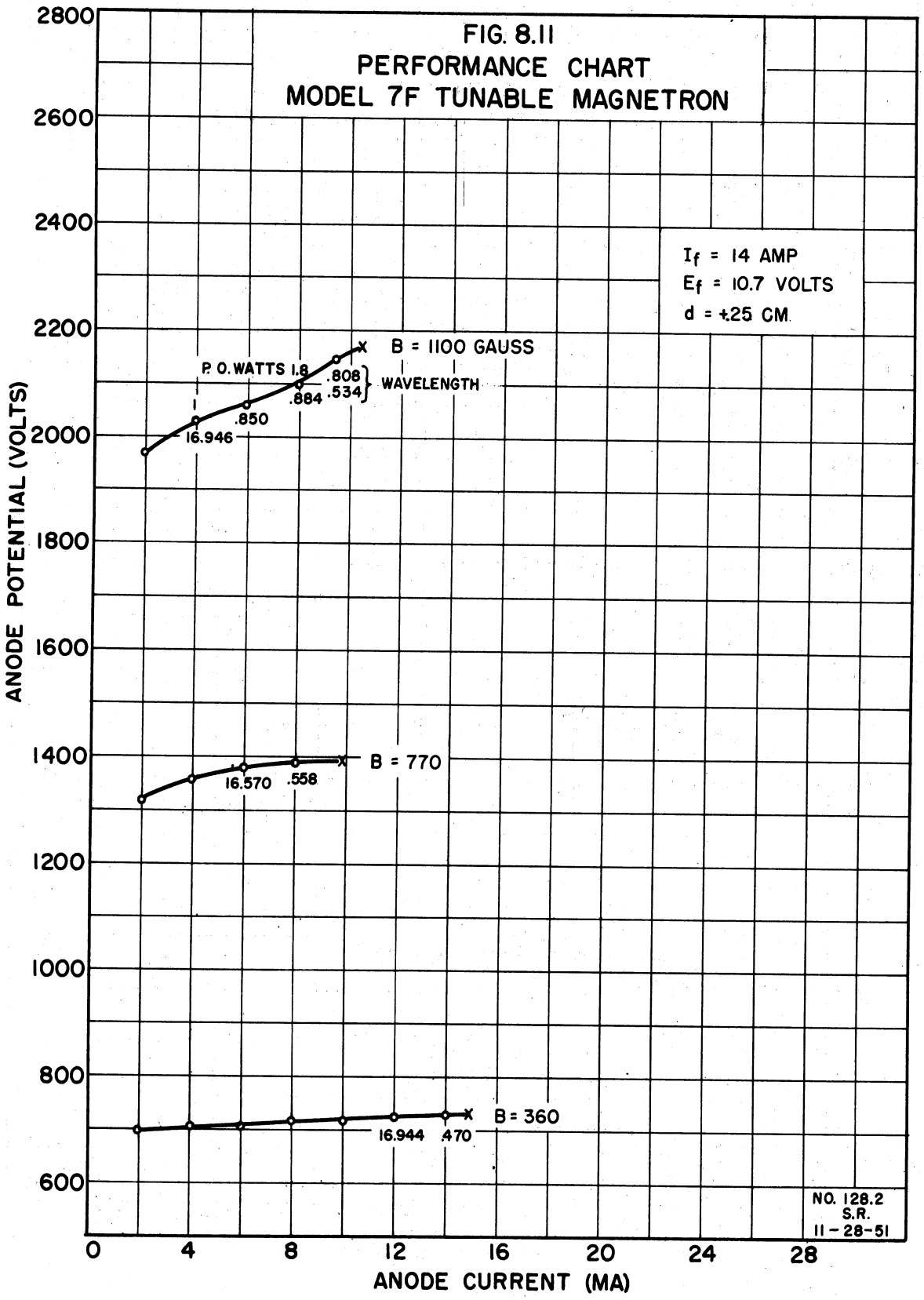
FIG. 8.11
PERFORMANCE CHART
MODEL 7F TUNABLE MAGNETRON
I_f = 14 AMP
E_f = 10.7 VOLTS
d = ±.25 CM
B = 1100 GAUSS
P. O. WATTS 1.8
.808
.884
.534
WAVELENGTH
.850
16.946
B = 770
16.570
.558
B = 360
16.944
.470
NO. 128.2
S.R.
11-28-51
ANODE POTENTIAL (VOLTS)
2800
2600
2400
2200
2000
1800
1600
1400
1200
1000
800
600
0
4
8
12
16
20
24
28
ANODE CURRENT (MA)

the distance between the lines at the second position is twice that of the first; the distance at the thid position is 3 times the first and 3/2 that of the second.

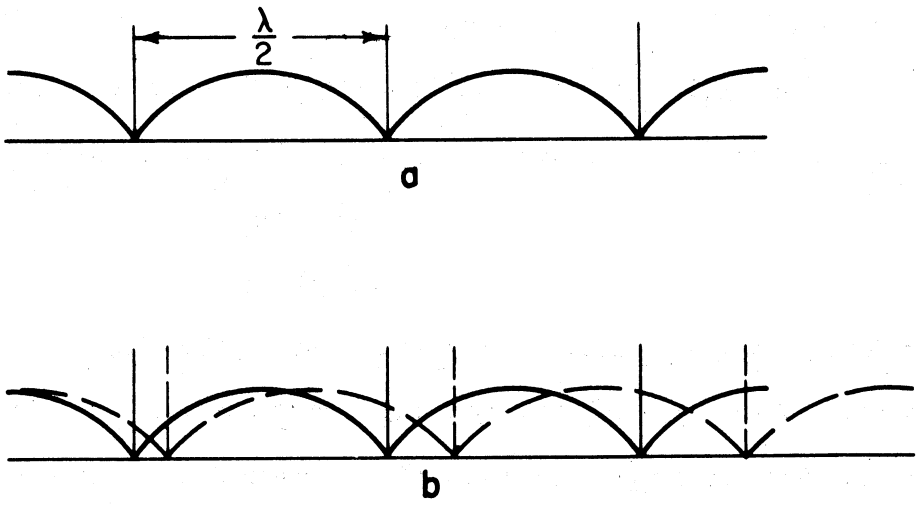

FIG. 8.12
WAVEMETER BEHAVIOR FOR SINGLE FREQUENCIES AND FOR DOUBLETS SHOWING DISPERSION INCREASE WITH PLUNGER POSITION

Now, then, it is noted that these doublets appear with large values of B and cathode-anode potential in the large current range for a particular performance curve. Observation of the characteristic in Fig. 8.8, for which the average magnetic field density, B, in the cathode-anode space is 770 gauss, shows that λ at first increases abnormally then decreases in the normal fashion. It is noted that a dip in the curve appears at this transition point. This same process is seen to occur in the next

characteristic (B = 950) where 2 successive points have λ = 14.784 cm; however, the next point is a doublet, each point being of λ less than 14.784 cm. This takes place in the other curves also, but for B = 1240, doublets appeared earlier on the curve with respect to mode jump such that measurements were made for 2 successive points, where it is seen that pushing has taken place for each part of the doublet. Fig. 8.9, for which d = - .38 cm and Q_L is less than for Fig. 8.8, shows a greater number of doublets. The B = 1100 curve is the most interesting here. λ increases in the first portion of the curve, splitting then occurs, each part of the doublet pushes, and, furthermore, the dispersion of the doublet increases when approaching the mode-jump-current boundary.

When a doublet appears, the crystal current for each part may be less than that for the single frequency of the preceeding point although the total output power is greater. This behavior is like the intensity due to 2 spectral lines which gradually disperse as shown in Fig. 8.13.

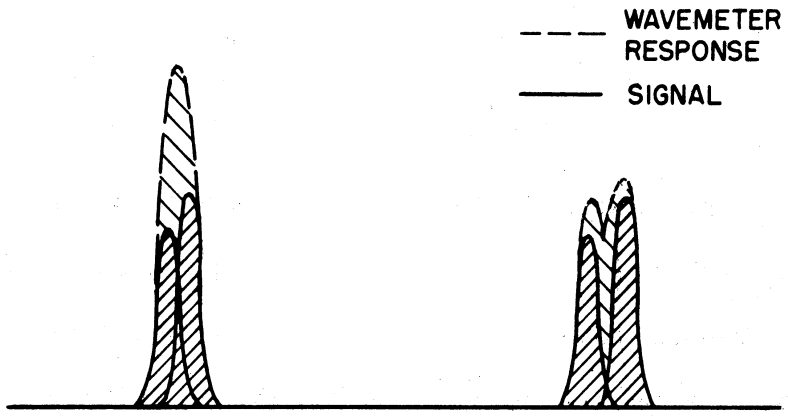

FIG. 8.13
WAVEMETER RESPONSE FOR CLOSE SPACED AND SEPARATED DOUBLETS

Note, too, that mode-jump currents decrease with lengthening cavity, or decreasing Q_L.

The performance as a function of heater power is given by Fig. 8.14. Doublets are seen to appear earlier on the performance curve as the heater power increases. Both pushing for each part of the doublet and the peculiar transition from increasing to decreasing λ occur as current increases. Fewer doublets appear as Q_L gets smaller with d larger than - .38 cm. Mode-jump current as a function of heater power is seen in Fig. 8.15.

Further analysis of this structure has been stopped in order to devote more time to voltage-tunable tubes. The above information is presented for the record to enable the resumption of the problem at a later date with the least amount of repetition.

9. Model 13 Low-Power External Cavity Interdigital Magnetron (J. Boyd)

In the study of the Model 9 structure for the application of voltage tuning at microwave frequencies, Dr. J. S. Needle has shown experimentally (Technical Report No. 11) and Dr. H. W. Welch theoretically (Technical Report No. 12) that the circuit is one of the important parameters which limits the power output of a voltage-tunable magnetron. The desirable circuit characteristics set forth in the above reports are low conductance and an inductive susceptance which varies slowly with frequency. It is concluded that if the electrons "see" the above circuit characteristics in the interaction space the generation of significant microwave voltage-tunable power is assured.

It has become apparent from the above considerations that a waveguide structure would be a more desirable circuit for the magnetron than a coaxial line. The Sylvania 3J22, an external-cavity interdigital

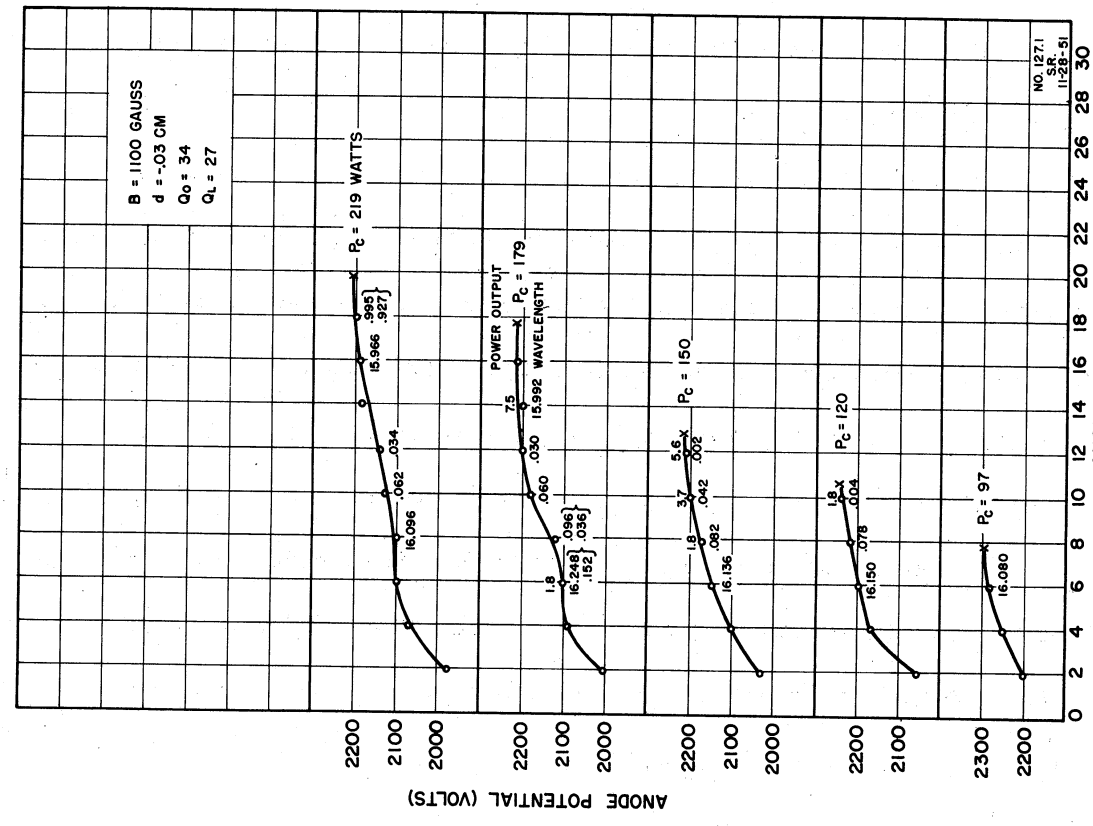

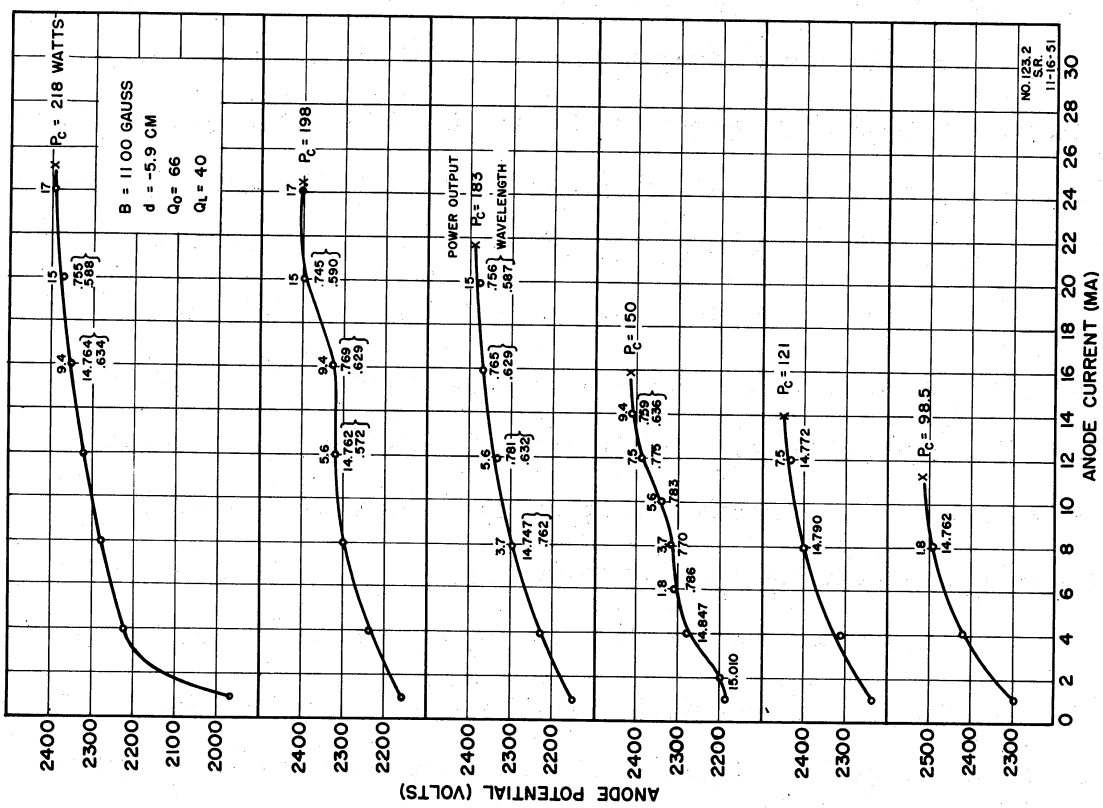

FIG. 8.14

PERFORMANCE CHARACTERISTICS VS. HEATER POWER FOR MODEL 7F NO. 55 MAGNETRON

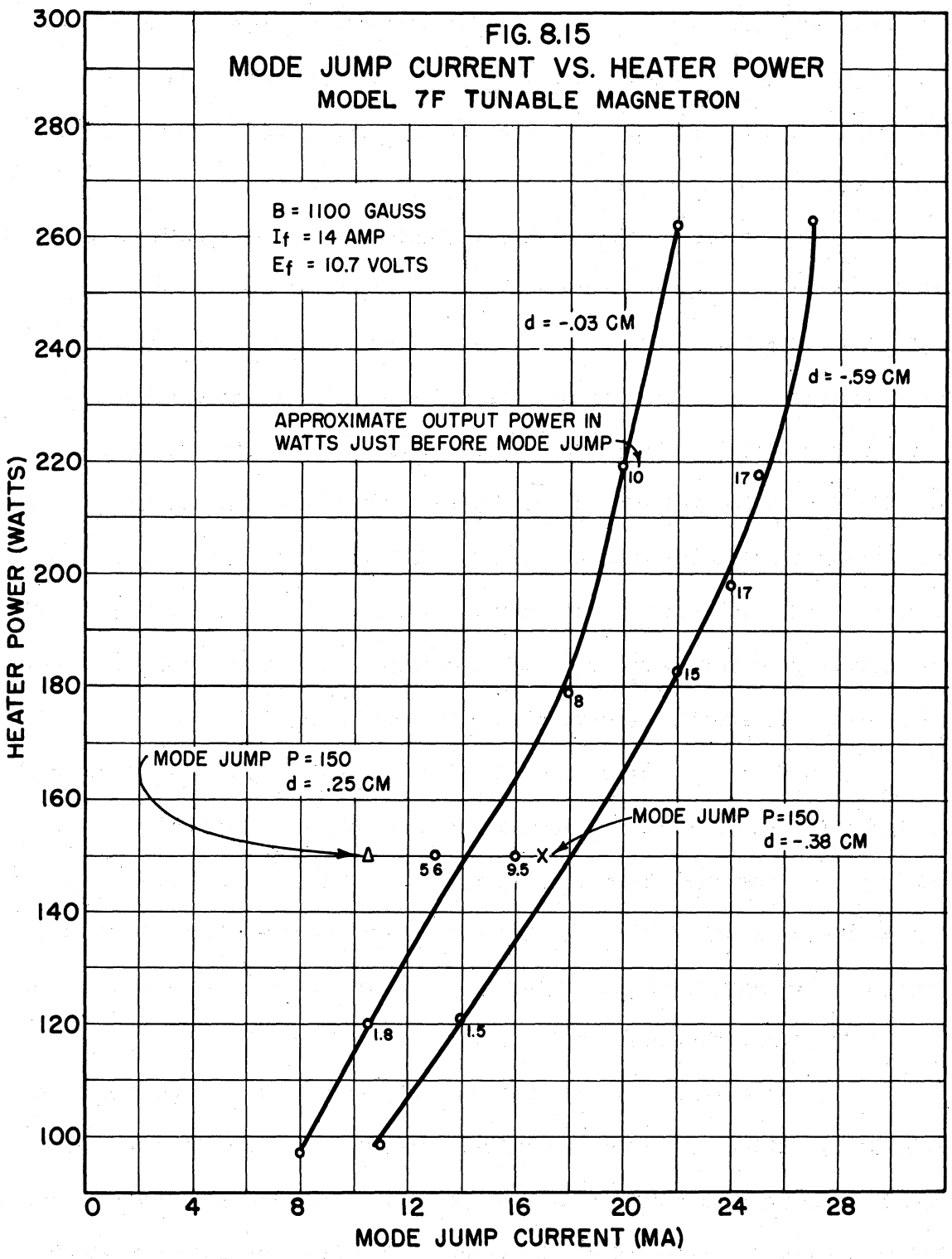
FIG. 8.15
MODE JUMP CURRENT VS. HEATER POWER
MODEL 7F TUNABLE MAGNETRON
B = 1100 GAUSS
If = 14 AMP
Ef = 10.7 VOLTS
d = -.03 CM
d = -.59 CM
APPROXIMATE OUTPUT POWER IN WATTS JUST BEFORE MODE JUMP
10
17
17
15
8
MODE JUMP P = 150
d = .25 CM
MODE JUMP P=150
d = -.38 CM
5 6
9.5
1.8
1.5
HEATER POWER (WATTS)
MODE JUMP CURRENT (MA)
300
280
260
240
220
200
180
160
140
120
100
0
4
8
12
16
20
24
28

magnetron which was designed for use in a mechanically-tunable resonator, has been used in several preliminary experiments. These experiments were conducted in order to determine the operating characteristics of this interdigital magnetron with various circuit arrangements. These experiments will now be discussed.

In the first experiment a mechanically-tunable rectangular cavity was used. The dimensions of the cavity are 2-1/2" x 5/16" x 7-1/2", the length is varied by movable plungers in both ends. The 3J22 was mounted in the center of this cavity and operating data taken for various positions of the plungers. It was found that the frequency of oscillation is determined entirely by the position of the plungers. The tube was mechanically tunable from 12 to 18 cm with a maximum c-w power output of 60 mw. This type of cavity has a high Q but does not meet the requirements of having an iductive susceptance which varies slowly with frequency. A magnetic loop-type coupling was used.

With the plungers removed and the cavity filled with steel wool, with short circuiting plates beyond the steel wool, it was possible to voltage tune the tube from 16 cm to 13.84 cm (7.8%). This range of tuning required only 100 volts change in plate voltage (from 700 to 800 volts). C-w maximum output of 140 mw was obtained. The lowering of the Q in this manner thus makes voltage tuning possible.

In the second experiment the 3J22 was mounted in the center of a 23-inch section of x-band waveguide. Magnetic loop coupling was used, the loop being placed very near the tube. The tube operated at a frequency below the cutoff frequency of the guide. Therefore the guide presented an inductive susceptance to the tube. Even though this susceptance is not

a slowly varying function of frequency it was possible to voltage tune the tube from 17.27 cm at 720 volts to 12.48 cm at 960 volts (25 per cent). A maximum c-w power output of 1.6 watts was obtained at an efficiency of 13.3 per cent; however, in the region of 14 to 15 cm the power output was too small to be measured. The fact that the wave was attenuated very rapidly in the guide was demonstrated by using shorting plungers in the guide. As expected for operating frequencies below the guide cutoff frequency, it was found that the plungers did not affect the operation of the tube until they were brought very near the tube.

For experiment three the 3J22 was mounted in a section of 3" x 1-1/2" waveguide, which was connected at each end to a tapered-ridge-to-coaxial-line junction (Fig. 9.1). One of the output terminals was connected through several feet of lossy line to a 50-ohm termination, and power for measuring was coupled out by means of the other coaxial terminal. On pulsed tests the tube was operated from 5.78 cm to 13.85 cm (41 per cent). The tube was then tested c-w and found to have operated over approximately this same range, with substantially constant power output. An attempt was made to obtain complete operating characteristics of the tube in this arrangement, however, the tube failed before these tests were completed. Other tubes will be available in the near future. The incomplete c-w operating data show that the tube tuned from 14.02 cm at 1300 volts to 10.228 cm at 1500 volts (16.5 per cent), with a power output of approximately 0.35 mw. The power output could be doubled by connecting the two output terminals together, utilizing a line stretcher to adjust the phasing for maximum power.

Further tests with this arrangement are planned as soon as more 3J22 tubes are obtained.

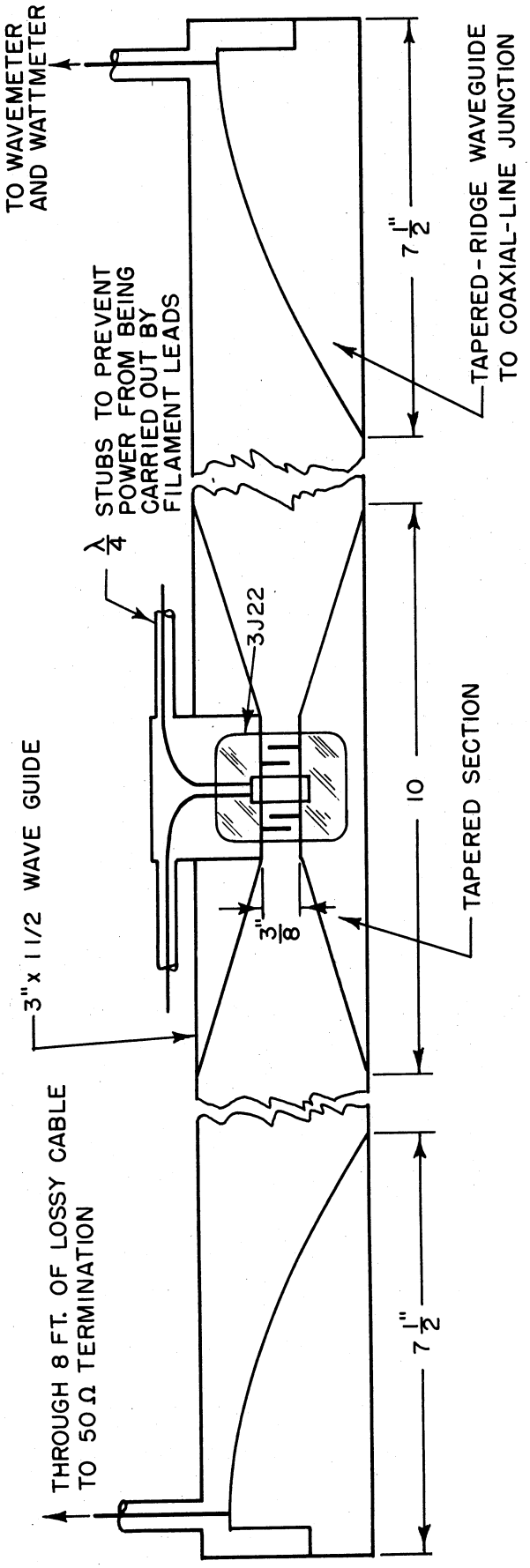

FIG. 9.1
SCHEMATIC DIAGRAM OF CIRCUIT
ARRANGEMENT USED IN EXPERIMENT NO. 3

The circuit arrangement used in experiment three seems to possess the characteristics necessary for voltage-tunable operation. With both ends of the waveguide matched to a 50-ohm coaxial line by means of a tapered-ridge waveguide, the admittance as "seen" by the electrons in the interaction space is determined by the type of termination used on the coaxial-line output terminals. The junctions used have a very wide band characteristic. Therefore, when the coaxial line is terminated in its characteristic impedance, "looking" into the waveguide the conductance is the characteristic conductance of the waveguide and the susceptance is a slowly varying function of frequency. The waveguide structure offers a good possibility of obtaining the desired low conductance. Another requirement is that the capacity between anode teeth be as small as possible.

Plans are being made to design an interdigital magnetron which will operate in an external cavity similar to that used in experiment three: The following specifications have been set up for this tube:

$E_p \leq 3000$ volts

$B < 2000$ gauss

$P_o = 5$ watts

$C_p \cong 1\ \mu\mu f$

$\lambda = 10$ cm (center frequency)

10. The Trajectron, a Tube for Study of Magnetron Space Charge (W. Peterson)

The purpose of this experiment is to attain a more complete understanding of the magnetron by studying the space charge in a smooth-bore d-c magnetron.

It is proposed to measure an electron's position as a function of time after it leaves the cathode. The tube will be used for this

work is a d-c smooth-bore magnetron with an electron gun in the same envelope arranged so that a beam of electrons can be sent into the magnetron space charge in an axial direction just grazing the cathode. The exit point of the beam will show on a fluorescent screen. This tube has been named the trajectron. A photograph of this tube appears in Fig. 10.1.

Theoretically, the Z-direction forces are independent of the r and θ displacements and velocities, and the r and θ forces are independent of the Z-position or velocity. Thus, so far as r and θ are concerned, the beam electrons move in the same manner as the emitted electrons. To find the displacement of an electron in T seconds, the beam velocity is adjusted so that the beam electrons spend T seconds in the magnetron space charge. The r and θ displacements are read from the fluorescent screen.

The first models of the trajectron were sealed-off tubes and were not successful. They were difficult to build, and difficult to modify. The kovar used in the glass seals on the early models seriously distorted the magnetic field, making it impossible to align the exploring beam, and even interferred with the operation of the magnetron diode. These tubes also became gassy after a short period of operation.

It was decided that the most expedient way of overcoming these difficulties would be to use a continuously-pumped system with teflon gasket seals. This has worked out well; the present tube is rugged, easily constructed and can be modified readily. To change a cathode, fluorescent screen, electron gun, or all three, requires only about an hour plus the time required for activation of the cathodes.

When the trajectron was first rebuilt as a continuously-pumped tube, the kovar was removed only from the magnetron diode section. The

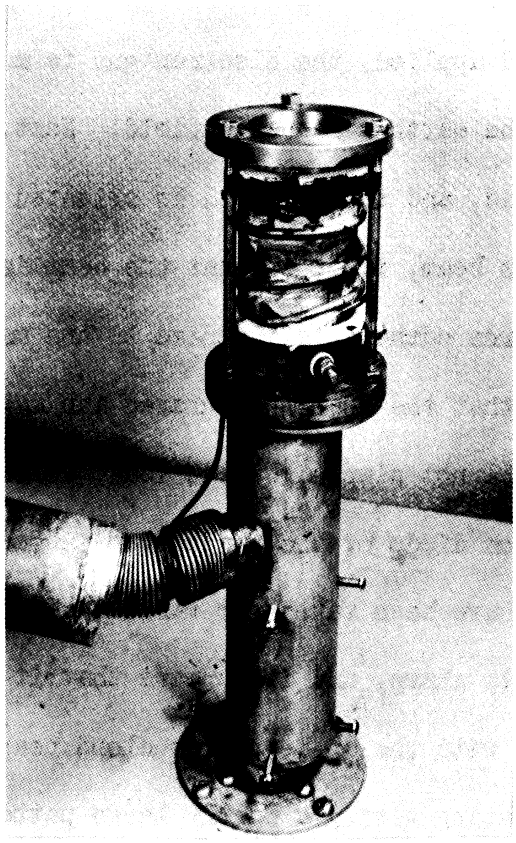

FIG. 10.1
VIEW OF TRAJECTRON NO. 3

beam still could not be aligned satisfactorily, although there was a great improvement. At this point it was noticed that the earth's magnetic field definitely affected the beam and had to be taken into account. The tube was rebuilt without any iron or kovar. In fact, there are now no glass-to-metal seals in the trajectron. The tube was also mounted in a manner so that the beam can be aligned by the following procedure: first, with no magnetic field applied, the electron gun is mounted so that the beam is parallel to the earth's magnetic field. Next, the voltage is applied to the solenoid, and the solenoid is oriented in such a way that it does not affect the beam, i.e., so that the beam is on the axis of the solenoid. The magnetron cathode is inserted in the magnetron diode, and the diode aligned so that the beam just grazes the magnetron cathode. The beam alignment is still not simple, but at least it can be achieved.

The magnetron diode of the trajectron is working well, and voltage-current data have been taken for various magnetic fields. The current cutoff is quite sharp, and it appears that it will be possible to operate the magnetron with the space-charge cloud near the anode while the electron beam is operating giving a fairly large pattern on the fluorescent screen.

The magnetron voltage-current curves indicated points of negative resistance at voltages well below cutoff. Usually a single voltage-current curve contained several such points. These points scaled with various magnetic fields in such a manner that they always occurred when the space-charge cloud was at a radius between 1.8 and 2.75 r_c. Fig. 10.2 shows a typical volt-ampere curve and Fig. 10.3 shows points where negative resitance has been observed for a wide range of magnetic field. These points

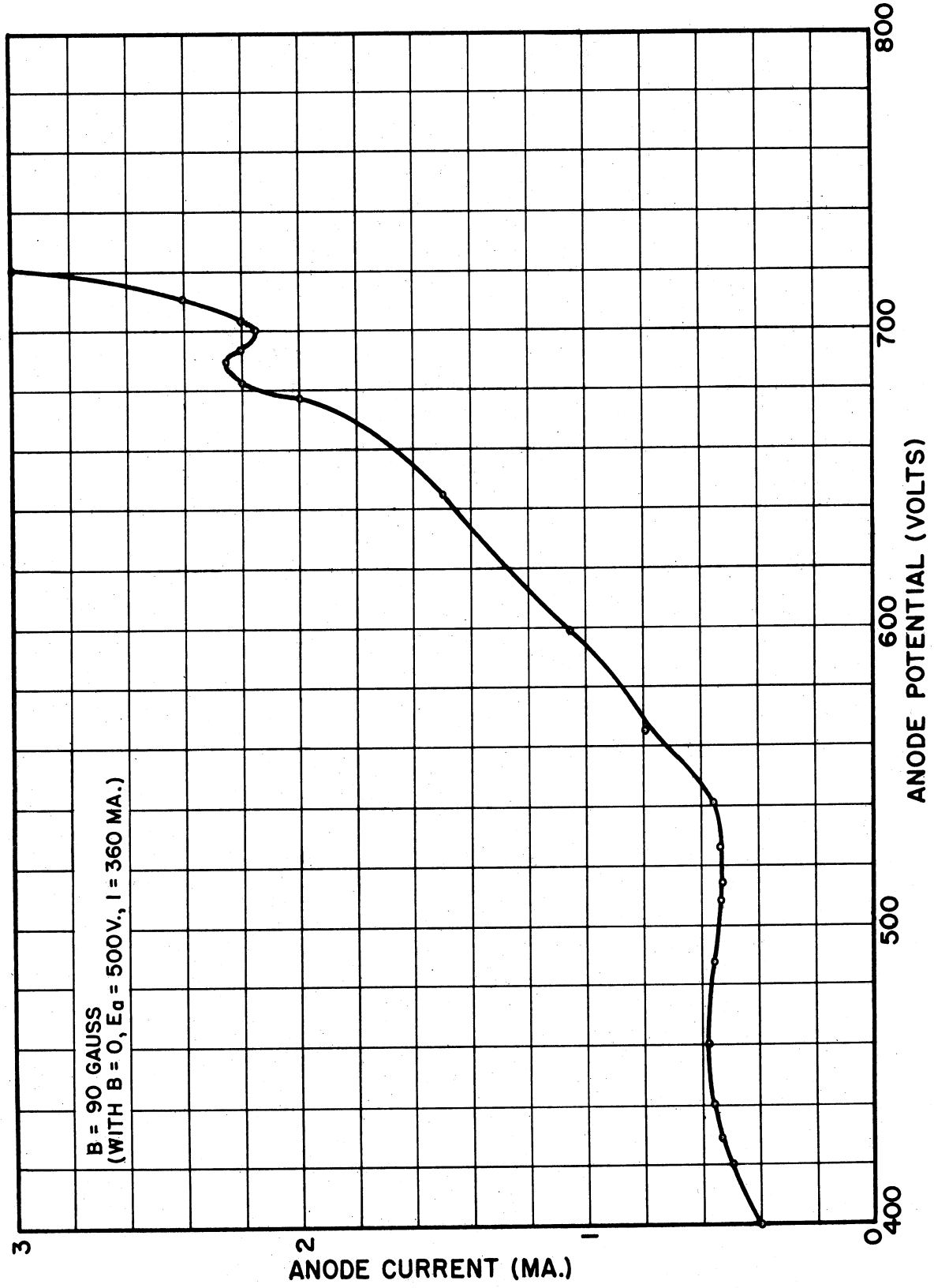

FIG. 10.2
TYPICAL MAGNETRON DIODE VOLT-AMPERE CURVE SHOWING NEGATIVE RESISTANCE

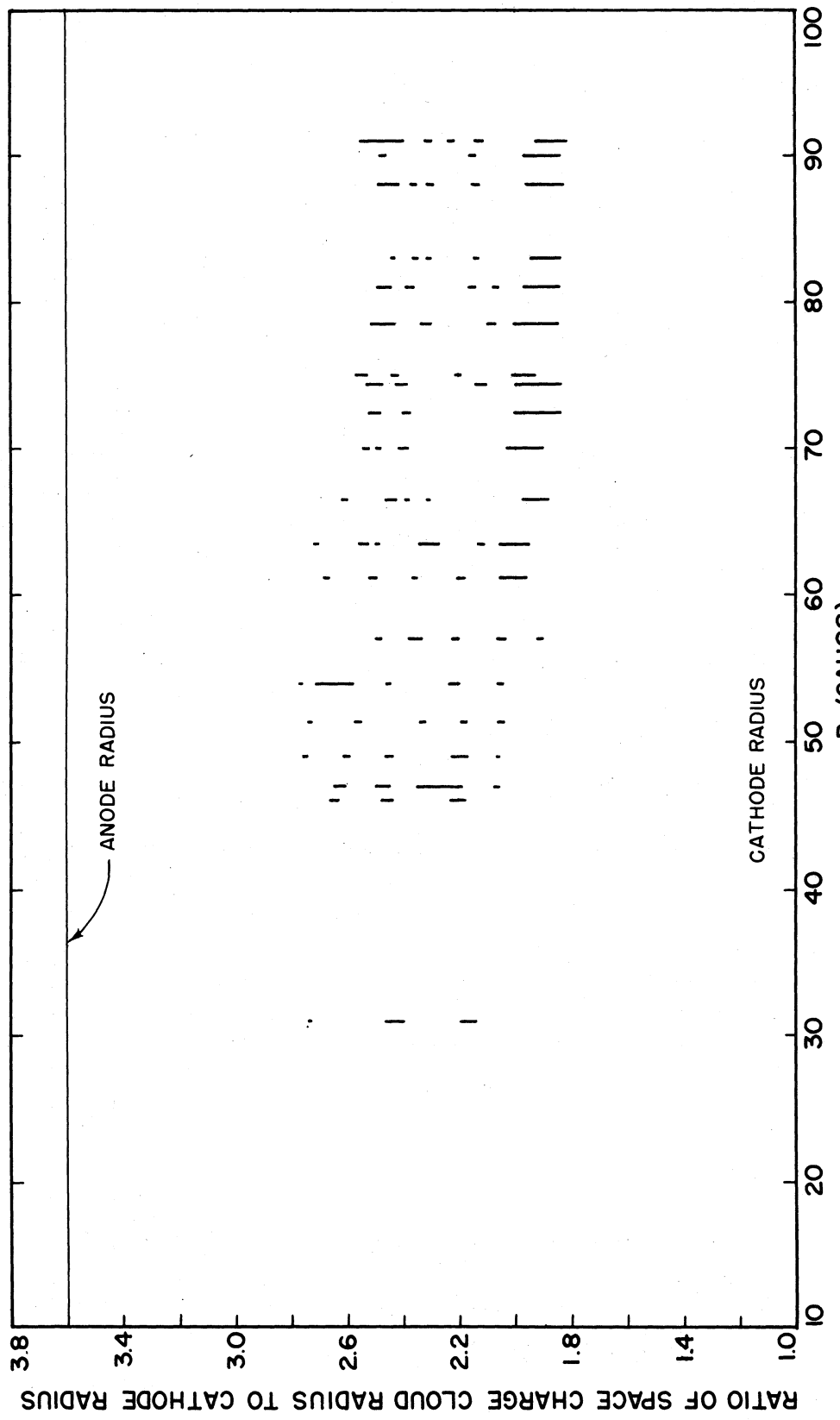

FIG. 10.3
POINTS WHERE NEGATIVE RESISTANCE HAS BEEN OBSERVED IN THE MAGNETRON DIODE

were taken with two different cathodes and with several cathode temperatures. This experiment will be repeated, and also perhaps a change in the character of the trajectories can be observed which may throw light on the cause of this phenomenon.

The electron beam has been aligned quite well and observations were made of trajectories with a dummy brass cathode in the diode section. It was found that the spot enlarged considerably when it was deflected. The trajectron was operated once with an emitting cathode, and this effect was more pronounced. Some new electron guns which will produce a better beam have been ordered. When the beam is as good as can be obtained from a conventional gun, the tube will be aligned carefully and data taken. This should certainly be during the first quarter under the ensuing contract.

IV. CONCLUSIONS

11. Summary of Results

Due to the nature of the research being done under this contract it is impossible to conclude by a given date every phase of the work. Only by a review of the results accomplished within a given period can progress be accurately evaluated. The following are considered to be the most important results of this project during the past year.

a. The study of the propagation of electromagnetic waves in a magnetron-type space charge has been completed and the results presented in Technical Report No. 8.

b. A statistical approach to the study of the space-charge equilibrium in a d-c magnetron has been completed, the results of which are presented in Technical Report No. 10.

c. The "insertion magnetron," an external cavity magnetron of new design has been built and operated. Voltage tuning has been obtained with a coherent signal from 1600 to 2600 megacycles per second. High-Q operation is also obtainable with this structure. The initial results of the study including the design and construction of the tube are presented in Technical Report No. 11.

d. A study of the dynamic frequency characteristics of the magnetron space charge including frequency pushing and voltage tuning has been completed during this period. The results of this work presented in Technical Report No. 12 have led to a considerable insight to magnetron operation.

e. The possibilities of an external cavity magnetron of the interdigital type have been studied and found encouraging. As a result of this study a magnetron has been designed principally for voltage-tunable use operating into a waveguide structure.

f. The rectangular cavity interdigital magnetron shows great promise as a high power, f-m or mechanically-tunable structure. The results obtained from the mechanically-tunable tube lead one to believe that with this structure one may obtain tuning greater than 1.2 to 1 above 7000 mc.

g. The study of the coaxial f-m structure (Models 6 and 7) has been brought to a point where this study may be conveniently stopped to be resumed at a later date. This has been done to allow more effort to be placed on voltage-tunable tubes. It is felt that this structure holds promise for an f-m tube and study should be resumed in the future.

h. The trajectron has been developed to a state where accurate measurements can be taken in the near future. Less than one third of an engineer's time has been devoted to this work.

12. Work in Prospect

The further development of voltage-tunable tubes will receive the major attention of this laboratory. Problems involving the control of noise of these structures and the increase of power output will be stressed. The Model 13 interdigital structure for waveguide operation will be developed as part of this program. The Model 8 rectangular tube will continue to receive attention since it appears to have excellent possibilities as an f-m structure, a high-power structure or a mechanically-tunable structure. The trajectron study will be continued at its present reduced rate and is to be the only experimental work connected directly with the general understanding of magnetron behavior.

APPENDIX

V. APPENDIX

13. Tubes Constructed Within the Period Covered by this Report (R. F. Steiner)

Tubes constructed in the period covered by this report are presented in Table 13.1. Construction was started on twenty different tube structures. Sixteen tubes were operated hot on the test bench and fourteen are still operable. Three tubes were lost during construction and one tube was only partially constructed for display purposes. Of the two tubes which were operated, but at present inoperable, one failed due to an extremely small leak and the other has a burned out cathode.

14. New Laboratory Facilities (J. R. Black)

Two new rooms have been added to the University of Michigan Vacuum Tube Laboratory space in this period. Each of the new rooms has a floor space of approximately 260 square feet bringing the total floor space of the laboratory to 2900 square feet.

Most of the laboratory facilities are described in Technical Report No. 7 along with pictures of the equipment. Approximately two-thirds of the equipment in the laboratory has been provided by the University of Michigan while the remainder has been provided by the Signal Corps. It should be pointed out that this laboratory enjoys the position of being able to draw on the laboratory equipment and facilities of the entire University.

Fig. 14.1 is an overall view of one of the new laboratory rooms in which the voltage-tunable magnetrons are tested. A close-up

TABLE

Tube No.	Model No.	Date Assembled	History	Operated	Present Condition
45	7E	11-50	1. Tube became gassy - repumped	Yes	Operable
46	Experimental Space Charge Study	1-51	1. Tube became gassy - repumped	Yes	Operable
47	Experimental Space Charge Study	2-51		Yes	Inoperable
48	9C	3-51	1. Has Model 13 oxide cathode	Yes	Operable
49	9B	3-51	1. Has tungsten cathode	Yes	Operable
50	9B	4-51	1. Originally used Model 19 tungsten cathode 2. Leak repaired 3. Replaced cathode with Model 22 oxide cathode	Yes	Operable
51	9B	4-51	1. Tube lost in construction - over-heated during glassing	No	Inoperable
52	9B	5-51	1. Has Model 24 cathode (Tungsten with magnetic pole pieces) 2. Glass seal cracked due to heat shock from cathode heater	No	Inoperable
53	9B	5-51	1. Cone-shaped tungsten cathode	Yes	Operable

TABLE I3.1 (Cont'd)

Tube No.	Model No.	Date Assembled	History	Operated	Present Condition
54	9B	7-51	1. Lost due to overheated anode bars during glassing	No	Inoperable
55	7F	6-51	1. Has Model 23 cathode 2. Sparking occurred due to cathode being inserted too far 3. Tube repaired	Yes	Operable
56	8B	6-51	1. During operation cathodes opened	Yes	Inoperable
57	9B	11-51	1. Inserted "L" cathode (heater shorted) 2. Inserted nickel cathode having 1/16" x .200" slot	Yes	Operable
58	9B	8-51	1. Has Model 24 cathode	Yes	Operable
59	9B	10-51	1. Has oxide cathode with 100 x 100 Ni mesh	Yes	Operable
60	9D	7-51	1. Has Model 22 cathode	Yes	Operable
61	9B	7-51	1. Tube used for display (only partially assembled)	No	Inoperable
62	9B	7-51	1. Originally used "L" cathode (heater shorted) 2. Replaced with Ni cathode having 100 x 100 mesh Ni strip 1/16" x .200 sintered on axial direction	Yes	Operable
63	8C	9-51	1. Had to be continuously pumped because of porous copper, old cavity parts were used for this tube	Yes	Operable

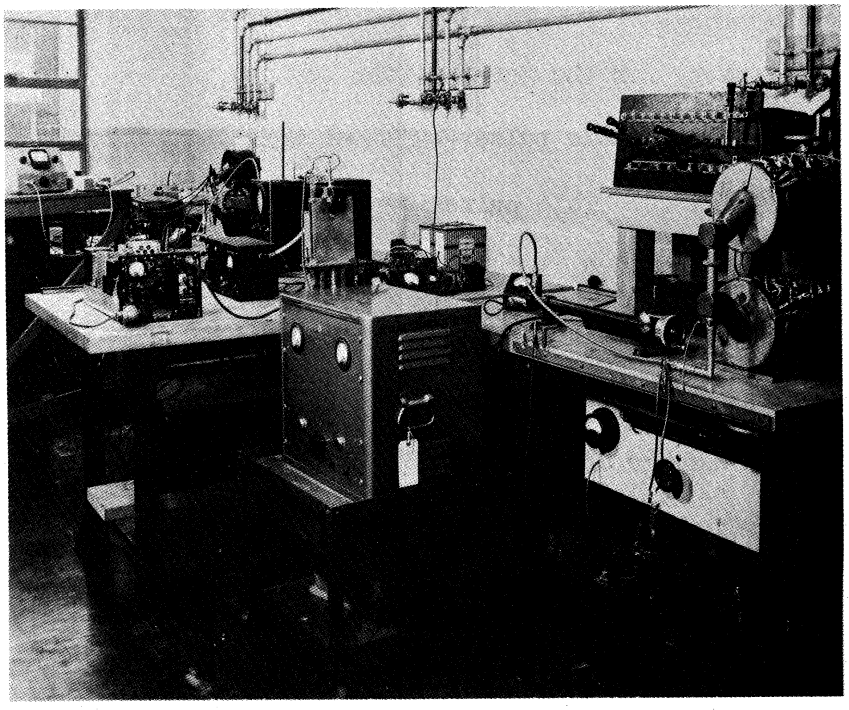

FIG. 14.1
GENERAL VIEW OF ROOM 3515

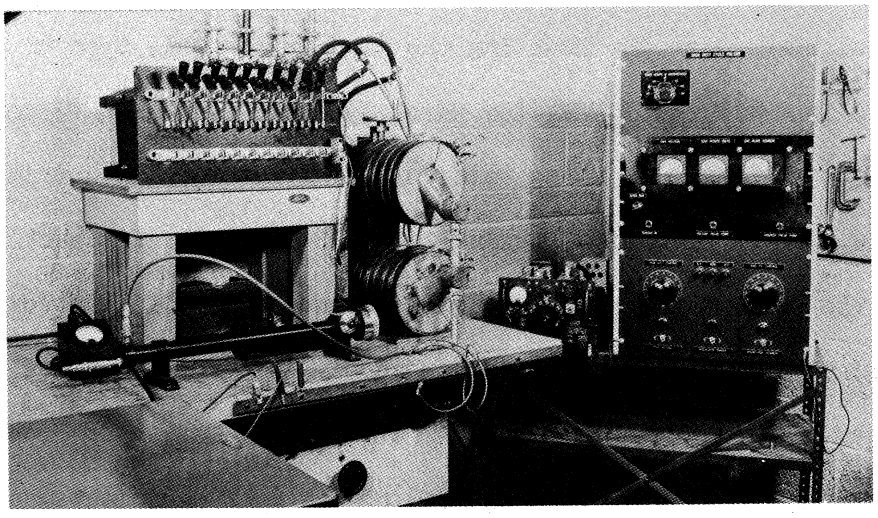

FIG. 14.2
MODEL 9 COAXIAL TEST BENCH

view of the equipment to the right of this picture is given in Fig. 14.2 showing a test setup for the Model 9 tube series.

A high-duty cycle pulser built at this laboratory is shown to the right of Fig. 14.2. This pulser is designed to produce a substantailly square pulse of 0.5, 1.0, 2.0, 20, 50, 100 and 120 microsecond duration. The voltage is continuously variable from 0 to - 8000 volts and the maximum current is 3 amperes.

At the center of Fig. 14.2 is shown an electromagnet and cavity for the Model 9 series of magnetrons. The electromagnet, built at this laboratory, is capable of producing 10,000 gauss across a 1" gap using 1-1/2 inch diameter solid pole pieces. The gap width between the pole pieces is variable between zero and 8 inches by means of the wheel shown at the top of the magnet yoke.

To the left of the electromagnet (Fig. 14.2) can be seen a resistance control box for the electromagnet and a coaxial wavemeter.

Fig. 14.3 shows a close-up view of a Model 9 test set employing a parallel plane line for mounting the magnetron. This type of line is described in the Proc. I.R.E. for March 1950[1] and is a transformed coaxial line. The advantage of using this form of line over the coaxial type is in its ease of mechanical tuning. An APR-5-A and a filament supply are seen on the bench alongside the parallel-plate line. In the foreground is a General Electric regulated power supply used for the plate voltage source.

Fig. 14.4 is a close-up view of the test equipment used for the investigation of the operation of an interdigital magnetron in a waveguide.

---

1 W. B. Wholey and N. Eldred, "A New Type of Slotted Line Section," Proc. I.R.E., Vol. 38, No. 3, March 1950.

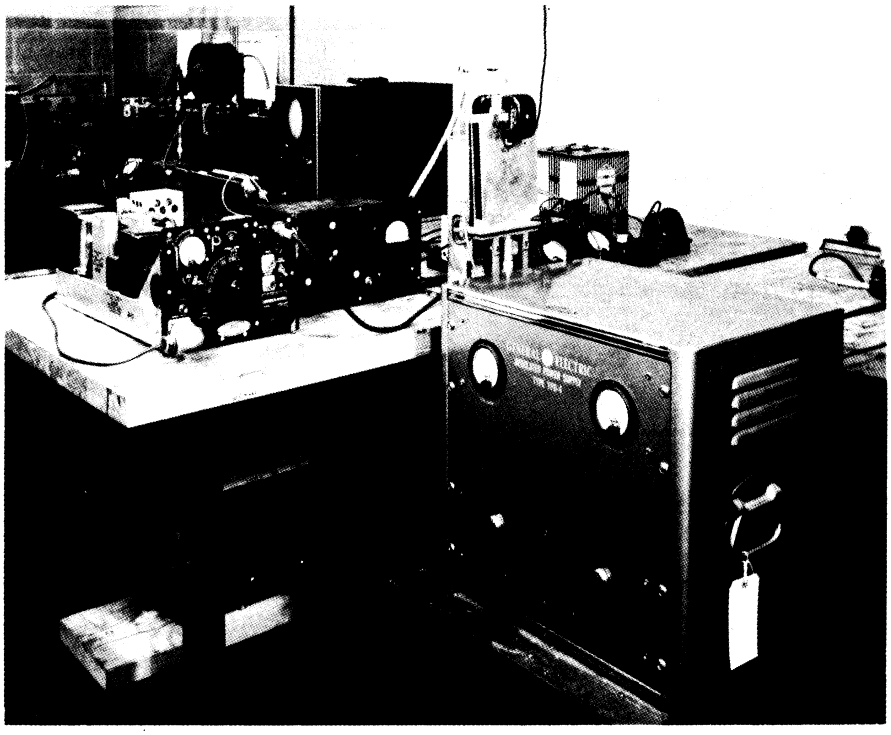

FIG. 14.3
MODEL 9 PARALLEL PLATE TEST BENCH

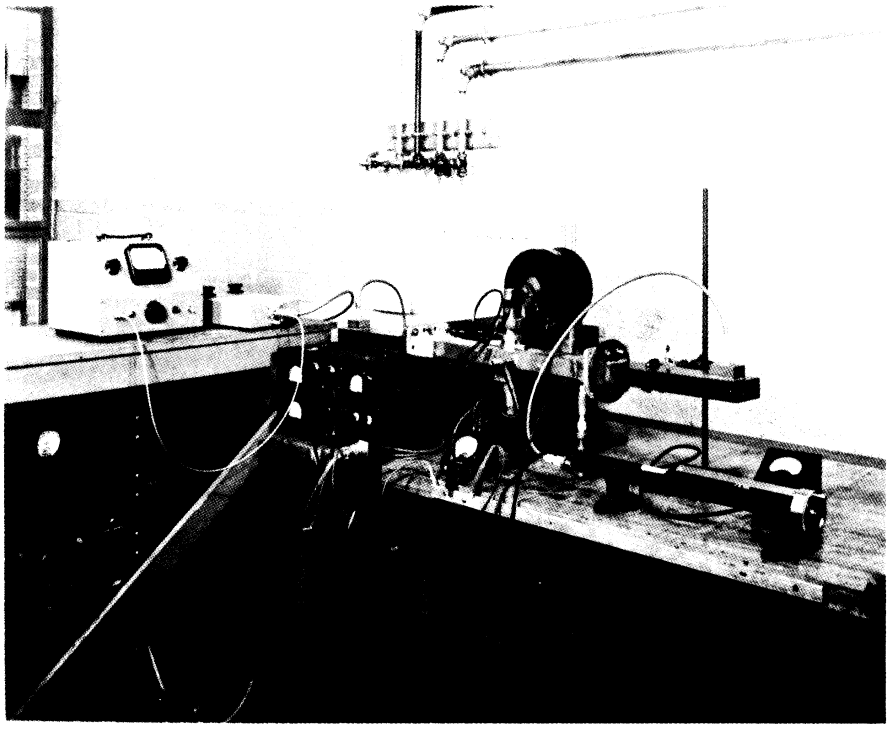

FIG. 14.4
WAVEGUIDE ARRANGEMENT FOR
INTERDIGITAL MAGNETRON

This is the equipment shown at the rear of the room in Fig. 14.1. A schematic drawing of this waveguide circuit arrangement is given in Fig. 9.1. On the bench in front of the electromagnet can be seen the filament supply for the magnetron. On the table to the left is a Hewlett-Packard Bolometer Mount, Model 430A and a tunable Bolometer Mount, Model 475B. Beneath this table is a high voltage plate supply.

Figs. 14.5 and 14.6 show the test equipment installed in room 3506-A. This room had been built into the assembly laboratory room and originally was used for desk space when theoretical work was emphasized.

The test bench in Figs. 14.5 and 14.6 is arranged for either hot testing or cold testing magnetrons. Two electromagnets are shown in these photographs for use with the Model 8A double anode high power magnetron. A General Radio slotted line used for cold tests can be seen on an adjustable r-f line carriage. This carriage makes possible the convenient use of either the small cold test coaxial line, a high-power coaxial line or a waveguide. Two combination filament supplies and magnet controls are shown at the back of the bench. A Model ISS-4SE, Type 107 spectrum analyzer mounted on a movable table to the left of the electromagnets is employed for cold tests. A Model 707-B oscillator using a waveguide structure tuner built at this laboratory can be seen in front of the spectrum analyzer where it is used as a local oscillator.

To the far left of Fig. 14.5 is shown a portion of a power supply used for hot tests which has a variable voltage output up to 15,000 volts at 7.5 kva.

New space has been acquired for welding facilities, the power hack saw, the metal cutting band saw, the sand blaster, and for the storage

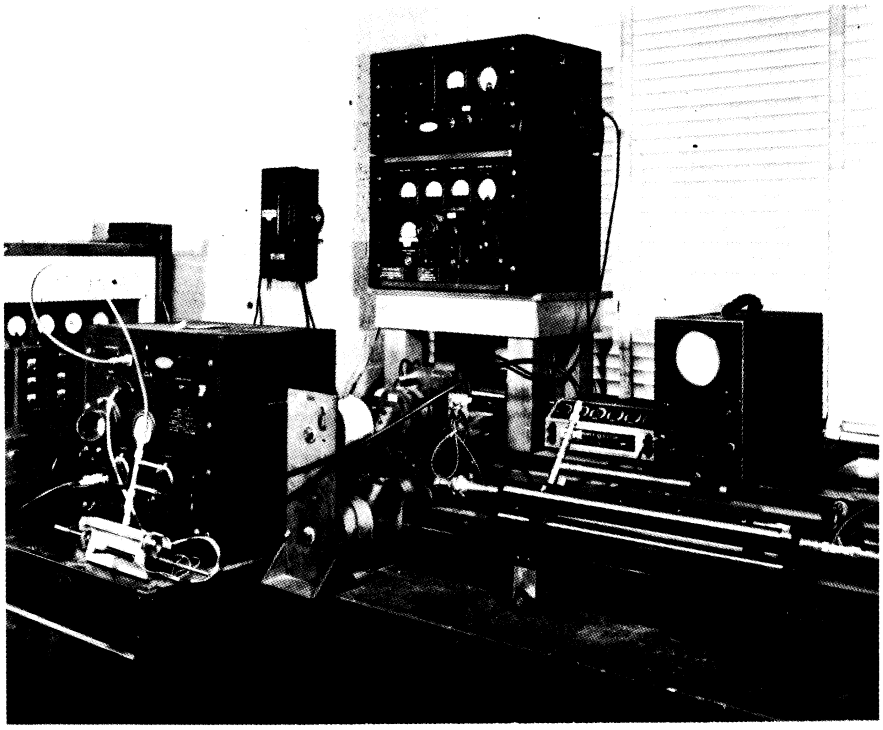

FIG. 14.5
VIEW OF TEST BENCH IN ROOM 3506 - A

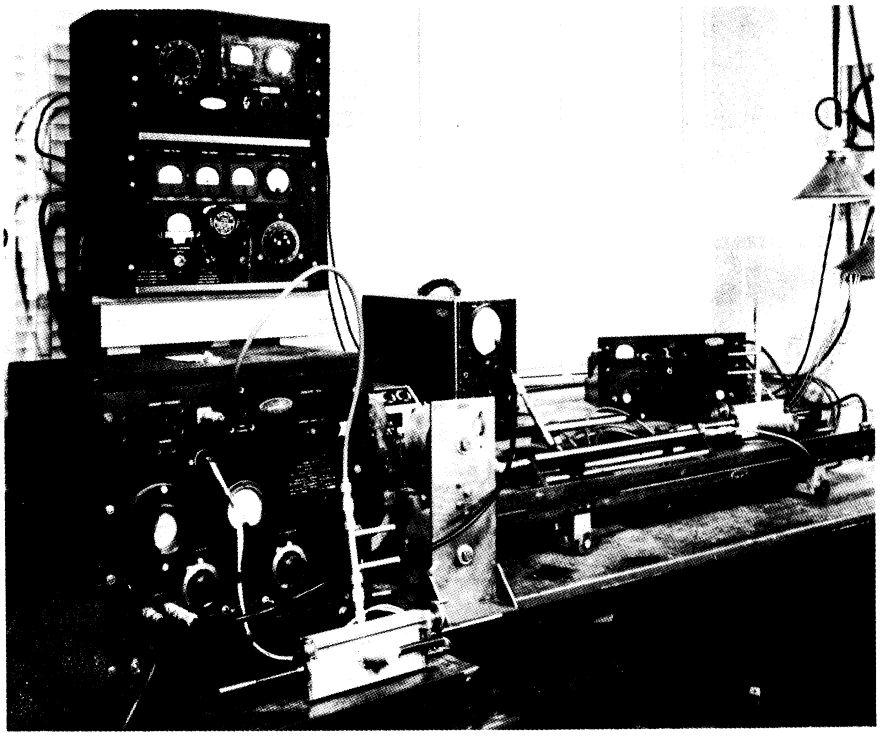

FIG. 14.6
TEST BENCH IN ROOM 3506-A

of stock for the machine shop. The space made free in the machine shop by this new storage space is utilized by a Monarch 10" tool makers' lathe and a LeBlond 16" lathe.

15. Construction Techniques (R. F. Steiner)

Most of the construction techniques employed at the University of Michigan Vacuum Tube Laboratory are of standard type well known to the art. These are discussed in Technical Report Nos. 3 and 7. The assembly of the Model 9B, however, was thought unique and is presented here:

Assembly of Model 9B Insertion Magnetron

An assembly drawing of this tube is presented in the Appendix.

Brazing Operations

Three gold-copper solder (37% Au) brazes are required to assemble this tube.

1st braze: Anode bars (Part 3) to kovar cylinder (Part 7) in the H_2 bottle.

2nd braze: Anode vanes (Part 5) to the outer anode ring (Part 2) are brazed at 1040°C in the vertical two-chamber H_2 furnace.

3rd braze: The subassemblies from the first two brazing operations are assembled together and the copper ring (Part 6) is brazed to the ends of the bar anode. This final braze is made at 1020°C in the vertical two-chamber furnace.

In the first braze the parts are mounted on a pre-oxidized stainless steel jig which holds them in accurate alignment. One ring of .015 inch Au-Cu wire is used.

The second braze uses a stainless steel jig with accurately machined radial slots which align the copper vanes axially and

longitudinally relative to the outer anode ring. One small U-shaped .015 inch Au-Cu wire is dropped over each vane and forced against the outer anode ring with U-shaped stainless steel wires to insure proper wetting of the parts.

The final braze is accomplished by using a .0015 inch Au-Cu washer between the anode bars and the anode cap. A stainless steel alignment jig is used to keep the outer anode ring assembly from touching the center conductor assembly, while the anode cap is being brazed.

Glassing Procedure

The glassing of this tube requires six steps. In the first step (Fig. 15.1-A) the vane anode kovar cylinder is held securely by means of a specially made split stainless steel jig held in the headstock of a Model F Litton glass lathe. The center conductor of the tube is held accurately in a chuck at the tailstock end of the lathe.

A glass cylinder 1/16" long cut from standard 7052 glass tubing to fit over the 5/16" kovar center conductor is sealed to the kovar 1/16" away from the copper of the bar anodes. Heat is applied mostly to the kovar to insure proper sealing of the glass. Caution must be taken in making seal to prevent the copper anodes from the melting.

The second step shown in Fig. 15.1-B uses the same jig for holding the vane anode kovar cylinder in the lathe headstock while the tailstock chuck is replaced with a wooden collet which holds the proper size glass for sealing to this kovar cylinder. The kovar center conductor is held in position by a longitudinally-slotted kovar cylinder which just fits inside the center conductor. A .050 nickel wire bent into an S shape is spotted to one end of this slotted kovar cylinder to keep the

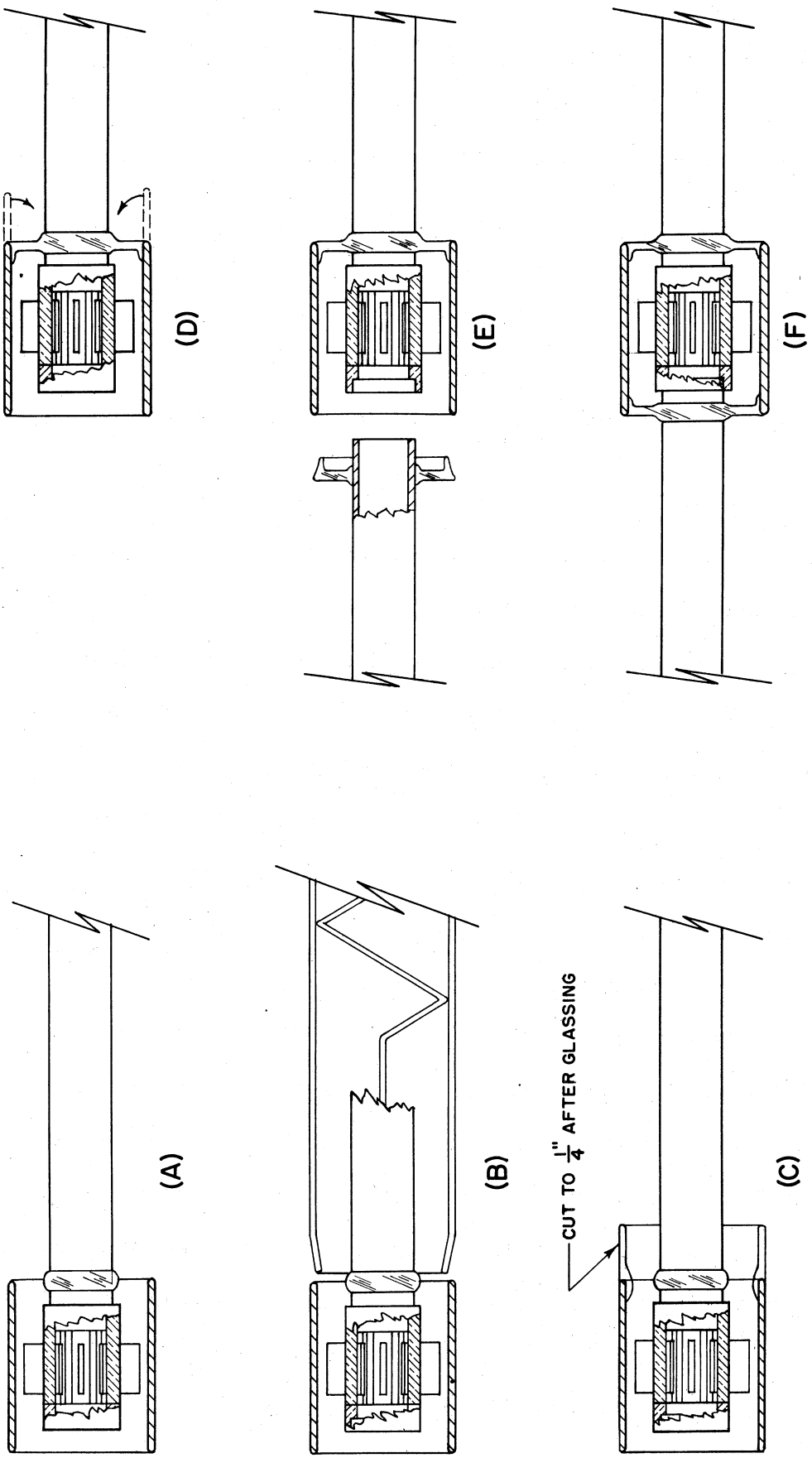

FIG. 15.1
MODEL 9B MAGNETRON ASSEMBLY GLASSING OPERATION

far end of the kovar center conductor in line while the galss is sealed to the vane anode kovar cylinder. The kovar is pre-oxidized on the inside to a depth of approximately 1/8 inch. The glass tubing is then tapered slightly on the end, placed inside the kovar which is then heated until the glass wets to it securely. Care must be taken not to heat the outer kovar near its center, since this would damage the Au-Cu braze joint to the anode vanes.

After the above described glass-metal seal is made the glass is cut with a torch to about 1/4 inch length (see Fig. 15.1-C) in preparation for the fourth operation of sealing the outer glass cylinder to the glass bead on the center conductor.

In this fourth step the tube is held as described in the first operation. Scribed lines on the center conductor and the outer kovar cylinder facilitate azimuthal alignment. A split stainless steel jig machined to simultaneously fit both diameters of the tube is used to locate the scribed lines accurately. Longitudinal alignment is checked with a dial indicator. The center conductor is pulled out .012 inch beyond its final desired position to allow for differential expansion while glassing.

After the glass has been brought to a workable temperature a flat graphite paddle is used to lap the glass down to the glass bead on the center conductor. When this point is reached heat is then applied to the kovar near the glass bead to assure a good seal. Meanwhile paddling continues until a straight seal is reached. Uniformity of the thickness of the disc seal can be controlled by applying heat where thicker glass is needed using the speed of the lathe to throw the glass outwardly or inwardly, whichever is required.

This glass disc seal being a compressive type seal is cooled and annealed outward from the center conductor. This type of annealing insures a very strong seal.

In order to accomplish the fifth step shown in Fig. 15.1-E a glass disc is sealed to the slipt fit end of the center conductor kovar cylinder. This is done by holding the kovar tubing in one end of the lathe and a piece of glass tubing in the other end, sealing the glass to the kovar, and blowing the glass out against a specially made carbon form held firmly on the lathe. The glass is then cut with a torch, to form the disc shown.

The tube is now ready for the final step in assembly as shown in Fig. 15.1-F. Two torches are needed in order to heat the tube properly and to anneal it. One torch is used to gently heat the center conductor at the first glass seal. Meanwhile the second torch is used to gradually heat the slip fit center conductor in preparation for sealing the glass disc to the outer kovar cylinder. When the glass is hot the torch is then directed on the outer kovar cylinder which is oxidized and heated to a bright red while the glass disc is pushed into place. The glass wets the kovar and then is further heated to create a uniform thickness throughout the disc seal. The slip fit end is not inserted all the way. A .012 gap is maintained here. Both torches are used in the annealing process using the same method as that of step 4. Annealing from the center conductors, to the glass, and then to the outer kovar cylinder makes a strong compressive kovar-to-glass seal.

Chemical Cleaning of the Tube

The tube is placed in a warm solution of Oakite No. 32 for five minutes, washed in distilled water and then immersed in a solution of

bright dip (8 parts H_2SO_4, 4 parts H_2NO_3, and 1 part of H_2O) for one-half minute. The tube is then rinsed in distilled water. If any oxide remains the tube is again immersed into the Oakite solution.

Finally the tube is thoroughly rinsed in distilled water followed by a methanol rinse. Clean compressed air is used to dry the tube.

SECTION 16

ASSEMBLY DRAWINGS OF TUBES AND SPECIAL CAVITIES

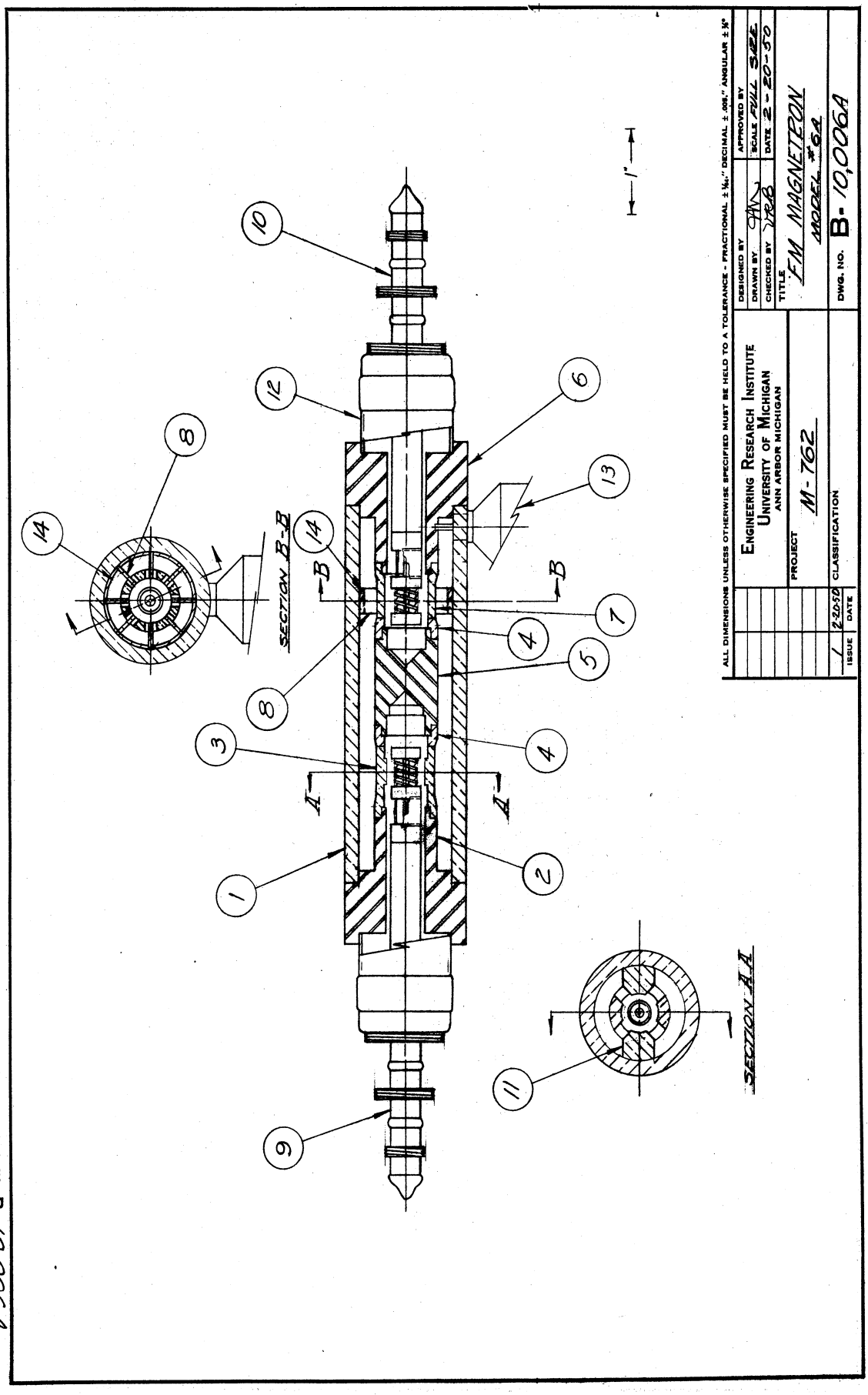
SECTION B-B
SECTION A-A
1"
ALL DIMENSIONS UNLESS OTHERWISE SPECIFIED MUST BE HELD TO A TOLERANCE - FRACTIONAL ± 1/64," DECIMAL ± .005," ANGULAR ± 1/2°
ENGINEERING RESEARCH INSTITUTE
UNIVERSITY OF MICHIGAN
ANN ARBOR MICHIGAN
PROJECT M-762
DESIGNED BY
DRAWN BY JAW
CHECKED BY
APPROVED BY
SCALE FULL SIZE
DATE 2-20-50
TITLE FM MAGNETRON MODEL #64
ISSUE 1
DATE 2-20-50
CLASSIFICATION
DWG. NO. B-10,006A
DWG. NO. B 10,006A

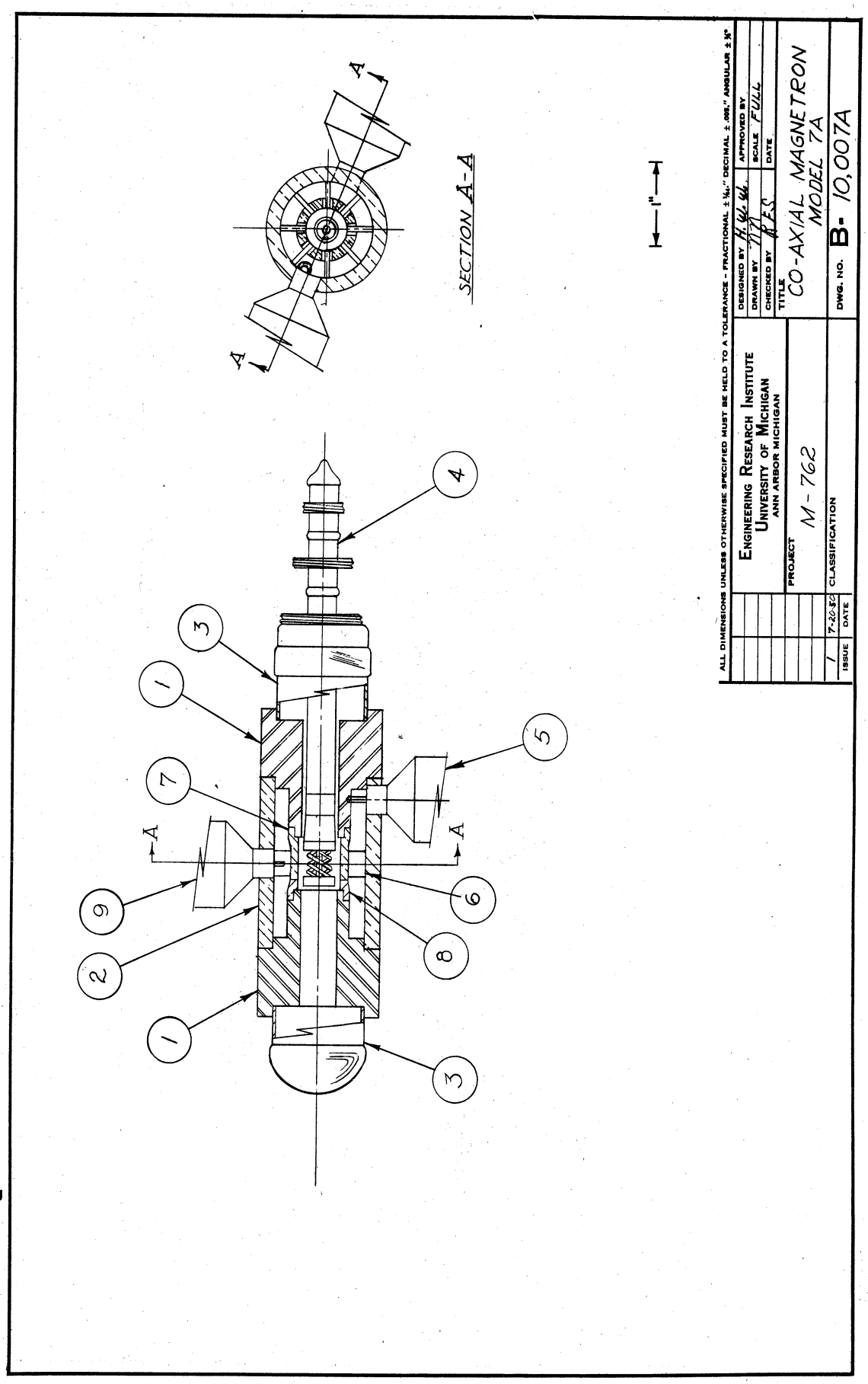

ALL DIMENSIONS UNLESS OTHERWISE SPECIFIED MUST BE HELD TO A TOLERANCE - FRACTIONAL ± 1/64" DECIMAL ± .005" ANGULAR ± 30'

ENGINEERING RESEARCH INSTITUTE
UNIVERSITY OF MICHIGAN
ANN ARBOR MICHIGAN

PROJECT M-762

ISSUE	DATE	CLASSIFICATION
1	7-20-52	

DESIGNED BY H.W.W.
DRAWN BY W.F.S.
CHECKED BY R.E.S.
APPROVED BY
SCALE FULL
DATE

TITLE CO-AXIAL MAGNETRON MODEL 7A

DWG. NO. B-10,007A

DWG. NO. B

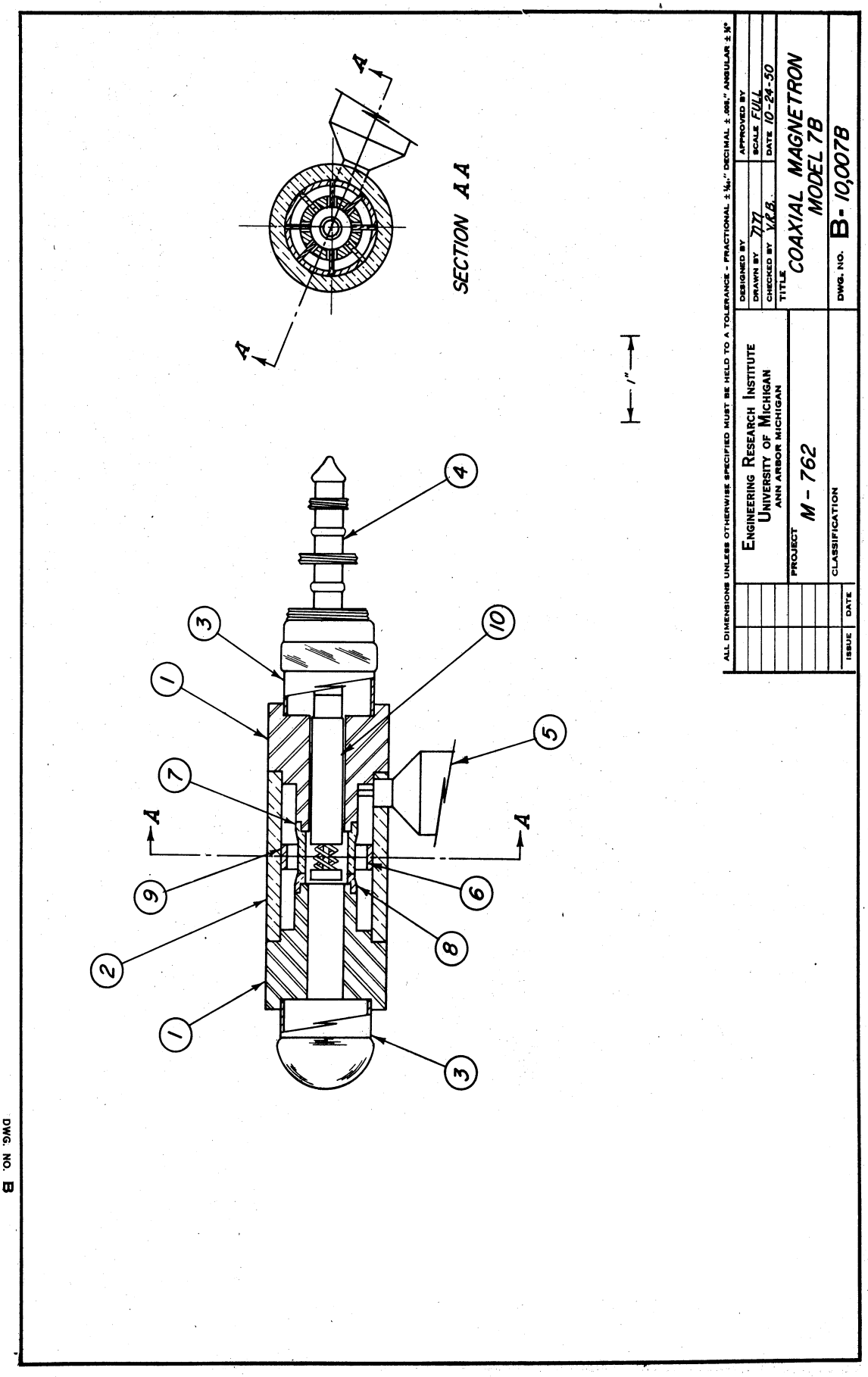
SECTION A A
A
A
1
2
3
4
5
6
7
8
9
10
1"
ALL DIMENSIONS UNLESS OTHERWISE SPECIFIED MUST BE HELD TO A TOLERANCE - FRACTIONAL ± 1/64" DECIMAL ± .005" ANGULAR ± 1/2°
ENGINEERING RESEARCH INSTITUTE
UNIVERSITY OF MICHIGAN
ANN ARBOR MICHIGAN
PROJECT M - 762
CLASSIFICATION
ISSUE
DATE
DESIGNED BY
DRAWN BY ZIZZ
CHECKED BY V.R.B.
APPROVED BY
SCALE FULL
DATE 10-24-50
TITLE COAXIAL MAGNETRON MODEL 7B
DWG. NO. B-10,007B
DWG. NO. B

1 - POLE PIECE (HRS)
2 - CAVITY SHELL (CU)
4 - CATHODE CONNECTIONS
5 - OUTPUT PIPE
6 - FILLER RING (FOR MODE SEPARATION)
7 - CAVITY CENTER CONDUCTOR
10 - CATHODE LINE BY-PASS
11 - INTERACTION SPACE

ALL DIMENSIONS UNLESS OTHERWISE SPECIFIED MUST BE HELD TO A TOLERANCE - FRACTIONAL ± 1/64," DECIMAL ± .005," ANGULAR ± 1/2°

ISSUE	DATE

ENGINEERING RESEARCH INSTITUTE
UNIVERSITY OF MICHIGAN
ANN ARBOR MICHIGAN

PROJECT
M - 762

CLASSIFICATION

DESIGNED BY R.W.D.
DRAWN BY [illegible]
CHECKED BY [illegible]
APPROVED BY
SCALE - FULL
DATE 10-24-50

TITLE
CO-AXIAL MAGNETRON
MODEL 7D

DWG. NO. B- 10,007D

DWG. NO. B-10,007D

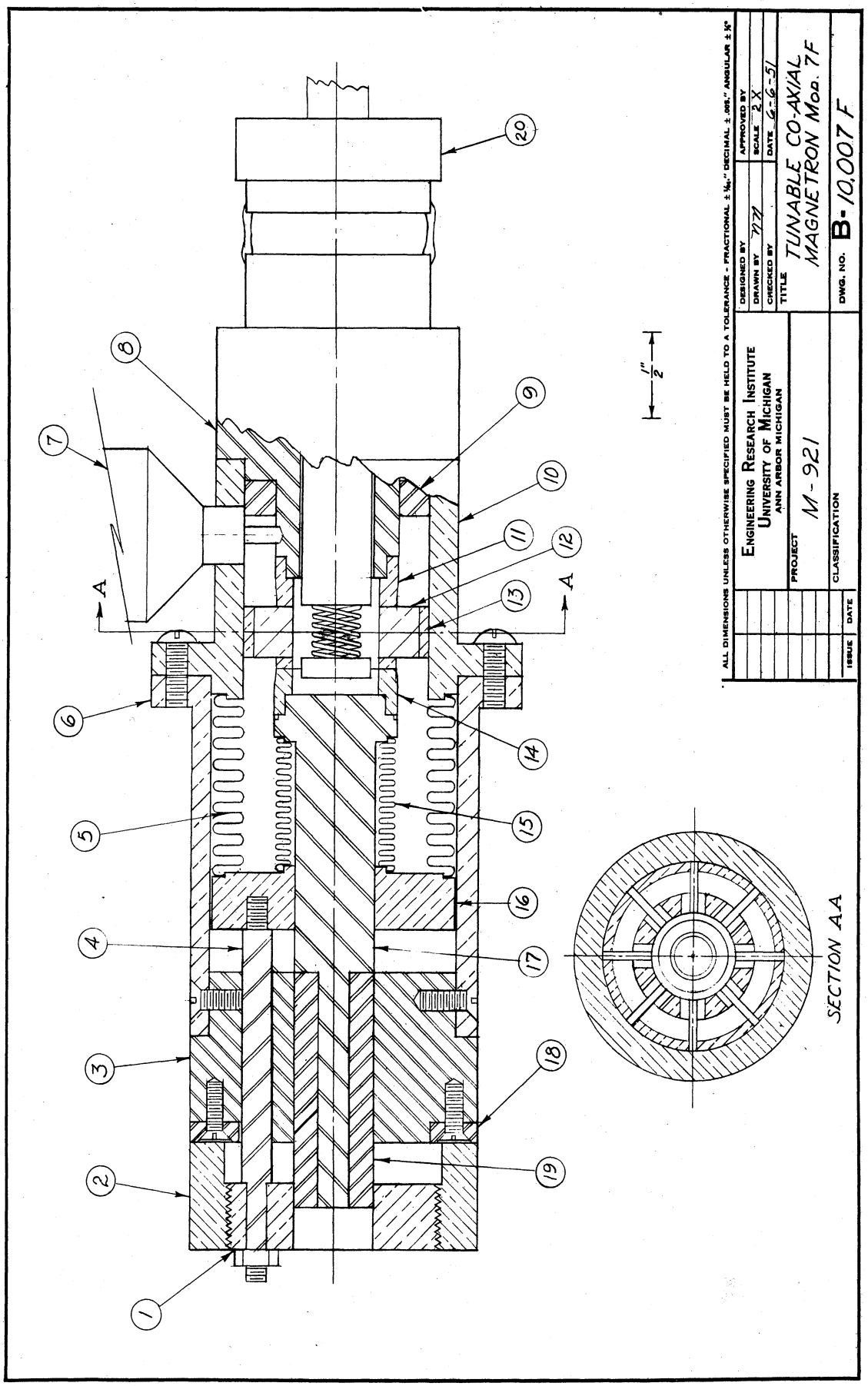
20
8
9
7
10
11
12
13
A
A
6
14
5
15
16
4
17
3
18
2
19
1
1"
2
SECTION AA
ALL DIMENSIONS UNLESS OTHERWISE SPECIFIED MUST BE HELD TO A TOLERANCE - FRACTIONAL ± 1/64" DECIMAL ± .005" ANGULAR ± 1/2°
ENGINEERING RESEARCH INSTITUTE
UNIVERSITY OF MICHIGAN
ANN ARBOR MICHIGAN
PROJECT M-921
CLASSIFICATION
ISSUE
DATE
DESIGNED BY
DRAWN BY RR
CHECKED BY
APPROVED BY
SCALE 2X
DATE 6-6-51
TITLE TUNABLE CO-AXIAL MAGNETRON Mod. 7F
DWG. NO. B-10,007 F
DWG. NO. B

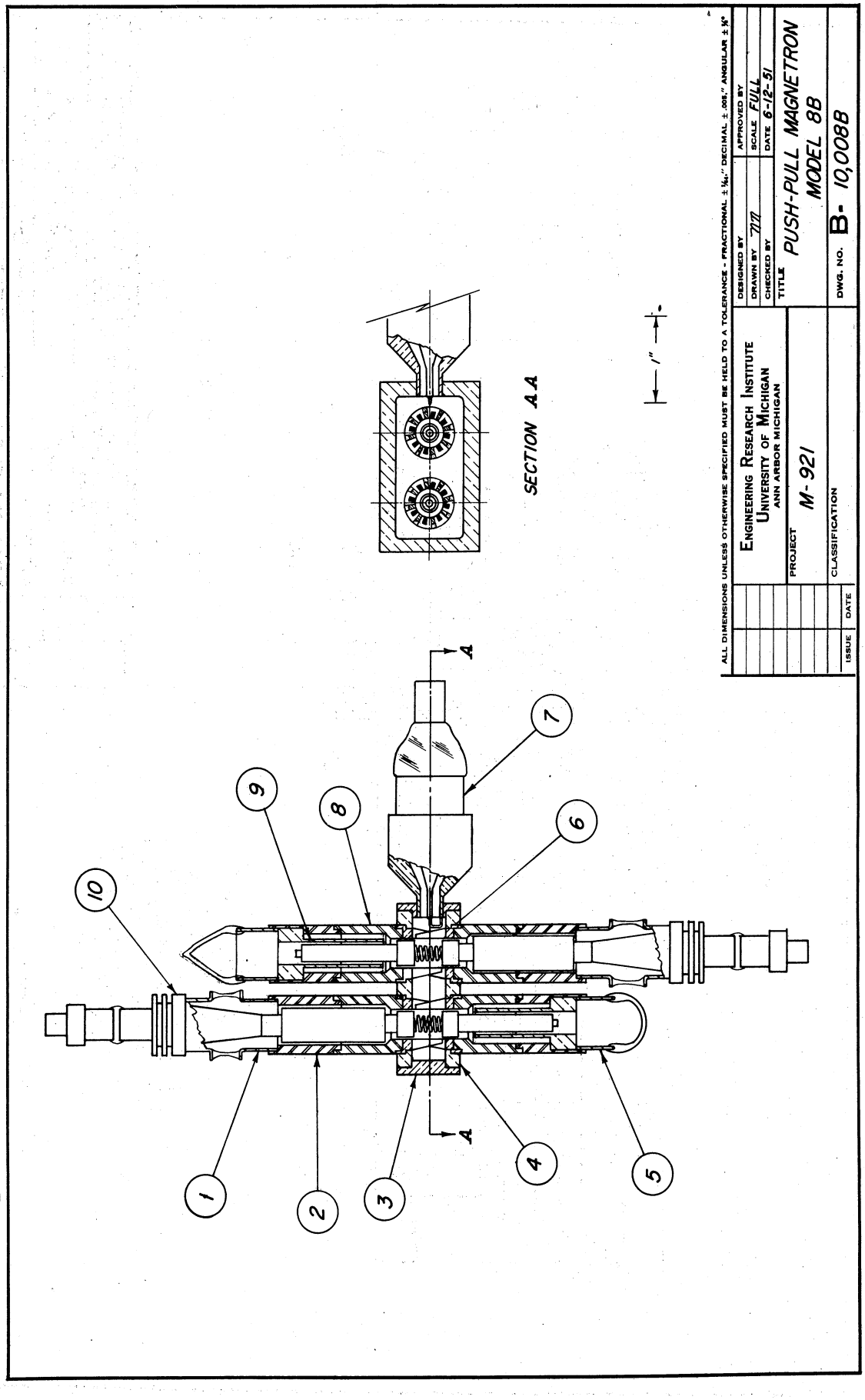
SECTION A-A
1"
A
A
1
2
3
4
5
6
7
8
9
10
DWG. NO. B
ALL DIMENSIONS UNLESS OTHERWISE SPECIFIED MUST BE HELD TO A TOLERANCE - FRACTIONAL ± 1/64" DECIMAL ± .005," ANGULAR ± 1/2°
ENGINEERING RESEARCH INSTITUTE
UNIVERSITY OF MICHIGAN
ANN ARBOR MICHIGAN
DESIGNED BY
DRAWN BY TJM
CHECKED BY
APPROVED BY
SCALE FULL
DATE 6-12-51
TITLE PUSH-PULL MAGNETRON
MODEL 8B
PROJECT M-921
DWG. NO. B- 10,0088
CLASSIFICATION
ISSUE
DATE

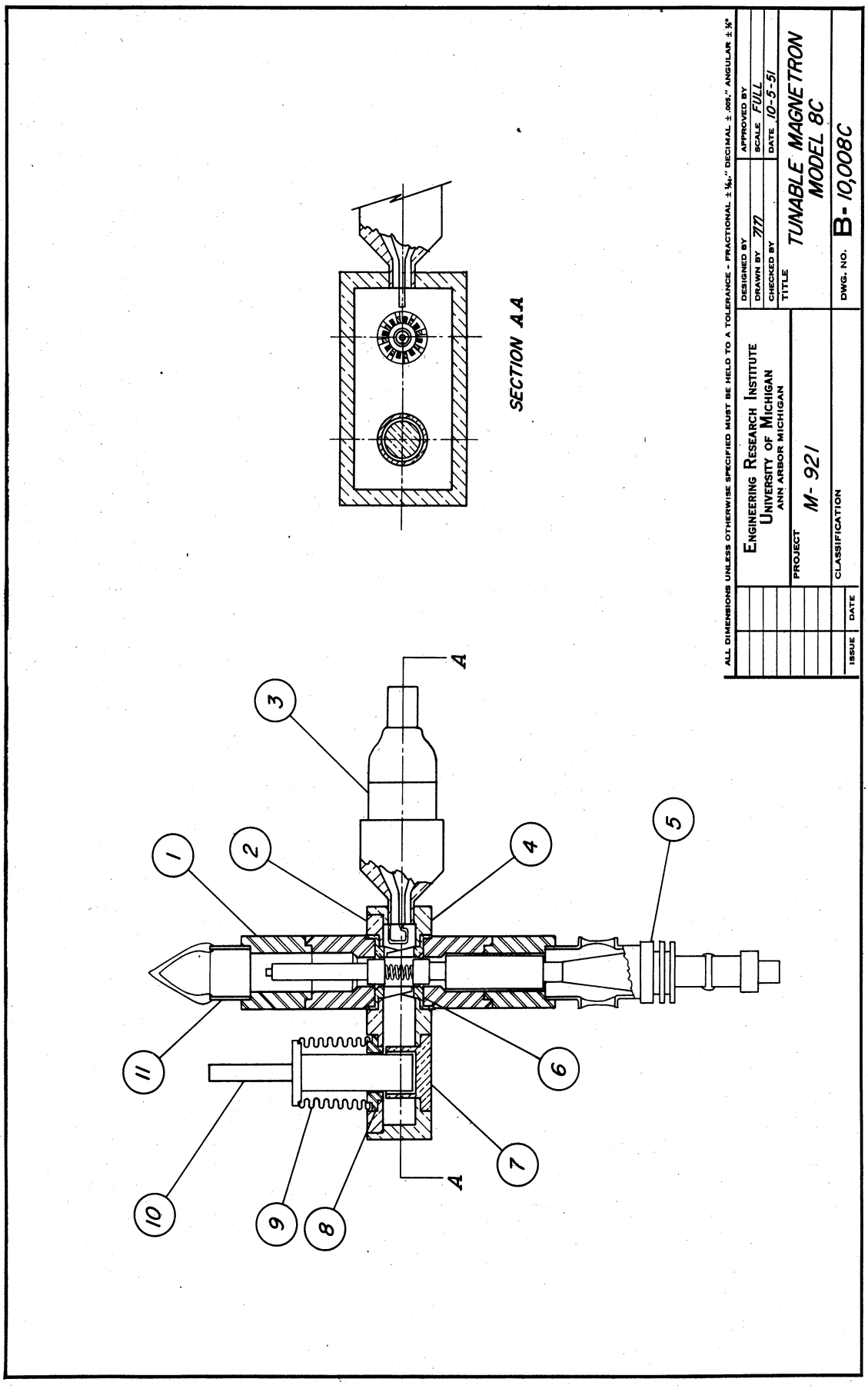
SECTION A-A
A
A
1
2
3
4
5
6
7
8
9
10
11
ALL DIMENSIONS UNLESS OTHERWISE SPECIFIED MUST BE HELD TO A TOLERANCE - FRACTIONAL ± 1/64," DECIMAL ± .005," ANGULAR ± 1/2°
ENGINEERING RESEARCH INSTITUTE
UNIVERSITY OF MICHIGAN
ANN ARBOR MICHIGAN
PROJECT M-921
CLASSIFICATION
ISSUE
DATE
DESIGNED BY
DRAWN BY
CHECKED BY
APPROVED BY
SCALE FULL
DATE 10-5-51
TITLE TUNABLE MAGNETRON MODEL 8C
DWG. NO. B-10,008C
DWG. NO. B

DWG. NO. B-10,009 B

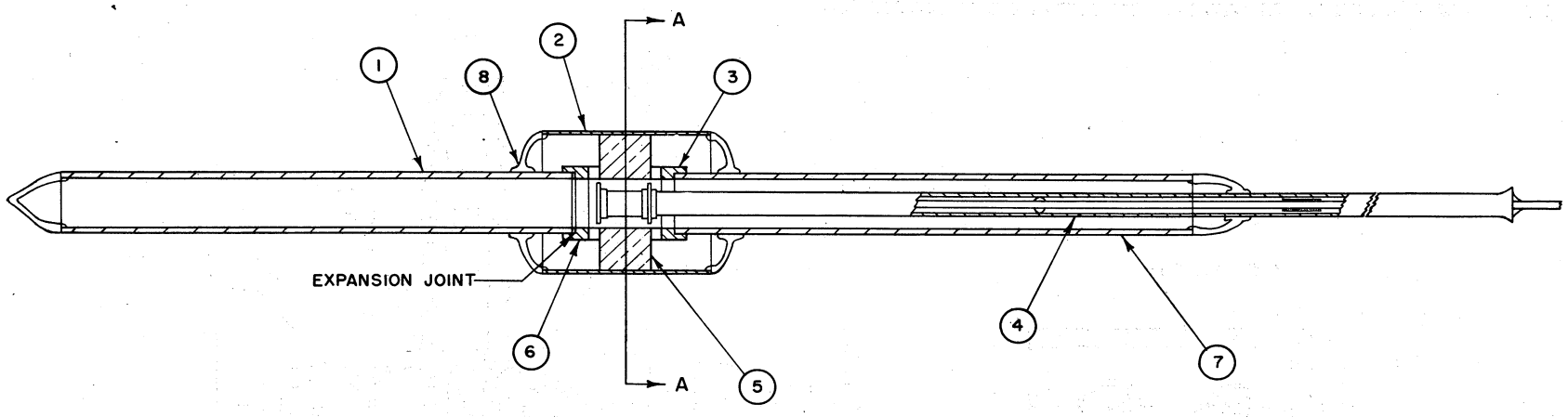

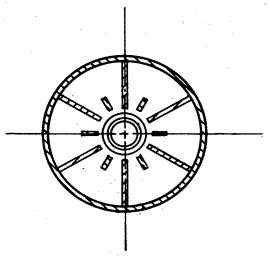

SECTION AA

1-INNER SLEEVE (KOVAR)
2-OUTER SLEEVE (KOVAR)
3-BAR-SUPPORT RING (CU)
4-CATHODE STEM (KOVAR)
5-VANE (CU)
6-BAR-SUPPORT RING (CU)
7-INNER SLEEVE (KOVAR)
8-GLASS SEAL

1" / 2

ALL DIMENSIONS UNLESS OTHERWISE SPECIFIED MUST BE HELD TO A TOLERANCE - FRACTIONAL ± 1/64," DECIMAL ± .005," ANGULAR ± ½°

ISSUE	DATE			
		ENGINEERING RESEARCH INSTITUTE UNIVERSITY OF MICHIGAN ANN ARBOR MICHIGAN	DESIGNED BY R.S.M.	APPROVED BY
			DRAWN BY M.M.	SCALE 2X
			CHECKED BY	DATE 1-22-51
		PROJECT M-921	TITLE LOW-POWER MAGNETRON MODEL 9B	
		CLASSIFICATION	DWG. NO. B-10,009 B	

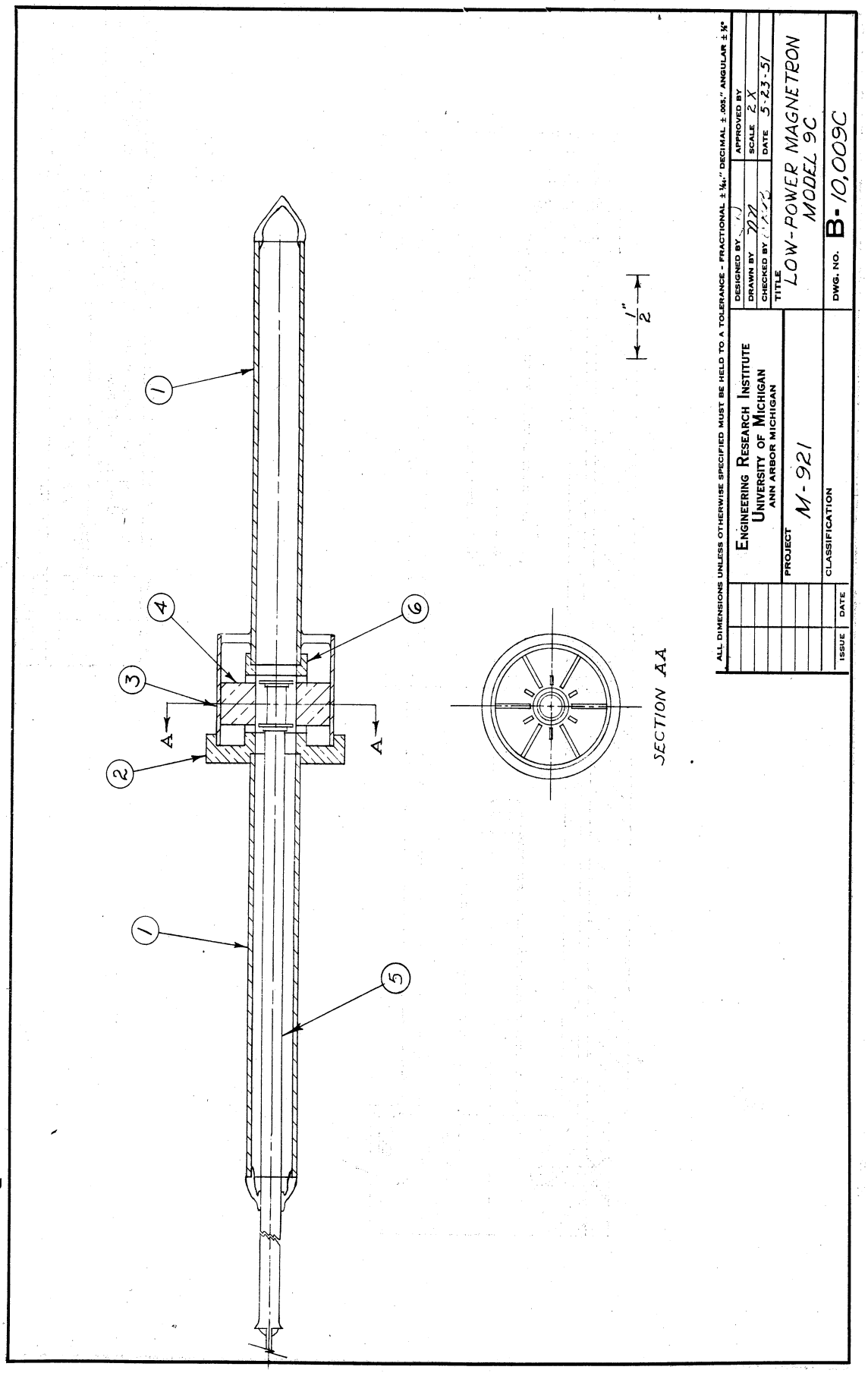
1
2
3
4
5
6
A
A
1/2"
SECTION AA
ALL DIMENSIONS UNLESS OTHERWISE SPECIFIED MUST BE HELD TO A TOLERANCE - FRACTIONAL ± 1/64" DECIMAL ± .005" ANGULAR ± 1/2°
ISSUE
DATE
CLASSIFICATION
ENGINEERING RESEARCH INSTITUTE
UNIVERSITY OF MICHIGAN
ANN ARBOR MICHIGAN
PROJECT
M-921
DESIGNED BY
DRAWN BY
CHECKED BY
APPROVED BY
SCALE 2 X
DATE 5-23-51
TITLE
LOW-POWER MAGNETRON
MODEL 9C
DWG. NO. B-10,009C
B
DWG. NO.

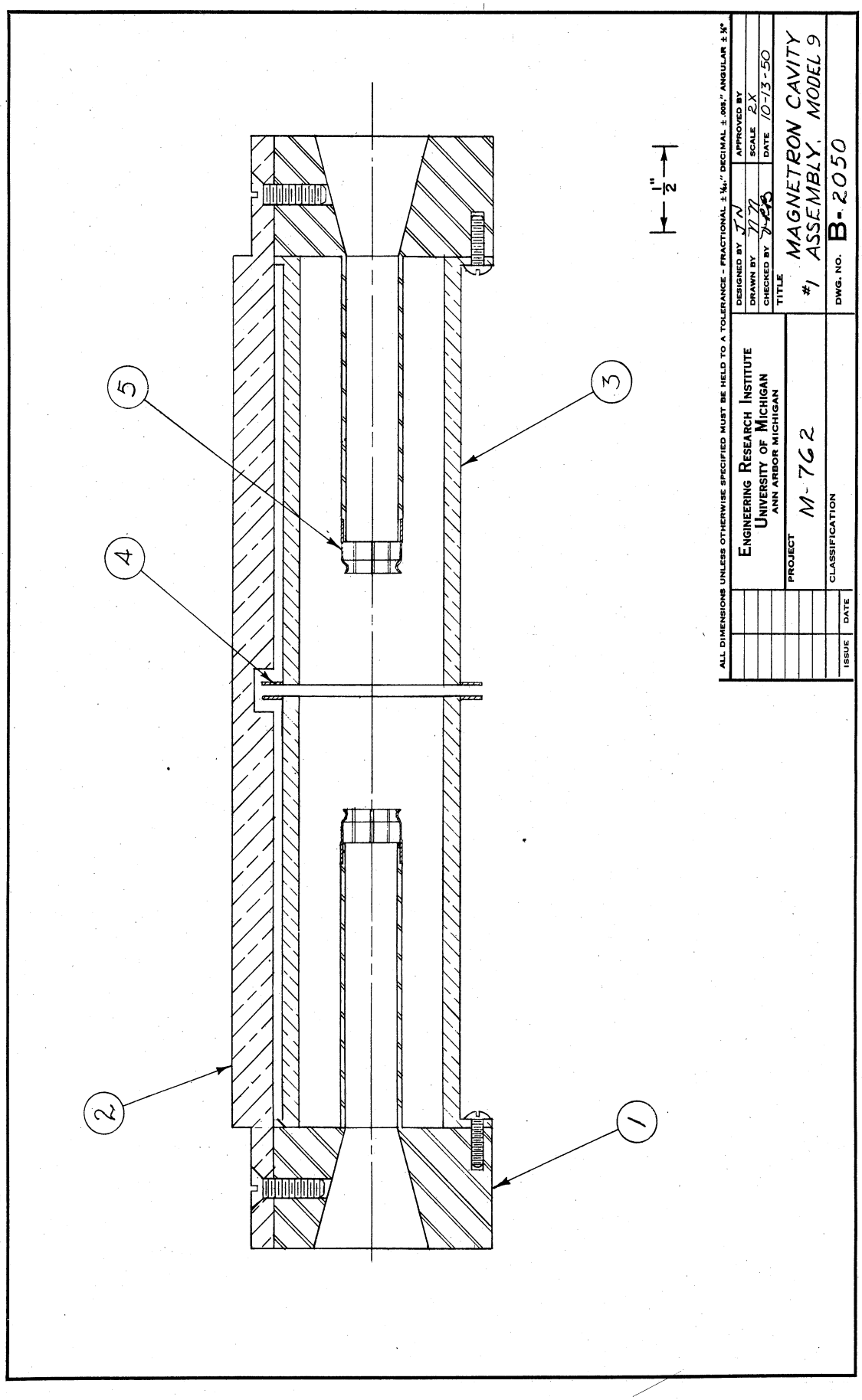
1
2
3
4
5
1/2"
ALL DIMENSIONS UNLESS OTHERWISE SPECIFIED MUST BE HELD TO A TOLERANCE - FRACTIONAL ± 1/64" DECIMAL ± .005" ANGULAR ± 1/2°
ENGINEERING RESEARCH INSTITUTE
UNIVERSITY OF MICHIGAN
ANN ARBOR MICHIGAN
PROJECT M-762
DESIGNED BY JN
DRAWN BY
CHECKED BY
APPROVED BY
SCALE 2X
DATE 10-13-50
TITLE MAGNETRON CAVITY #1 ASSEMBLY, MODEL 9
CLASSIFICATION
DWG. NO. B-2050
ISSUE
DATE
B
DWG. NO.

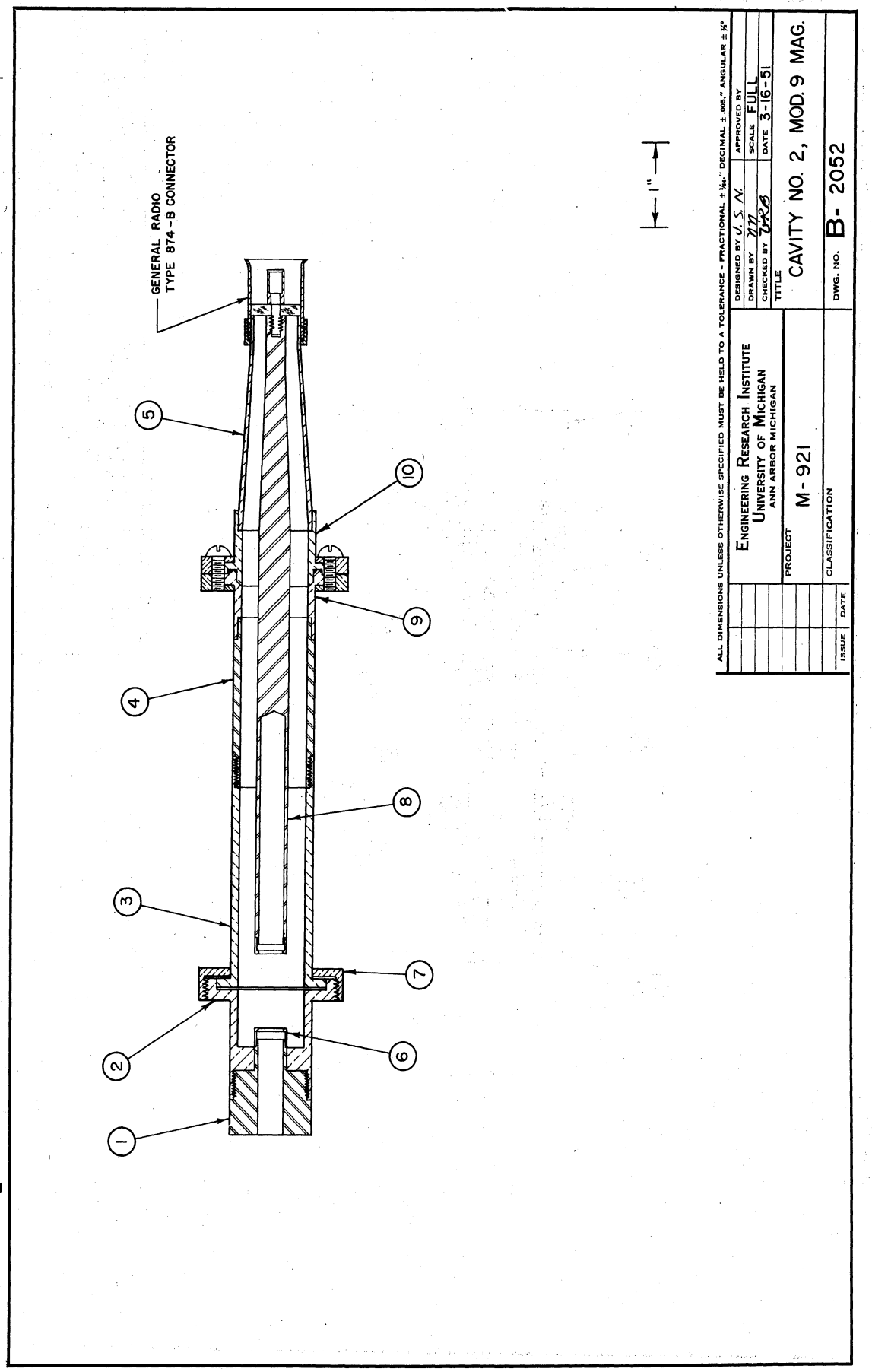
GENERAL RADIO
TYPE 874-B CONNECTOR
1
2
3
4
5
6
7
8
9
10
1"
ALL DIMENSIONS UNLESS OTHERWISE SPECIFIED MUST BE HELD TO A TOLERANCE - FRACTIONAL ± 1/64," DECIMAL ± .005," ANGULAR ± 1/2°
ENGINEERING RESEARCH INSTITUTE
UNIVERSITY OF MICHIGAN
ANN ARBOR MICHIGAN
DESIGNED BY U. S. N.
DRAWN BY
CHECKED BY
APPROVED BY
SCALE FULL
DATE 3-16-51
PROJECT M-921
TITLE CAVITY NO. 2, MOD. 9 MAG.
CLASSIFICATION
DWG. NO. B-2052
ISSUE
DATE
DWG. NO. B

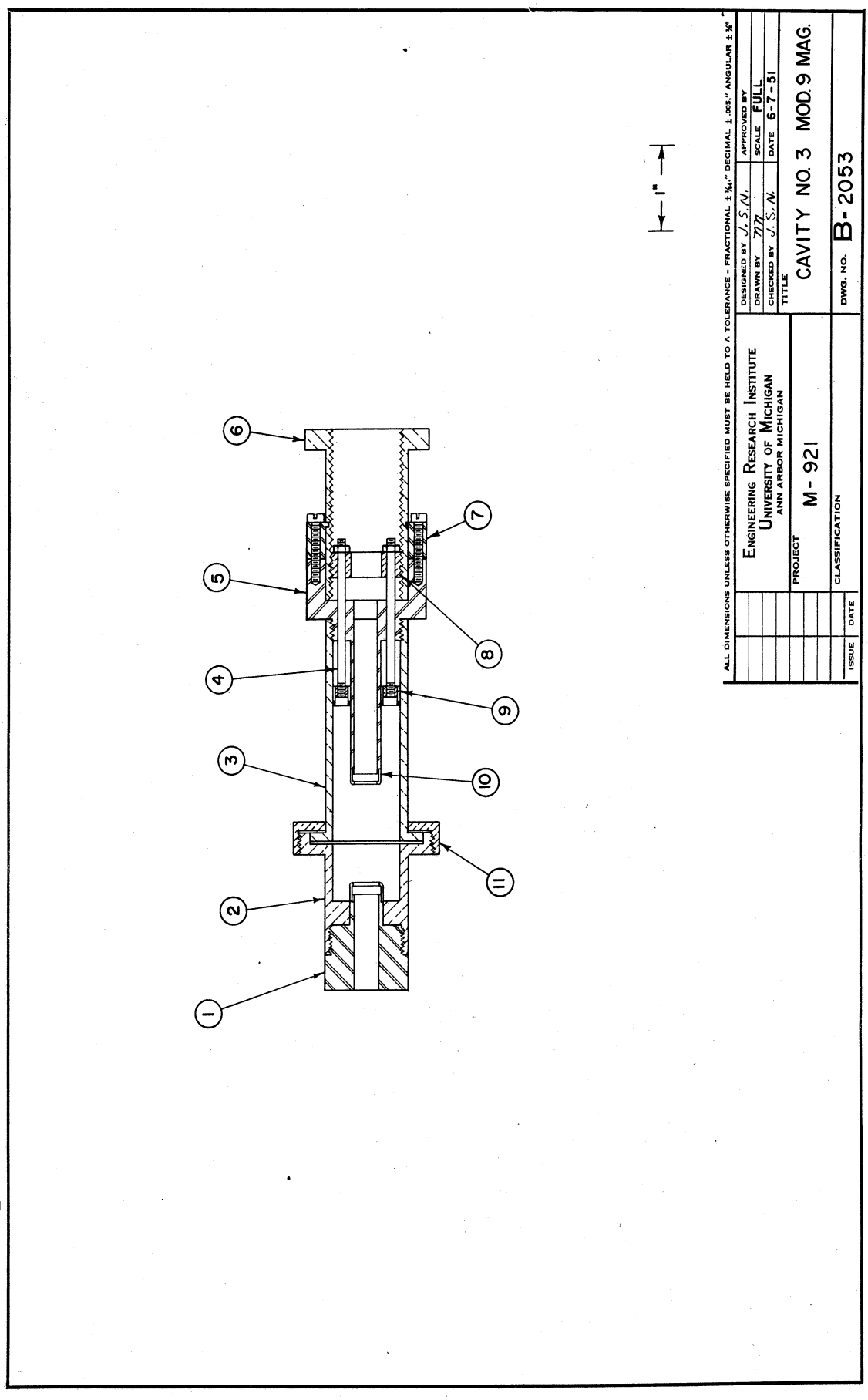
1"
1
2
3
4
5
6
7
8
9
10
11
ALL DIMENSIONS UNLESS OTHERWISE SPECIFIED MUST BE HELD TO A TOLERANCE - FRACTIONAL ± 1/64," DECIMAL ± .005," ANGULAR ± 1/2°
ENGINEERING RESEARCH INSTITUTE
UNIVERSITY OF MICHIGAN
ANN ARBOR MICHIGAN
DESIGNED BY J. S. N.
DRAWN BY
CHECKED BY J. S. N.
APPROVED BY
SCALE FULL
DATE 6-7-51
TITLE
CAVITY NO. 3 MOD. 9 MAG.
PROJECT
M-921
CLASSIFICATION
DWG. NO. B-2053
ISSUE
DATE
DWG. NO. B

DISTRIBUTION LIST

22 copies - Director, Evans Signal Laboratory
Belmar, New Jersey
FOR - Chief, Thermionics Branch

12 copies - Chief, Bureau of Ships
Navy Department
Washington 25, D. C.
ATTENTION: Code 930A

12 copies - Director, Air Materiel Command
Wright Field
Dayton, Ohio
ATTENTION: Electron Tube Section

4 copies - Chief, Engineering and Technical Service
Office of the Chief Signal Officer
Washington 25, D. C.

2 copies - Mr. John Keto
Director, Aircraft Radiation Laboratory
Air Materiel Command
Wright Field
Dayton, Ohio

2 copies - H. W. Welch, Jr., Research Physicist
Electronic Defense Group
Engineering Research Institute
University of Michigan
Ann Arbor, Michigan

1 copy - Engineering Research Institute File
University of Michigan
Ann Arbor, Michigan

W. E. Quinsey, Assistant to the Director
Engineering Research Institute
University of Michigan
Ann Arbor, Michigan

W. G. Dow, Professor
Department of Electrical Engineering
University of Michigan
Ann Arbor, Michigan

Gunnar Hok, Research Engineer
Engineering Research Institute
University of Michigan
Ann Arbor, Michigan

J. R. Black, Research Engineer
Engineering Research Institute
University of Michigan
Ann Arbor, Michigan

J. S. Needle, Instructor
Department of Electrical Engineering
University of Michigan
Ann Arbor, Michigan

G. R. Brewer
Electron Tube Laboratory
Research and Development Laboratory
Hughes Aircraft Company
Culver City, California

Department of Electrical Engineering
University of Minnesota
Minneapolis, Minnesota
ATTENTION: Professor W. G. Shepherd

Westinghouse Engineering Laboratories
Bloomfield, New Jersey
ATTENTION: Dr. J. H. Findlay

Columbia Radiation Laboratory
Columbia University
Department of Physics
New York 27, New York

Electron Tube Laboratory
Department of Electrical Engineering
University of Illinois
Urbana, Illinois

Department of Electrical Engineering
Stanford University
Stanford, California
ATTENTION: Dr. Karl Spangenberg

National Bureau of Standards Library
Room 203, Northwest Building
Washington 25, D. C.

Radio Corporation of America
RCA Laboratories Division
Princeton, New Jersey
ATTENTION: Mr. J. S. Donal, Jr.

Department of Electrical Engineering
The Pennsylvania State College
State College, Pennsylvania
ATTENTION: Professor A. H. Waynick

Document Office - Room 20B-221
Research Laboratory of Electronics
Massachusetts Institute of Technology
Cambridge 39, Massachusetts
ATTENTION: John H. Hewitt

Bell Telephone Laboratories
Murray Hill, New Jersey
ATTENTION: S. Millman

Radio Corporation of America
RCA Victor Division
415 South 5th Street
Harrison, New Jersey
Building 55
ATTENTION: Hans K. Jenny

Magnetron Development Laboratory
Power Tube Division
Raytheon Manufacturing Company
Waltham 54, Massachusetts
ATTENTION: Edward C. Dench

Vacuum Tube Department
Federal Telecommunication Laboratories, Inc.
500 Washington Avenue
Nutley 10, New Jersey
ATTENTION: A. K. Wing, Jr.

Microwave Research Laboratory
University of California
Berkeley, California
ATTENTION: Professor L. C. Marshall

General Electric Research Laboratory
Schenectady, New York
ATTENTION: P. H. Peters

Cruft Laboratory
Harvard University
Cambridge, Massachusetts
ATTENTION: Professor E. L. Chaffee

Collins Radio Company
Cedar Rapids, Iowa
ATTENTION: Robert M. Mitchell

Research Laboratory of Electronics
Massachusetts Institute of Technology
Cambridge, Massachusetts
ATTENTION: Professor S. T. Martin

Department of Electrical Engineering
University of Kentucky
Lexington, Kentucky
ATTENTION: Professor H. Alexander Romanowitz

Department of Electrical Engineering
Yale University
New Haven, Connecticut
ATTENTION: Dr. H. J. Reich

Department of Physics
Cornell University
Ithaca, New York
ATTENTION: Dr. L. P. Smith

Mrs. Marjorie L. Cox, Librarian
G-16, Littauer Center
Harvard University
Cambridge 38, Massachusetts

Mr. R. E. Harrell, Librarian
West Engineering Library
University of Michigan
Ann Arbor, Michigan

Mr. C. L. Cuccia
RCA Laboratories Division
Radio Corporation of America
Princeton, New Jersey

Dr. O. S. Duffendack, Director
Phillips Laboratories, Inc.
Irvington-on-Hudson, New York

Air Force Cambridge Research Laboratories
Library of Radiophysics Directorate
230 Albany Street
Cambridge, Massachusetts

Air Force Cambridge Research Laboratories
Library of Geophysics Directorate
230 Albany Street
Cambridge, Massachusetts
ATTENTION: Dr. E. W. Beth

Raytheon Manufacturing Company
Research Division
Waltham 54, Massachusetts
ATTENTION: W. M. Gottschalk

General Electric Research Laboratory
Schenectady, New York
ATTENTION: Dr. A. W. Hull

Sanders Associates Inc.
135 Bacon Street
Waltham 54, Massachusetts
ATTENTION: Mr. James D. LeVan

Sperry Gyroscope Company
Library Division
Great Neck, Long Island, New York

Sylvania Electric Products, Inc.
70 Forsyth Street
Boston 15, Massachusetts
ATTENTION: Mr. Marshall C. Pease

Dr. D. L. Marton
Chief, Electron Physics Section
National Bureau of Standards
Washington 25, D. C.

National Research Council of Canada
Radio and Electrical Engineering Division
Ottawa, Canada

Mr. Stanley Ruthberg
Electron Tube Laboratory
Bldg 83
National Bureau of Standards
Washington 25, D. C.